Materials Advances

ROYAL SOCIETY OF CHEMISTRY

REVIEW

View Article Online
View Journal | View Issue

Cite this: *Mater. Adv.*, 2025, 6, 8277

Immobilization of pyrene-tagged metal complexes onto solid supports by π-stacking interactions: syntheses and applications

Elham Sanaei and Gholamhossein Mohammadnezhad *

This review explores the development of metal complexes, based on their metal center, immobilized non-covalently onto diverse supports through functional anchors such as pyrene fragments. Additionally, it covers novel synthesis strategies and presents various practical applications, such as biosensors and biofuels, and generally industrial applications. Since pyrene fragments play a key role in the structure of these metal complexes, their significant effects on functionality are highlighted. Not only the number of pyrene fragments but also numerous supports, including graphene oxide (GO), reduced graphene oxide (rGO), carbon nanotubes (CNT), edge-plane graphite (EPG), graphitic carbon nitride (g-C_3N_4), pyrene-modified gold (Au), and indium tin oxide (ITO), can have a significant influence due to their extraordinary properties. Furthermore, it indicates how a non-covalent interaction between the pyrene fragment and the solid support can provide an efficient catalyst through π-stacking interactions compared to its homogeneous counterpart. In order to reduce leaching, maintain activity and selectivity, and improve recyclability, both homogeneous and heterogeneous properties are combined together in this approach.

Received 6th June 2025,
Accepted 26th September 2025

DOI: 10.1039/d5ma00598a

rsc.li/materials-advances

Department of Chemistry, Isfahan University of Technology, Isfahan 84156-83111, Islamic Republic of Iran. E-mail: mohammadnezhad@iut.ac.ir, g_m1358@yahoo.com; Fax: +98-31-3391-2350; Tel: +98-31-3391-3279

Elham Sanaei

Elham Sanaei received her Bachelor's degree in Applied Chemistry from the Isfahan University of Technology in 2023. She has completed her BSc project in the field of covalent organic frameworks. Her research interests include heterogeneous metal complexes, polymer nanocomposites, and smart hydrogels. Currently, she is exploring the broader applications of her research in various areas, such as environmentally friendly catalysis and targeted drug delivery, as an inorganic and polymer researcher.

Gholamhossein Mohammadnezhad

Gholamhossein Mohammadnezhad is a full professor of Inorganic Chemistry at the Isfahan University of Technology (IUT), Iran, where he has been a faculty member since 2012. He received his PhD degree from Shahid Beheshti University (SBU), Iran, in 2012. He worked as a visiting professor at Friedrich Schiller University Jena and the University of Cologne, Germany, on several occasions between 2014 and 2025, fostering international collaborations. His research focuses on: (i) single-source precursors, particularly metal alkoxides, for the synthesis of high-surface-area advanced nanomaterials, metal oxides, and nanocomposites and (ii) the preparation and immobilization of inorganic complexes such as pincer-based and carboxamide complexes. The applications of the synthesized compounds are explored in catalysis, photocatalysis, electrochemistry, and biology. His work has resulted in over 80 peer-reviewed publications. He also serves as an Associate Editor for the Inorganic Chemistry Research Journal and is a member of the Iranian Chemical Society.

1. Introduction

A major goal in homogeneous catalysis is to develop sophisticated ligands that possess properties beyond their traditional role of binding to a metal and providing a well-defined stereoelectronic effect. Adding a functional group to a ligand can modify the properties of a metal complex through ligand-based reactivity under external stimuli. The properties of the complex can be tuned by several functionalities, such as hydrogen bonding interactions, proton-responsive sites, redox-sensitive components, and photoresponsive units. Additionally, more effective homogeneous catalysts that take advantage of weak reversible non-covalent interactions are of prime importance.[1–4] Although homogeneous catalysts are highly active and selective, they face crucial challenges in their separation from products, which prevents industries from using them for large-scale material production. Furthermore, catalyst recycling is another major flaw in the industrial use of homogeneous catalysts.[5]

Molecular complexes can be immobilized to combine the benefits of homogeneous and heterogeneous catalysis, such as selectivity and recyclability, respectively. Several methods can be used to achieve this goal, including covalent bond formation, ion pairing, adsorption, and encapsulation. Such heterogenization onto various supports, for instance, mesoporous materials, microporous structures, and polymers, has already been achieved using many of these strategies.[6,7] The most common technique for immobilizing catalytic species is forming a covalent bond between the ligand and the solid support. Two significant disadvantages of this approach should be considered. First, it depends on both a stable surface and functionalization of extra ligands, which could raise the catalyst preparation cost, and the second drawback is the alterations in the reactivity of the original catalyst. Conversely, non-covalent interactions avoid further functionalization, potentially preserving the catalyst's intrinsic characteristics.[5] Furthermore, the non-covalent method is more straightforward to apply in synthetic processes and is less likely to reduce catalyst activity.[8,9] In this regard, non-covalent interactions, specifically π-stacking, have become an interesting candidate for substantial development of biological science, demanding comprehensive investigations. Particularly, the immobilization of enzymes on carbon nanotube surfaces holds high potential to achieve novel, high-performance bio-devices with notable biomolecular functions, such as advanced biosensors and biofuel cells. This process can be applied in an aqueous environment through the significant role of pyrene in enhancing the hydrophilicity of the CNT surface, as verified by TEM and FTIR analyses.[10–12]

Nevertheless, this method must be pursued with caution due to the fact that many of these catalysts are highly sensitive to changes in ionic strength, immobilization conditions, support nature, and the type of selected complex.[5,13] The latter must be carefully designed to ensure stability against leaching. Hence, new strategies, such as controlled-reversible immobilization *via* investigating the effects of temperature and solvent polarity, have been developed for the immobilization of these sensitive complexes onto solid supports to enhance the recyclability of the catalysts and supports.[13] Although the immobilization approach through π–π stacking resulted in catalytic performance that was comparable to its homogeneous counterpart, some challenges are associated with the non-covalent interactions between the catalyst and the support, such as slight deactivation due to the robustness of non-covalently immobilized complexes towards recycling, which may compromise long-term stability and increase the leaching risk. For instance, by aligning the active center of the enzymes correctly on the CNT surface, these enzymes can achieve efficient direct electron transfer without the need for external mediators, which is an appropriate measure to overcome the above-mentioned obstacles. Additionally, the immobilization of a His-tagged enzyme onto CNTs, facilitated by a pyrene fragment, promotes direct electron transfer due to the conductivity of the supports. Not only does stronger π–π stacking enhances the robustness of immobilization and the recyclability feature, but it may also reduce the catalyst release. Indeed, weaker interactions, which can result from certain solvents or temperatures, may improve electronic communication but increase the risk of leaching.[5,8,12,13]

This review aims to explore various pyrene-tagged metal complexes immobilized onto suitable solid supports through π-stacking interactions. To achieve this goal, several aspects are considered, including different supports for the immobilization of pyrene-tagged complexes, the role of pyrene structure, and immobilized pyrene-tagged complexes with various metal centers. These complexes are categorized based on their metal centers from early-transition to late-transition metal groups. Additionally, the extent of recycling improvement through different analyses of several catalysts was reviewed. The main objective of these studies is to explore the transformation of homogeneous catalysts into the heterogeneous ones and to evaluate their impact on recyclability while preserving selectivity. The results unambiguously demonstrate that the presence of pyrene fragments within the catalyst structure is pivotal for enhancing overall catalyst performance. Furthermore, the considerable influence of the pyrene fragment's location, which may affect the behavior of the resulting catalyst, is highlighted.[14]

2. Different supports for the immobilization of pyrene-tagged complexes

There are two efficient ways of achieving the immobilized pyrene-tagged complexes through π–π interactions between the complexes and supports, including (a) carbon-based nanomaterials or (b) modified pyrene-tagged supports. A limited range of such superb supports have been reported, specifically those based on highly efficient carbon nanomaterials, including graphene oxide (GO), reduced graphene oxide (rGO), carbon nanotubes (CNT), edge-plane graphite (EPG), graphitic carbon nitride (g-C_3N_4) and modified gold (Au) and indium tin oxide (ITO).[5,6,15–19]

Besides their intrinsic π–π interaction ability, carbon nanotubes, rolled-up graphene sheets, GO, and rGO have further promising properties, such as high specific surface area, stability,

and accessibility.[5] The other two types of commonly used supports, Au and ITO, are modified with the pyrene fragments. In these cases, the immobilization of the complexes is achieved through π–π stacking interactions between the pyrene-tagged support and pyrene-tagged complexes.[16,17]

3. Role of the pyrene structure

The pyrene molecule is the smallest polycyclic aromatic hydrocarbon with a peri-fused system and may form during the ignition of organic substances. Although its structure does not conform to Hückel's rule, it exhibits aromaticity with a highly symmetrical structure (D_{2h} point group).[20] It plays essential roles in organic chemistry, pharmaceutical industry, materials science, and many applications, such as biological probes,[21–23] photonic devices,[24,25] and liquid crystal materials.[26–30] Additionally, it is considered a prototypical molecule due to its predictable substitution reactions, diverse photochemistry, high fluorescence quantum yield, and efficient excimer emission.[31] Such modifications to pyrene fragments enable the construction of the surface that allow for changes, which is beneficial for various electrochemical applications, such as sensing, energy storage, and catalysis.[16] Catalysts containing pyrene fragments can be heterogenized thermodynamically through van der Waals non-covalent interactions (π-stacking) with a solid surface. The crucial role of the pyrene fragment in the adsorption of several complexes on the graphene surface was investigated by Peris and co-workers.[5] In addition to the presence of the pyrene moiety, the quantity of pyrene tags significantly affects both desorption and recyclability. Specifically, unlike the catalyst with a single pyrene that can only be recycled three times, the variant with two pyrene fragments retained its activity for up to twelve cycles.[2] The addition of external pyrene, as a π-stacking additive, decreased the catalytic activity of all reactions catalyzed by pyrene-tagged palladium complexes.[3] The general properties of immobilized pyrene-tagged complexes, which are hybrid and take advantage of both homogeneous and heterogeneous positive features, are summarized in Table 1.

4. Immobilized pyrene-tagged complexes with various metal centers

4.1. Pyrene-tagged chromium complexes

In 2021, Jaber, Schulz, and their co-workers developed a strategy to immobilize chiral chromium salen onto rGO, taking advantage of this novel catalyst.[32] Salen catalysts modified with one/two pyrene groups were synthesized to evaluate their stability during recycling and accessibility to active sites. Key intermediates **1** and **2** were obtained *via* click reactions between pyrene derivatives and 5-(azidomethyl)-3-(*tert*-butyl)-2-hydroxybenzaldehyde in high yields (Fig. 1). Classical condensation of **1** and **2** with (1*S*,2*S*)-cyclohexane-1,2-diamine produced Sym-**1** and Sym-**2**; the latter has a metal coordination site separated from the pyrene *via* four methylene groups. In order to synthesize **Unsym** ligands, 3,5-di-*tert*-butyl-2-hydroxybenzaldehyde reacted with **1** or **2**, with no requirement to isolate the intermediate ammonium mono-imine. In the next step, chromium was introduced into the coordinating sites of the four synthesized ligands *via* $CrCl_2$ in THF under an argon atmosphere, followed by subsequent oxidation in air, leading to **Sym-Cr(-1,-2)** and **UnSym-Cr(-1,-2)**. **UnSym-Cr-1** was selected to be immobilized onto the carbon surface by impregnating rGO suspension with a solution of the catalyst in CH_2Cl_2 (4 : 1 mass ratio) (Fig. 2). UV/vis analysis indicated that 90% of the complex had been immobilized, confirmed by weighing the resulting solid.

To examine the efficiency of these catalysts, they were evaluated in the asymmetric ring-opening (ARO) of epoxides and hetero-Diels–Alder (HDA) processes. Although the Sym-Cr-**1** and Sym-Cr-**2** catalysts indicated minor enantioselectivity, UnSym-Cr-**1** had a considerable enantiomeric excess and virtually complete conversion, which was ascribed to the presence of two *t*Bu groups that hindered intramolecular stacking and increased substrate access. In this regard, the recyclability of the UnSym-Cr-**1**@rGO catalyst was assessed through its application in the same reaction. UnSym-Cr-**1**@rGO maintained its high activity and selectivity over 5 runs of hydrodearomatization and with different substrates in 6–8 runs. The X-ray photoelectron spectroscopy (XPS) analysis confirmed no active species leaching from the spent **UnSym-Cr-1** based on the Cr/C ratios. The pyrene tags facilitated π-stacking interactions with rGO, improving dispersion but complicating recovery due to settling difficulties. Nevertheless, the immobilized catalysts generally outperformed the Jacobsen reference, leading to highly active species in the catalytic processes as a result of probable bimetallic interactions. This work successfully immobilized salen complexes on carbon *via* π–π interactions, opening opportunities for future asymmetric catalysis applications.

Table 1 The properties of homogeneous, heterogeneous, and immobilized pyrene-tagged complexes

	Homogeneous	Immobilized pyrene-tagged	Heterogeneous
Stability	High	High	Variable[a]
Selectivity	High	High	Moderate
Activity	High	Medium to high	Medium
Recyclability	Difficult	Easy	Easy

[a] Generally less than homogeneous counterparts.

4.2. Pyrene-tagged manganese complexes

New catalytic structures with abundant first-row transition metals (Ni, Co, Fe, and Mn) are of interest as replacements for expensive Re, Ru, and Ir catalysts in CO_2 reduction to valuable chemicals. In 2017, Reisner and co-workers reported the immobilization of a *fac*-[$MnBr(bpy_{pyr})(CO)_3$] complex (Mn_{pyr}, **7**) (bpy = bipyridine) onto a carbon nanotube electrode through a pyrene fragment for aqueous CO_2 reduction.[33] The pyrene-tagged ligand, 4-methyl-4′-(5-(pyren-1-yl)pentyl)-2,2′-bipyridine (bpy_{pyr}, **6**), was produced through the reaction of a lithiated 4,4′-dimethyl-bipyridine intermediate and 1-(4-bromobutyl)pyrene (**5**) (Fig. 3). The resulting ligand, bpy_{pyr}, was refluxed *via* [$MnBr(CO)_5$] to synthesize *fac*-[$MnBr(bpy_{pyr})(CO)_3$] (Mn_{pyr}, **7**). Subsequently, to immobilize the Mn complex, a two-step procedure was followed. Firstly, dispersed MWCNTs in

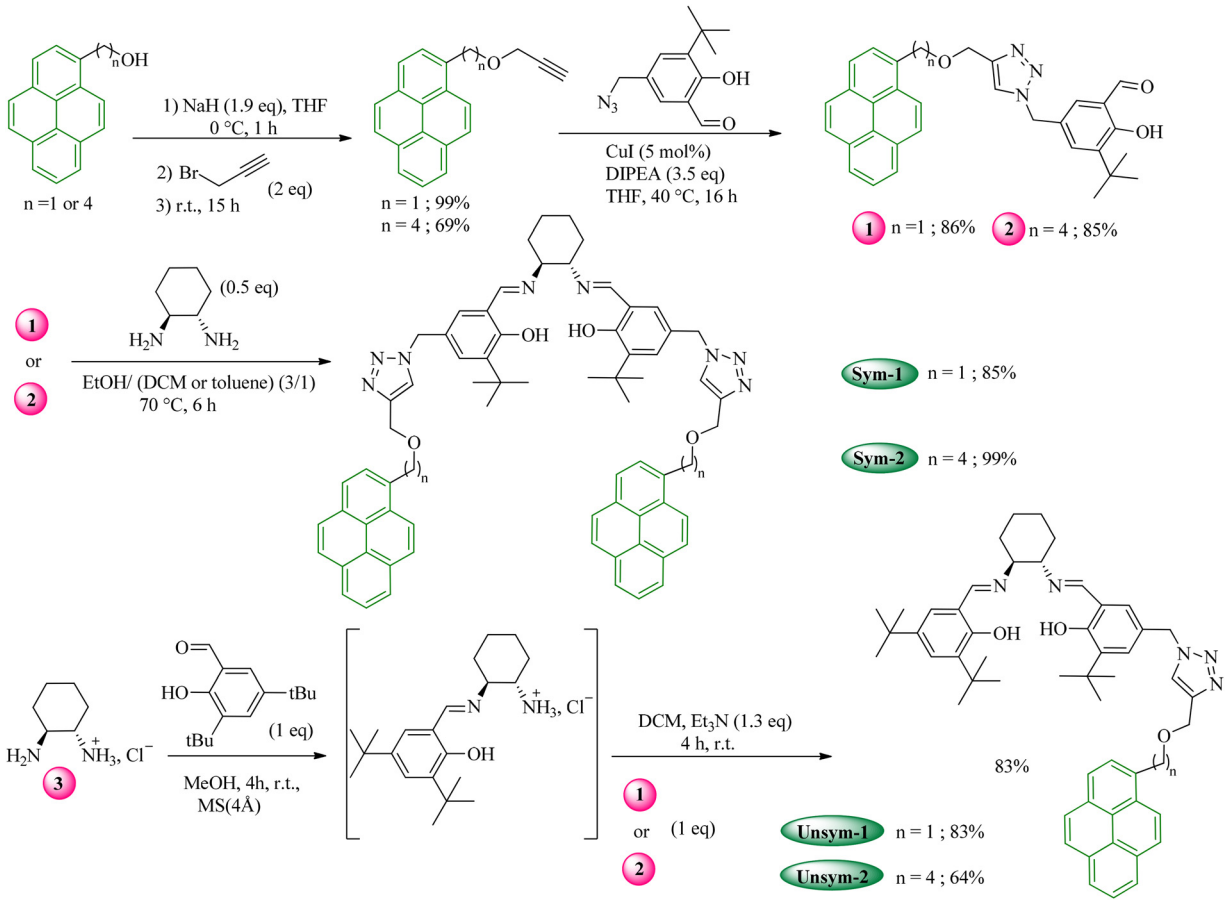

Fig. 1 The synthesis of salen ligands containing pyrene fragments. Reproduced with permission from ref. 32 copyright 2021, John Wiley and Sons.

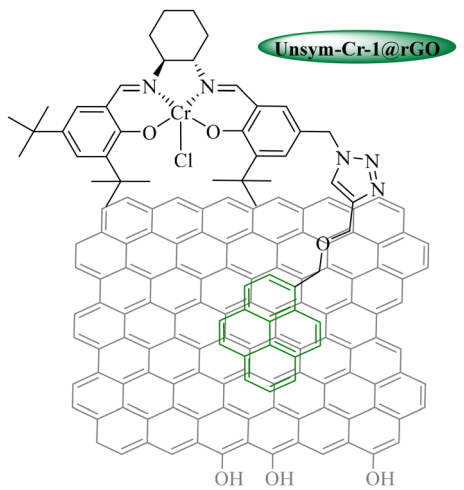

Fig. 2 The immobilized **UnSym-Cr-1**'s structure onto the graphene surface. Reproduced with permission from ref. 32 copyright 2021, John Wiley and Sons.

N-methylpyrrolidone (NMP) were drop cast and dried onto a glassy carbon electrode. Secondly, the MWCNT modified electrode was immersed in a Mn_{pyr} solution of anhydrous *N*,*N*-dimethylformamide (DMF), and the resulting CNT|Mn_{pyr} electrode was used for further experiments (Fig. 4).

Pyrene-modified catalysts on CNT sidewalls, which offer an exceptional conductivity and high surface area, allow insoluble catalysts to work in water, enable CO_2 reduction in water with low energy input and high reaction efficiency, and overcome limitations caused by diffusion in the bulk solution. It is noteworthy that catalyst loading adjustment controls product selectivity. Comparing [MnBr(bpy)$(CO)_3$] and the pyrene-anchored complex, *fac*-[MnBr(bpy_{pyr})$(CO)_3$] reveals some key differences. While the first complex is extremely active in organic solvents, the latter exhibits flexible catalytic activity in both organic and aqueous solutions. Generally, these distinctions indicate the effect of ligand selection and immobilization techniques on catalytic performance and selectivity in CO_2 reduction. Besides, surface loading can affect CO_2 reduction, leading to the formation of CO or formate ($HCOO^-$).

4.3. Pyrene-tagged rhenium complexes

In 2019, Warren and co-workers reported an immobilized pyrene-tagged rhenium(I) complex containing 2-(2′-quinolyl)benzimidazole (QuBIm-R) (R = H, Me, and Bn) (**8**) ligands on edge-plane graphite (EPG) electrodes for CO_2 reduction under aqueous conditions (Fig. 5).[18] In order to synthesize rhenium(I) complexes, ReQuBIm-R (**10**) derivatives were synthesized by reacting $Re(CO)_5Cl$ (**9**) with an equal amount of QuBIm-R ligand

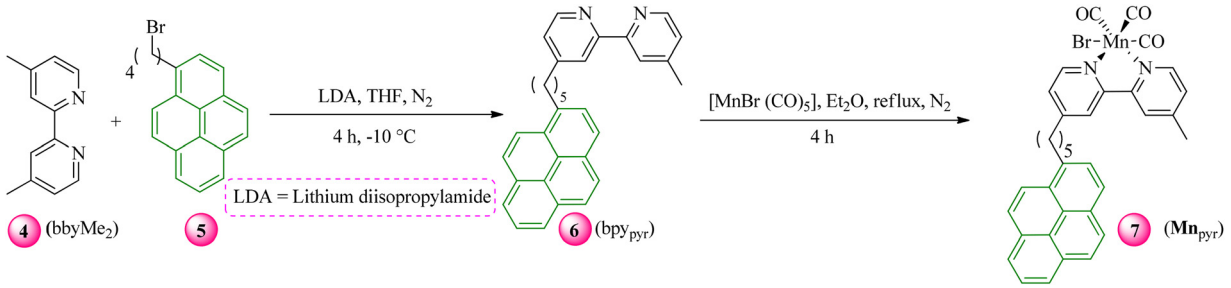

Fig. 3 The synthesis procedure for the preparation of pyrene-tagged Mn complexes. Reproduced with permission from ref. 33 copyright 2017, American Chemical Society.

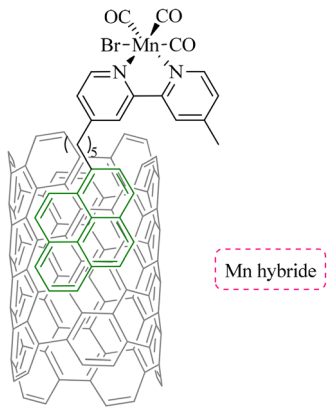

Fig. 4 The immobilization of pyrene-tagged Mn complexes onto CNTs. Reproduced with permission from ref. 33 copyright 2017, American Chemical Society.

in hot toluene, followed by reflux to yield bright-orange solids, filtration, and washing with cold toluene and diethyl ether. To study the heterogeneous electrochemical properties of the alkylated ReQuBIm-R complexes, each compound was introduced *via* drop-casting onto the EPG electrodes and subsequently rinsed thoroughly with water before cyclic voltammetry (CV) experiments. In the case of ReQuBIm-Pyr, an irreversible reduction wave at −1.38 V in argon-purged $KHCO_3$ buffer was observed. After several CV sweeps, the peak current density gradually decreased to the baseline level. A trend was also observed in alkylated ReQuBIm-H complexes and bare EPG electrodes, suggesting potential reductive exfoliation of graphite as a result of ionic intercalation. In contrast, ReQuBIm-Pyr displayed unique behavior in the presence of CO_2, showing a five-fold increase in the current density at a defined potential after four CV cycles while maintaining stable peak current density, unlike other alkylated ReQuBIm-R complexes. Based on controlled potential electrolysis (CPE) experiments, adsorbed ReQuBIm-Pyr onto EPG electrodes demonstrated steadier and higher current densities compared to the other ReQuBIm-R complexes. Additionally, ReQuBIm-Pyr drop cast onto EPG showed limited effectiveness in MeCN, reflecting the challenges faced by Re^{I}-based catalysts, while in contrast, it demonstrated significant current density in H_2O, highlighting the substantial impact of solvent on electrocatalyst performance. Moreover, ReQuBIm-Pyr films' activity in CPE experiments was evaluated by comparing the reported turnover number (TON) according to the quantity of the electroactive catalyst and the estimated theoretical TON. The results showed approximately similar values, indicating that most of the electroactive catalyst was active for CO_2 reduction.

In 2013, Brunschwig, Gray, and co-workers immobilized two kinds of pyrene-tagged Rh and Re complexes onto carbon electrodes through a pyrene-tagged bipyridine ligand (P), where P performs the role of a linker between the defined complexes and the surface (Fig. 6).[34] Immobilization of a rhodium proton-reduction catalyst, [Cp*Rh(P)Cl]Cl (**11**), and a rhenium CO_2-reduction catalyst, [Re(P)$(CO)_3$Cl] (**12**), afforded electrocatalytically active assemblies.

In order to synthesize these complexes and covalently attach pyrenyl moieties to bipyridine ligands, a synthetic approach was developed, which involves the reaction of 2,2′-bipyridyl-4,4′-carboxylic acid with 1-pyrenylmethylamine. The modified ligand was metalated to yield complexes **11** and **12**. In the next step, a high surface area carbon black was used to form conducting electrodes with superb electrocatalytic performance. In this regard, the electrodes were prepared by drop-casting a suspension of the carbon in NMP with the binder onto graphite and subsequent heating at 70 °C prior to immobilization. In order to functionalize the electrodes with catalysts, they were soaked in

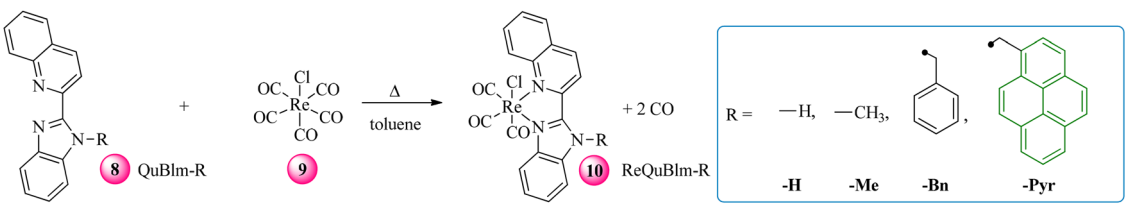

Fig. 5 The synthesis procedure of ReQuBIm-R complexes. Reproduced with permission from ref. 18 copyright 2019, American Chemical Society.

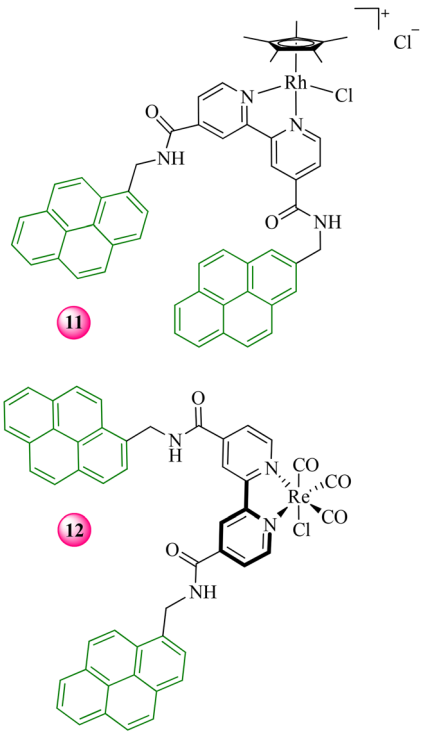

Fig. 6 The Rh and Re pyrene-tagged catalysts for immobilization. Reproduced with permission from ref. 34 copyright 2013, American Chemical Society.

CH_2Cl_2 solutions of **11** or **12** complexes, followed by washing to remove weakly bound species, resulting in strong electrocatalytic systems.

These catalysts were compared with their analogous structure to evaluate their efficiency. It was verified that the surface-immobilized catalyst **11** facilitates proton (H^+) reduction to hydrogen. Nevertheless, the addition of a proton source (*p*-toluenesulfonic acid) leads the catalyst to lose its redox reversibility; it increases the catalytic current for proton reduction, which can be continued until a steady-state current density is reached, indicating the catalyst's efficacy in promoting the hydrogen evolution reaction. Moreover, electrodes with catalyst **11** are more robust for H_2 production than those with catalyst **12** for CO_2 reduction. In controlled-potential electrolysis (CPE), electrodes with catalyst **12** showed current values approaching the background within the first hour. Generally, immobilizing molecular catalysts with pyrene groups is a viable technique for forming solar fuel cathodes.

4.4. Pyrene-tagged iron complexes

In 2010, Jousselme and co-workers reported a straightforward and adjustable method for functionalizing carbon nanotube electrodes with ferrocene by π-stacking interactions, resulting in the immobilization of redox groups on CNTs for use in sensors and catalytic applications (Fig. 7).[35] In order to synthesize 3-ferrocenyl-*N*-(pyren-1-ylmethyl)propanamide (**14**), 1-pyrenemethylamine hydrochloride was dissolved in, washed with, and dried with CH_2Cl_2, NaOH, and Na_2SO_4, respectively, and finally concentrated to obtain 1-pyrenemethylamine. This amine reacted with 2-[(3-ferrocenylpropanoyl)oxy]-1*H*-isoindole-1,3(2*H*)-dione (**13**) and triethylamine in CH_2Cl_2. Then, the crude product was purified, resulting in **14** as a yellow powder. A solution of **14** was added to a dispersed MWCNT solution in ethanol, treated ultrasonically, and filtered through a PTFE membrane to produce thin films of MWCNTs, which served as a working electrode in the electrochemical setup. Indeed, the simple π-stacking of pyrene allows for the uniform self-assembly of a single monolayer of molecules onto the MWCNTs. In the next step, bucky paper (BP) electrodes were utilized to investigate chemical functionalization through π–π interactions. The CV analysis of **14** in CH_2Cl_2 revealed π-stacking with CNTs, indicated by monoelectronic oxidation. However, washing the electrode with CH_3CN led to the desorption of ferrocene due to **14**'s solubility. To enhance stability, nanotubes were dispersed in ethanol, combined with a saturated **14** solution, and filtered to prepare the modified electrodes. The attachment of ferrocene was confirmed in MeCN through a reversible oxidation wave. Notably, no adsorption was observed with ferrocene alone, highlighting the pyrene fragment's critical role in promoting π-stacking. Nevertheless, based on cyclic voltammetry and XPS measurements, the covalent derivatization of CNTs with ferrocene moieties (in **13**), in comparison with π-stacking (**14**), results in a stable and reliable electrode material for glucose sensors.

In 2011, Cosnier and co-workers discovered that tris(bispyrenebipyridine)iron(II) complexes can serve as appropriate cross-linkers that enable biomolecules to adhere more easily to CNTs.[36] Complex tris[4,4′-bis(4-pyren-1-ylbutyloxy)bipyridinyl]iron(II) hexafluorophosphate (**17**) was synthesized in a multi-step process (Fig. 8). The ligand, 4,4′-bis(3-pyren-1-ylbutyloxy)bipyridine (**16**), was prepared by reacting 4-4′-bishydroxy-2-2′-bipyridine (**15**) with 1-(4-bromobutyl)-pyrene (**5**). Three equivalents of this ligand were then reacted with $Fe(ClO_4)_2$, followed by exchanging the ClO_4^- with hexafluorophosphates, leading to the corresponding complex (**17**), isolated as a purple solid.

Two techniques were applied for MWCNT electrode modification: dip-coating and electropolymerization. The first one allows for efficient immobilization through the generation of a homogeneous coating with a high surface area; however, through electropolymerization, the rate of electron transmission may be slowed down, providing an insulating coating. Since MWCNT electrodes have a high surface area and favorable interactions, they promote higher polymer formation in comparison to bare Pt electrodes during electropolymerization. The yield of electropolymerization on MWCNT electrodes was substantially higher than that on Pt electrodes, emphasizing how well MWCNT electrodes perform. According to biosensing results, the prepared biosensor *via* the dip coating approach with **17** shows the best performance. Additionally, the bioelectrodes demonstrated excellent sensing performance using glucose oxidase (GO_x) as a model enzyme (Fig. 9). The high sensitivity of the MWCNT/**17** configuration indicates its flexible supramolecular design that enabled maximum enzyme immobilization and efficient hydrogen peroxide diffusion. Electrochemical analysis confirmed successful MWCNT functionalization with transition metal complexes and

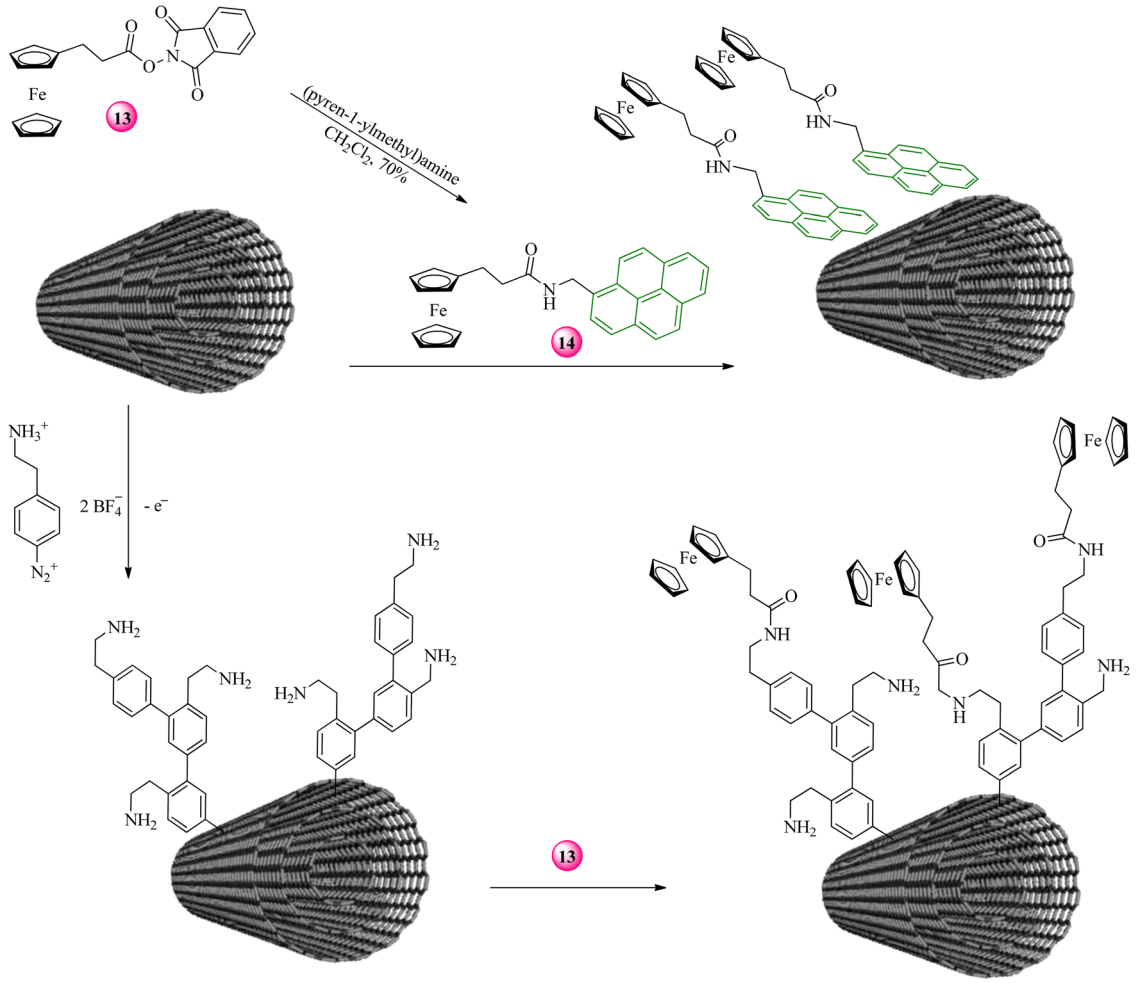

Fig. 7 Functionalization of MWCNTs with ferrocene *via* π-stacking of **14** or covalent grafting of **13**. Reproduced with permission from ref. 35 copyright 2010, Elsevier.

enzymes, which illustrates the potential of this bioelectrode configuration for sensitive and effective biosensing.

In 2012, Cosnier and co-workers introduced a novel technique for the direct synthesis of stable iron diamine complexes bearing mixed ligands on pyrene-tagged bipyridinyl functionalized CNTs *via* π-stacking interactions to take advantage of their beneficial features in biosensor devices.[37] To prepare the mixed ligand iron complex, $[Fe^{II}(L_1)_2L_2]^{2+}$ (L_1 = 4,4′-bis(biotin)-2,2′-bipyridine, L_2 = 2,2′-bipyridine-4,4′-dipyrene) (**20**), CNTs were functionalized by incubating them in a bipyridinyl ligand (**19**) solution (Fig. 10). The immobilized ligand was then electropolymerized on the CNT-modified electrodes in dry acetonitrile. Next, the modified electrode was incubated in a solution of MeCN containing the precursor complex $[Fe^{II}(L_1)_2S_2]^{2+}$ (**18**), followed by rinsing the electrode to remove unbound materials. The asymmetric mixed ligand complex (**20**) was immobilized onto modified CNTs *via* π-stacking involving pyrene fragments. Additionally, biotin moieties enabled the specific anchoring of biotinylated proteins through avidin–biotin interactions. In terms of that, a particular enzyme, biotinylated glucose oxidase (B-GO_x), was utilized to assess the effective attachment of a protein onto the CNT through the activity of the enzyme. Next, the immobilized mixed ligand Fe complex was compared to its counterpart, just without nanotubes. The amounts of immobilized B-GO_x were 4 times higher on the CNT modified electrode, this highlights the prominent role of CNTs in enhancing surface properties. Indeed, the efficiency of the complex is evidenced by the remarkable stability and reproducibility of electrode performance under physiological conditions, highlighting its potential as a promising candidate for future bioanalytical applications.

In 2013, Dichtel and his co-workers synthesized a series of immobilized tripodal compounds involving two kinds of pyrene-tagged ferrocene tripods, **25a** and **25b**, on single layer graphene (SLG), demonstrating higher kinetic stability in comparison with monovalent binding groups (Fig. 11).[38] These tripods feature varying numbers of methylene spacers and involve multiple synthetic steps. In order to obtain bromophenyl(tris-4-methoxyphenyl)propyne (**22**), iodo-4-bromobenzene, CuI, and $Pd(PPh_3)_2Cl_2$ were added to **21**, followed by the addition of degassed anhydrous THF and trimethylamine under an inert atmosphere. Afterward, to prepare red solid **23**, compound **22** was dissolved in anhydrous CH_2Cl_2, and then a solution of BBr_3 in CH_2Cl_2 was added slowly. In the next step, the

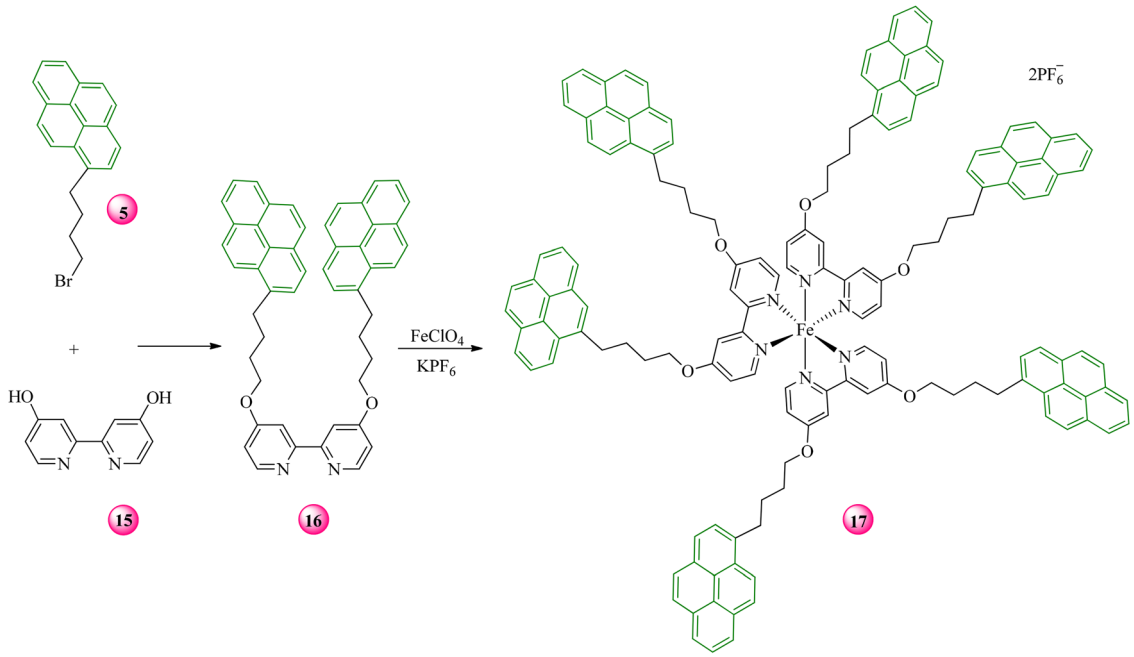

Fig. 8 The synthesis of the pyrene-tagged complex **17**. Reproduced with permission from ref. 36 copyright 2011, John Wiley and Sons.

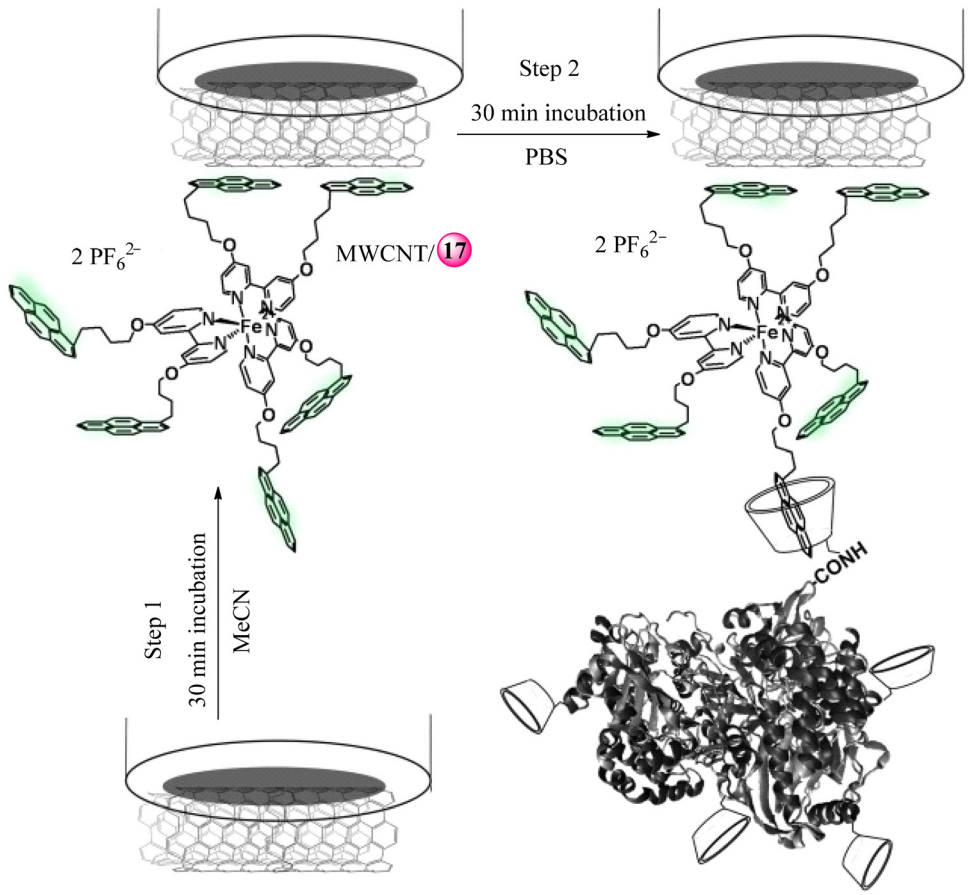

Fig. 9 The development of the glucose biosensor takes place in two steps: the supramolecular assembly of **17** with MWCNTs and β-cyclodextrin-GO_x. Reproduced with permission from ref. 36 copyright 2011, John Wiley and Sons.

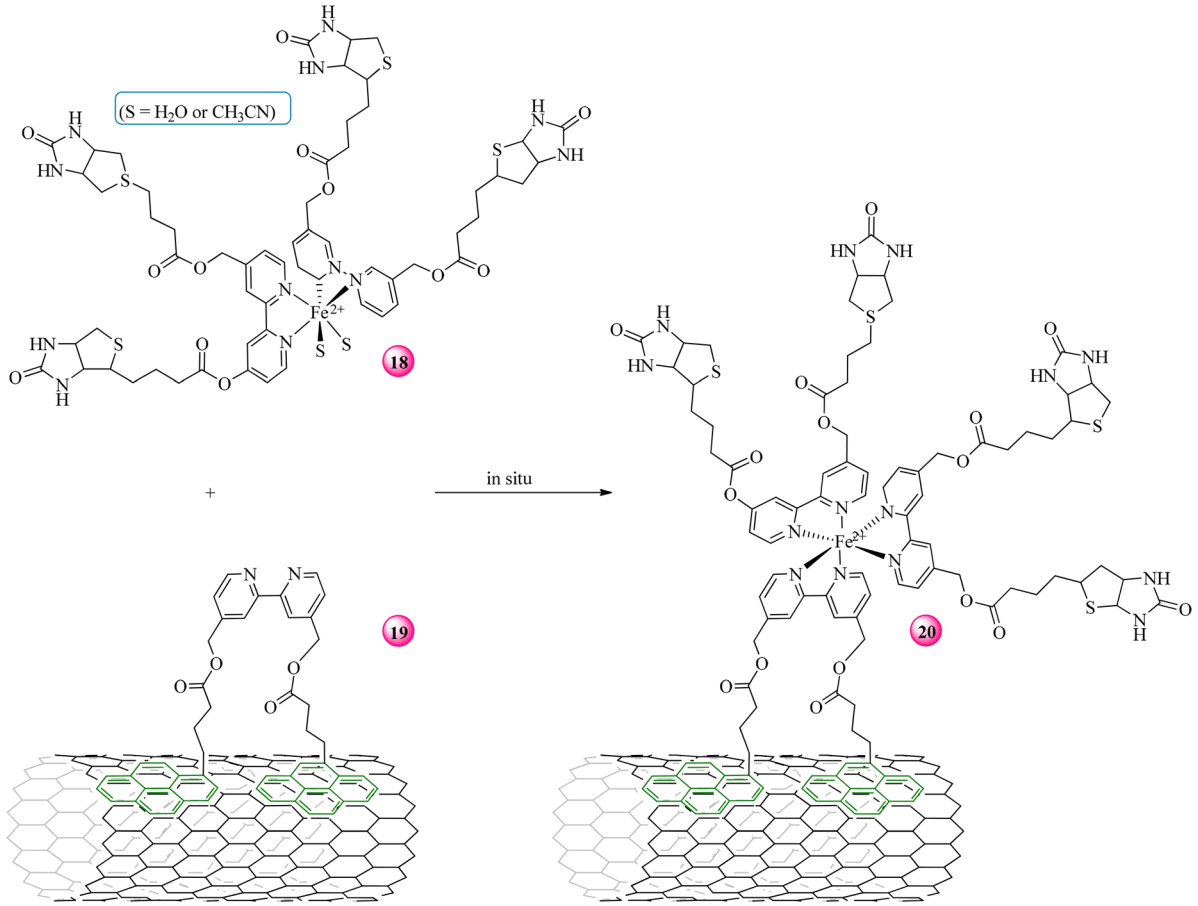

Fig. 10 The synthesis procedure involved the mixed ligand pyrene-tagged iron complex **20**. Reproduced with permission from ref. 37 copyright 2012, Royal Society of Chemistry.

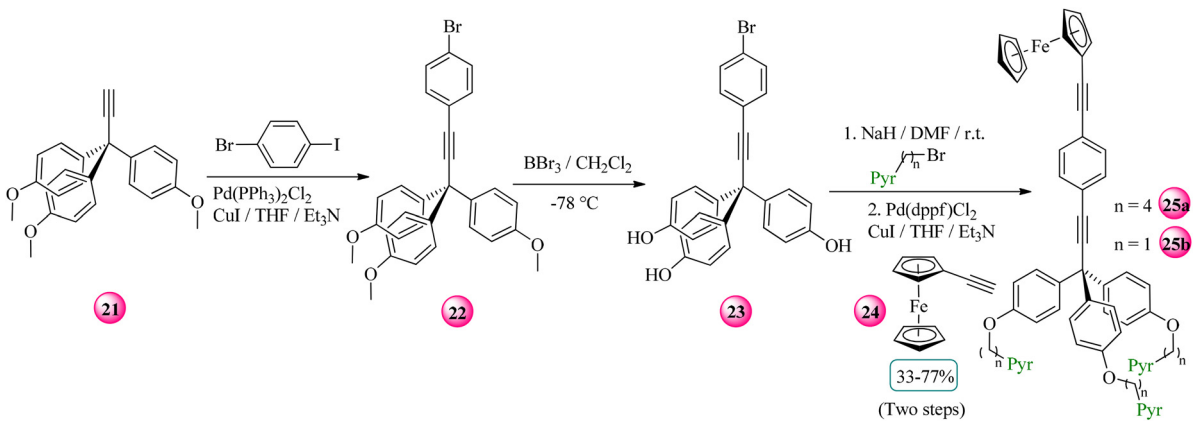

Fig. 11 The synthesis of **25a** and **25b** complexes. Reproduced with permission from ref. 38 copyright 2013, American Chemical Society.

varied number of methylene spacers led to either a 4-bromophenyl butylpyrene tripod or a 4-bromophenyl methylpyrene tripod. On the other hand, to synthesize ferrocene tripod **25a**, the 4-bromophenyl butylpyrene tripod, ethynylferrocene, CuI, and Pd(dppf)Cl_2 were charged into a flame-dried flask under an N_2 atmosphere, followed by the addition of anhydrous THF and trimethylamine. Subsequently, several work-up steps led to the final product. Similarly, for ferrocene tripod **25b**, the 4-bromophenyl methylpyrene tripod, ethynyl ferrocene, CuI, and Pd(dppf)Cl_2 were used under the same conditions. The assessment of tripods with different anchor sizes indicated a logarithmic link between the anchor area and the desorption rate, as well as a linear relationship between packing density and anchor size. Additionally, similar desorption rates for **25a** and **25b** (1.1×10^{-4} and 2.5×10^{-4} s^{-1}, respectively) suggested that convenient syntheses are much preferable to binding features. Notably, both **25a** and **25b** complexes, which show electrochemical

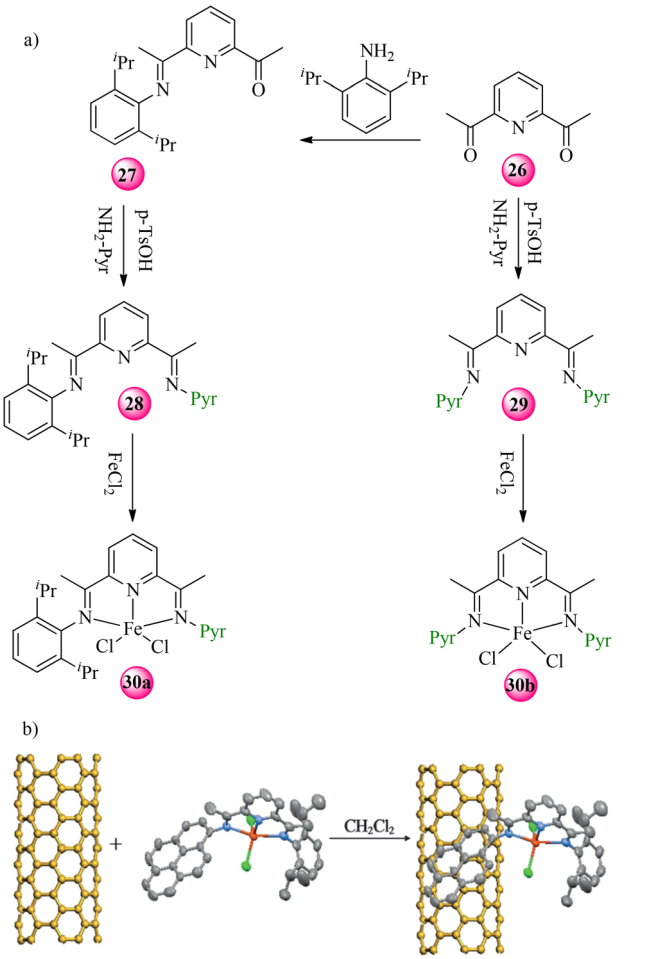

Fig. 12 (a) Synthetic procedure of **30a** and **30b**, (b) schematic representation of **30a** immobilization onto MWCNTs. Reproduced with permission from ref. 39 copyright 2014, John Wiley and Sons.

reversibility, desorb more rapidly than complex **141** (see Fig. 43). This behavior can be attributed to their increased solubility, enhancing the favorable interactions between the solvent molecules and the ferrocene-based complexes. Based on these findings, the use of larger feet (anchor) might be required to improve monolayer stability. This property is influenced by the nature of the headgroup and the solvent, which can be beneficial for particular applications.

In 2014, Sun, Durand, and co-workers utilized pyrene-tagged Fe precatalysts immobilized on CNTs by π-stacking for ethylene polymerization.[39] The Fe complexes (**30a** and **30b**) were synthesized by reacting $FeCl_2$ with 2-[1-(2,6-diisopropylphenylimino)-ethyl]-6-[1-(pyren-1-ylimino)ethyl]pyridine (**28**) and 2,6-bis[1-(pyren-1-ylimino)ethyl]pyridine (**29**) in THF at ambient temperature, respectively (Fig. 12). The formed solid was filtered, rinsed with diethyl ether, and dried under reduced pressure. In order to immobilize them, CH_2Cl_2 was added to the mixture of **30a** or **30b** and MWCNTs under a N_2 atmosphere. The immobilization of **30a** and **30b** was achieved after several consecutive steps, which included stirring the resulting suspension, filtration, washing the black powder with toluene, and finally drying under vacuum.

In order to evaluate the efficiency of these heterogeneous catalysts, they were tested in the presence of modified methyl aluminoxane (MMAO) as an activator in the ethylene polymerization (PE) reaction. According to the result, the MWCNT-**30a** system with different molar ratios of Al/Fe indicated a narrower molecular polydispersity with appropriate molecular weights (M_w) in comparison with their homogeneous analogues. Nonetheless, the activity of MWCNT-**30b** was not as high as its equivalent homogeneous counterpart, which can be attributed to the steric hindrance effect on the Fe center through the two pyrene fragments existing in the structure of **30b**. Besides, the impact of temperature on the reaction was also examined, which surprisingly demonstrated that higher temperatures led to lower catalytic activity. It can be deduced that weak π–π interactions of MWCNTs prevent them from stabilizing the active species at high temperatures. It is noteworthy that the M_w and polydispersity values of PE achieved by utilizing MWCNT-**30b** showed a moderate decrease at higher reaction temperatures due to the presence of one more pyrene group that exists to interact with the MWCNTs, in contrast to the trend found for MWCNT-**30a**. Generally, the heterogeneous precatalysts indicated better activity in the polymerization of ethylene by surface-initiated processes, producing well-dispersed MWCNTs into PE matrices.

In 2016, Robert and co-workers presented a non-covalent approach to attach a pyrene-appended iron triphenylporphyrin, containing six hydroxyl substituents at the *ortho* and *ortho*' positions of the phenyl rings (CAT_{Pyr}), to CNTs *via* π-stacking interactions.[40] In order to synthesize the CAT_{Pyr} complex (**36**), the pyrene-tagged porphyrin ligand (**35**), 5,10,15-tris(2,6-hydroxyphenyl)-20-(3-(pyren-1-yl)propyl)porphyrin, was dissolved in methanol and degassed under argon (Fig. 13). In the next step, $FeBr_2$ and 2,6-lutidine were added to this solution and were stirred at 60 °C. Subsequently, it was diluted with ethyl acetate and treated with HCl, resulting in a new catalyst, CAT_{Pyr}, which has the potential to be immobilized onto CNTs. The CAT_{Pyr} exhibited excellent catalytic activity for the reduction of CO_2 in water (pH = 7), demonstrating high selectivity, durability, and reaction rate. Based on the data from CV analysis, it has been revealed that the remarkable catalytic activities of iron complexes can be effectively maintained under heterogenized conditions in water, which exhibited a substantial current increase when exposed to a CO_2 atmosphere at specific potentials. In terms of porphyrin molecules, immobilization is a suitable method that keeps the surface of immobilized CAT_{Pyr} active during extended electrolysis with notable catalytic selectivity, generally maintaining high catalytic properties. Additionally, the authors declared that the efficiency associated with the catalytic system can be further improved by optimization of the CAT_{Pyr}/MWCNT ratio.

For non-covalent attachment of pyrene-tagged molecules onto the solid supports lacking inherent delocalized π-systems, pre-modification is inevitable. In this regard, the development of chemically modified electrodes with molecular selectivity depends on the surface integration of these molecules. Innovative procedures have been established, which involve the covalent attachment of pyrene molecules onto the surfaces, followed by

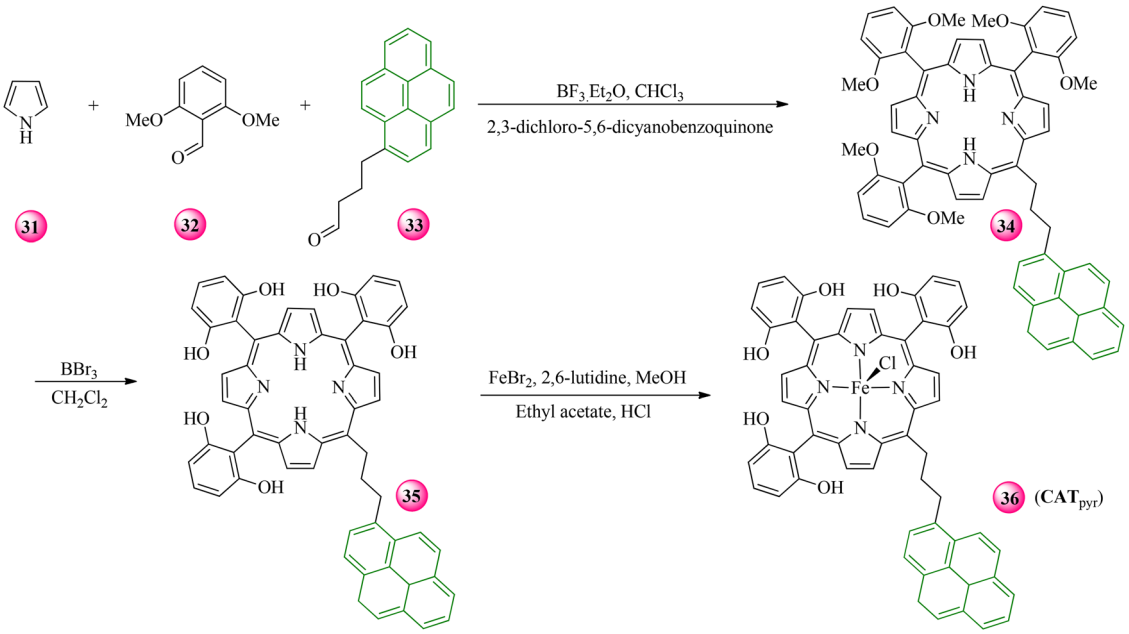

Fig. 13 The synthetic procedure for complex CAT_{Pyr}. Reproduced with permission from ref. 40 copyright 2016, American Chemical Society.

the non-covalent physisorption of pyrene-tagged complexes possessing redox properties (Fig. 14). This approach could be beneficial in various fields, such as energy systems, chemical sensing, electrochromic materials, and molecular electronics.[16,17]

In 2016, Yang and co-workers reported the non-covalent immobilization of a redox-active 1-pyrenylferrocene complex on the gold surface modified with *S*-(pyren-1-ylmethyl) ethanethioate (**37**) (Fig. 15).[16] Since organic thioacetate exhibited greater stability and resistance to oxidation than thiols, it could be isolated and purified more easily. Prior to surface attachment, the thioacetate protecting group was removed *in situ* using a base. Additionally, the pyrene-modified ferrocene derivative was synthesized through palladium-catalyzed cross-coupling reactions. In the following step, pyrene-tagged ferrocene was immobilized on the pre-functionalized gold electrode (**38**) through π-stacking *via* physisorption from the solution to prepare **39**. The pyrene-modified ferrocene provides well-defined redox-active tools for monitoring physisorption and electron transport at the interface. According to the electrochemical experiments, electron transfer along this interface was straightforward, allowing the ferrocene redox pair to behave in an ideal reversible way.

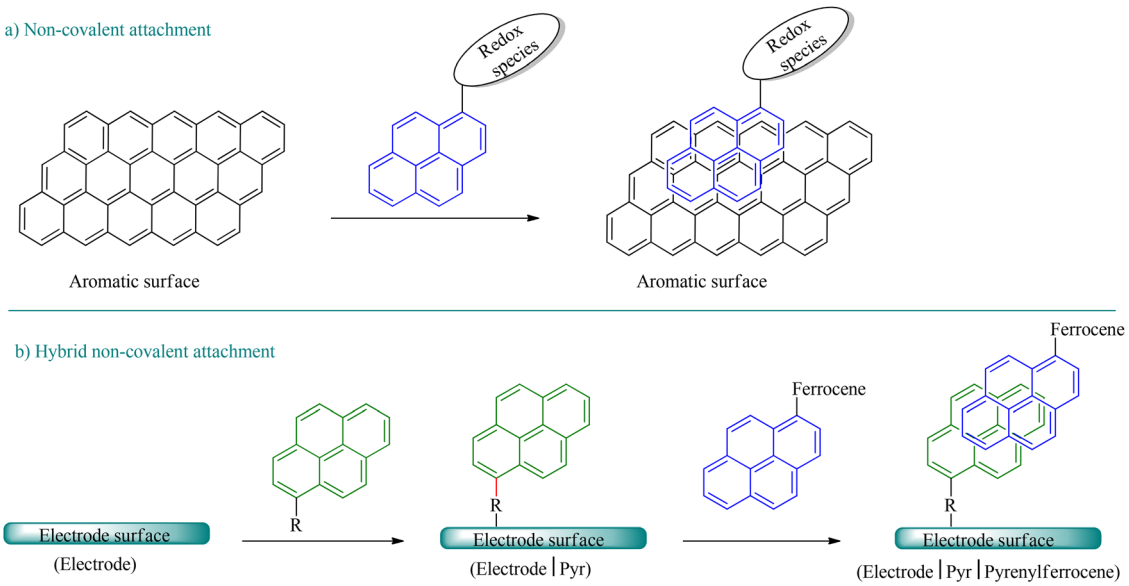

Fig. 14 An overview of (a) the non-covalent attachment method for molecular attachment to the electrode surface and (b) the procedure for hybrid non-covalent attachment. Reproduced with permission from ref. 17 copyright 2018, American Chemical Society.

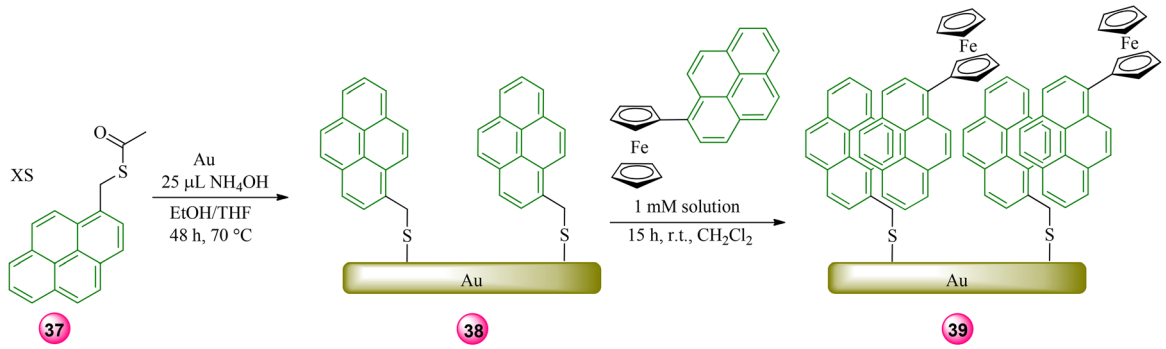

Fig. 15 The modification of gold electrodes through π–π interactions. Reproduced with permission from ref. 16 copyright 2016, Royal Society of Chemistry.

In 2018, Yang and co-workers developed hybrid noncovalent immobilization through the attachment of 1-pyrenylferrocene to indium tin oxide (ITO) electrodes modified with pyrene.[17] In this regard, ferrocene was chosen for its ideal redox properties, inertness, and facile functionalization, making it possible to compare the interfacial properties of both covalent and hybrid non-covalent approaches (Fig. 14). To compare the electron-transfer kinetics for covalent systems, vinylferrocene was directly attached to an ITO electrode (ITO|vinylferrocene). While in noncovalent immobilization, a cleaned ITO electrode was first functionalized by 1-vinylpyrene in anhydrous toluene, which led to the covalent attachment of pyrene to the ITO surface (ITO|Pyr). In the next step, ITO|Pyr samples were immersed in a 1-pyrenylferrocene solution for immobilization of the complex onto the modified ITO *via* pyrene–pyrene interactions, yielding ITO|Pyr|pyrenylferrocene (Fig. 16). The results showed that the transfer of electrons by the pyrene–pyrene interface has comparable kinetics (ten times faster) to analogous covalently attached systems. Studies indicate that several factors, such as the electrode/redox-active species distance, the extent of π-conjugation of the linker, and, in this case, the monolayer formation or the possibility of vinyl group polymerization, can influence the electron transfer kinetics. This hybrid approach successfully proposed a practical electron transfer system by utilizing non-covalent interactions.

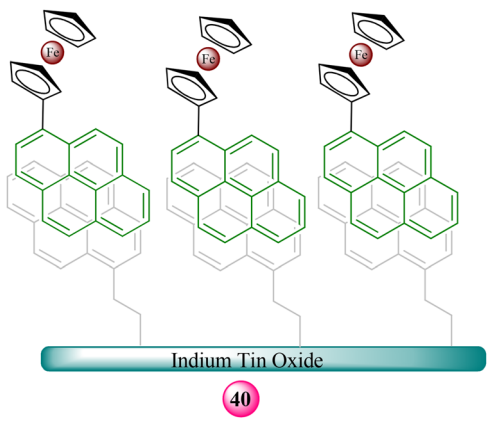

Fig. 16 The immobilization of the 1-pyrenylferrocene complex onto modified ITO (**40**). Reproduced with permission from ref. 17 copyright 2018, American Chemical Society.

4.5. Pyrene-tagged ruthenium complexes

In 2009, Wang and co-workers used a novel approach to control the immobilization and recycling of pyrene-tagged ruthenium complexes through the use of suitable solvents and temperature.[13] To synthesize an olefin metathesis catalyst bearing pyrene moieties, compounds **41**, (*E*)-(4-isopropoxy-3-(prop-1-enyl)phenyl)-methanol, and **42**, 4-(pyren-1-yl)butanoic acid, underwent a reaction to yield pyrene-tagged compound **43** (Fig. 17a). The pre-ligand (**43**) was further transformed into the corresponding ruthenium complex (**45**). Then, a typical experiment was carried out to noncovalently immobilize **45** onto SWCNTs using CH_2Cl_2 (Fig. 17b). This technique enables reversible immobilization and conducts faster metathesis reactions in homogeneous solution than the other reported solid-supported catalysts. In this regard, various representative ring-closing metathesis (RCM) reactions were performed to assess the efficiency of SWCNT-supported **45**. According to the obtained data, acetone can be employed as the solvent, and temperature can be controlled between 0 and 35 °C to enable the catalyst, immobilized onto SWCNTs, to be reused and recycled six/seven times for numerous di- or trisubstituted substrate dienes, even at low levels of catalyst loading (1.5 mol% Ru). Another benefit of this approach was the simple recovery of the immobilized catalyst in homogeneous solutions through filtration of the cooled-down mixture, which is more convenient than that for similar catalysts supported on soluble polymers. Recovery of SWCNTs from the deactivated heterogeneous catalyst was efficiently performed using CH_2Cl_2 or THF (about 98%). The results demonstrated that the π–π interaction between SWCNTs and pyrene fragments is reversible and depends on temperature and the polarity of the solvents.

In 2020, Ouali and co-workers reported active and recyclable pyrene-tagged terpyridine-based Ru catalysts immobilized onto the surface of cobalt magnetic nanoparticles (MNPs) supported by graphene for nitroarene transfer hydrogenation processes.[41] The proposed system relies on the arrangement of pyrene-tagged terpyridine ligands. Terpyridine ligands come in two variations: monomeric (one terpyridine per one pyrene) and multivalent (five terpyridines per one pyrene), Fig. 18.

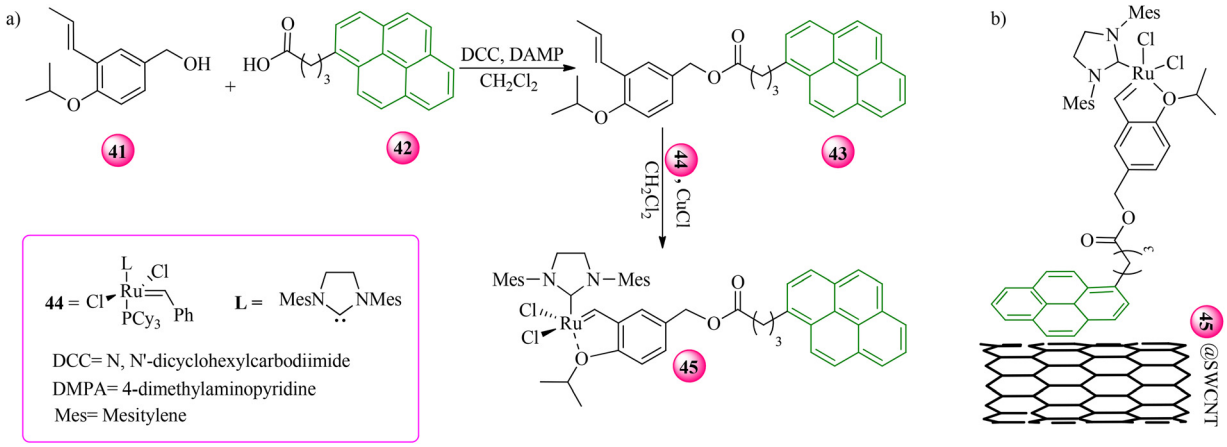

Fig. 17 The scheme of (a) the synthesis procedure for the pyrene-tagged ruthenium complex (**45**) and (b) immobilization of (**45**) on the SWCNT surface. Reproduced with permission from ref. 13 copyright 2009, American Chemical Society.

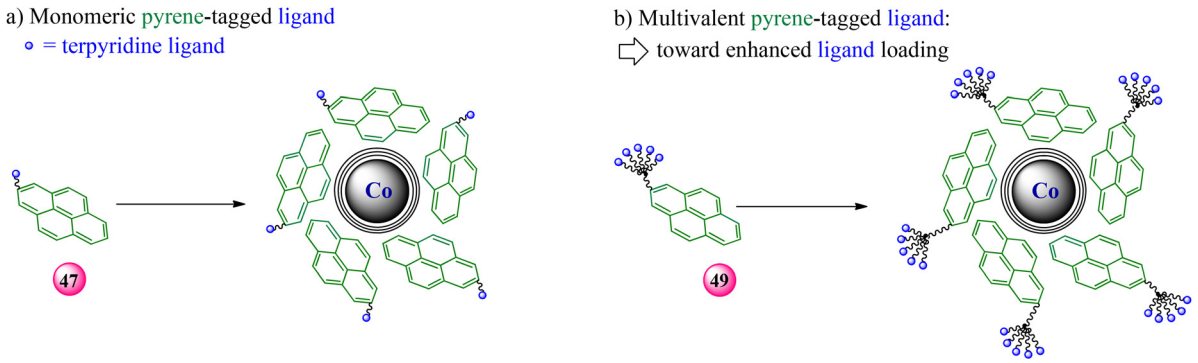

Fig. 18 Pyrene-tagged ligands with specific design, utilizing (a) a single terpyridine ligand (**47**) and (b) five terpyridine ligands (**49**), along with their corresponding anticipated hybrid MNPs. Reproduced with permission from ref. 41 copyright 2020, American Chemical Society.

The pyrene bearing one terpyridine moiety (**47**) was obtained through the coupling of 1-pyrenebutyric acid (**42**) and amine **46** (Fig. 19). Furthermore, a multi-valent ligand named **49**, containing five terpyridines, was synthesized *via* the reductive amination of an aldehyde-decorated dendron with amine **46**. They found that the formation and disruption of non-covalent interactions between **47** or **49** and MNPs are temperature-dependent. Therefore, the catalyst can leave the support at a higher temperature, where catalytic processes can occur, and rejoin it at a lower temperature for subsequent recovery *via* a magnet. It has been found that the multivalent ligand acted effectively in nitrobenzene transfer hydrogenation since it was

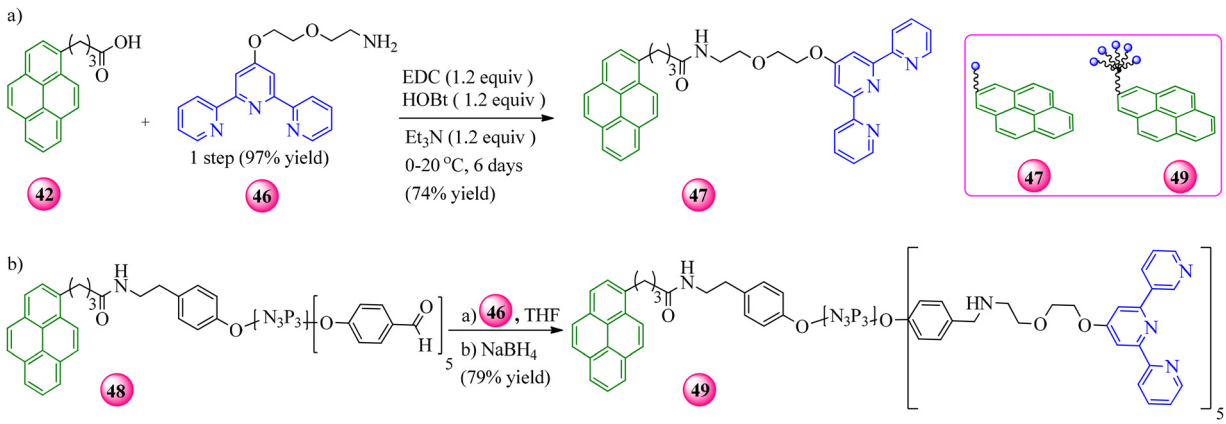

Fig. 19 A synthetic pathway for synthesis of the pyrene-tagged ligands, incorporating (a) one (**47**) or five terpyridine (**49**) moieties. Reproduced with permission from ref. 41 copyright 2020, American Chemical Society.

reused eight times without losing activity compared to six runs with monovalent terpyridine. Notably, the decreased loading aligns with an increase in the size of the ligand, probably due to steric hindrance at the π-stacking interface. In this study, the pyrene-tagged loading per gram of MNPs was remarkably lower than that of similar phosphine ligands containing one or five phosphines.[42] Such behavior could be attributed to the solvent medium, in this case, the absence of water, which is known to facilitate stronger stacking. This report was the first nonaqueous study of pyrene reversible interactions with Co/C MNP surfaces and opened up new prospects for their use as supports for different organic reactions.

Water oxidation is a crucial process to take advantage of the artificial photosynthesis procedure, converting solar energy into renewable fuel. In this regard, in 2011, Li, Sun, and their co-workers found a synthesis procedure for a pyrene-tagged Ru complex and immobilized it onto MWCNTs, coated onto an ITO glass electrode, as an optimal surface for catalyst loading and a medium that facilitates rapid electron and hole transfer to achieve efficient water oxidation.[43] On the one hand, the ITO electrode modified with MWCNTs was produced through the electrophoretic deposition of acid-treated MWCNTs onto ITO glass. On the other hand, in order to synthesize Ru(bpa)(Pyr–Py)$_2$ (**55**) (H_2bpa = 2,2′-bipyridine-6,6′-dicarboxylic acid and Pyr–Py = 4-(pyren-1-yl)-*N*-(pyridine-4-ylmethyl)butanamide) the pyridine-bearing pyrene (Pyr–Py) ligand was first prepared by the reaction of pyrenebutyric acid and aminomethylpyridine, which was then refluxed with the solvent-ligated complex Ru(bpa)(DMSO)$_2$ to provide complex **55** (Fig. 20). Afterward, the catalyst was immobilized by immersing the MWCNT-modified electrode in a methanol solution of complex **55** overnight. In order to evaluate the electronic behavior of **55** on the MWCNT-modified electrode, cyclic voltammetry was employed. It was confirmed that **55** is a highly effective catalyst for water oxidation, demonstrating a high water oxidation wave and two quasi-reversible redox couples of Ru^{II}/Ru^{III} and Ru^{III}/Ru^{IV}. Meanwhile, its homogeneous counterpart showed just a pair of CV waves belonging to Ru^{II}/Ru^{III}. In contrast, bare ITO or ITO electrodes coated by MWCNTs were not active in the same measurement range. Indeed, further investigation with a constant potential revealed that the counter and working electrodes released hydrogen and oxygen bubbles immediately, respectively, along with a sustained current. In contrast, the MWCNTs/ITO electrode lacking the catalyst remained essentially inert under the same conditions. Moreover, these features enable the complex **55** to be significantly efficient for water oxidation at a relatively low applied potential in neutral, non-buffered aqueous solutions.

In 2011, Ma and co-workers reported a series of immobilized bi(2,2′-bipyridyl)-pyrene ruthenium(II) complexes onto graphene sheets (B–Ru–P/GS nanohybrid) through a straightforward π-stacking self-assembly method for applications in electrochemiluminescence and photo sensing.[44] In order to synthesize B–Ru–P (**61**), initially, a mixture of 4-(pyren-1-yl)butanoic acid (**42**) and 4-(2-hydroxyethoxy)benzaldehyde (**56**) was reacted in

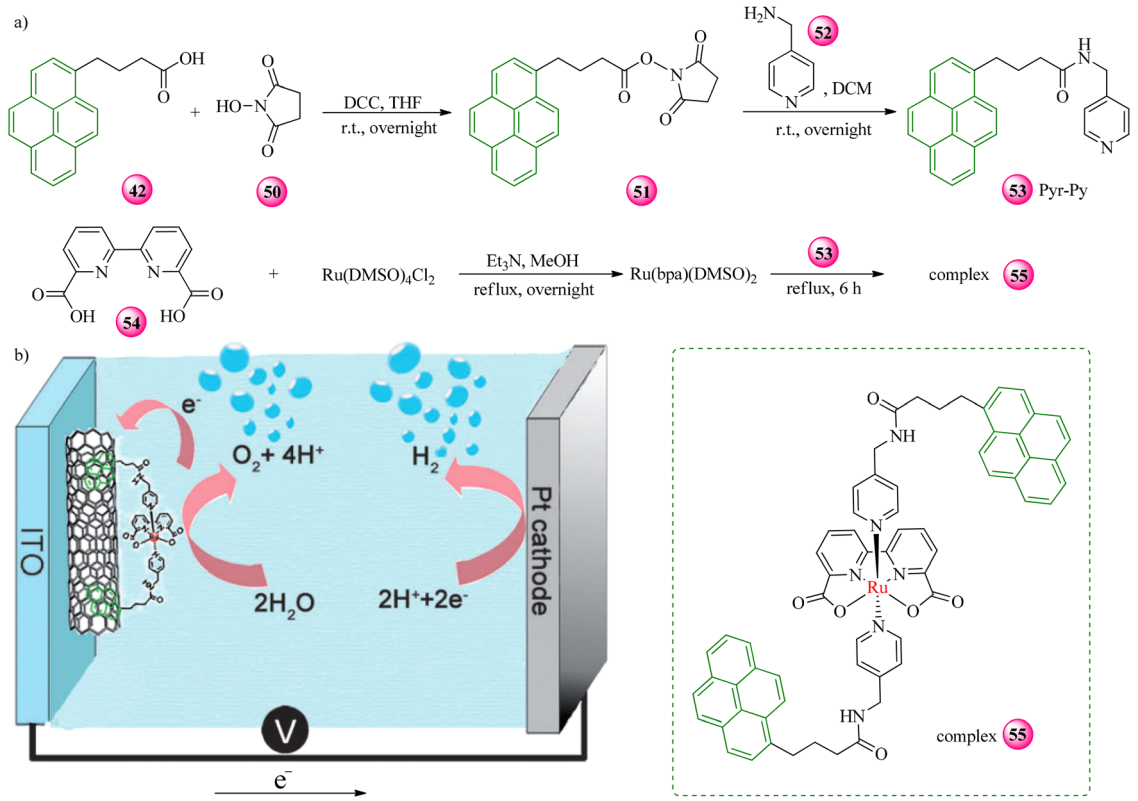

Fig. 20 Schematic representation of: (a) the synthesis procedure for complex **55** and (b) an electrochemical cell for water splitting, and structure of the molecular catalyst **55**. Reproduced with permission from ref. 43 copyright 2011, John Wiley and Sons.

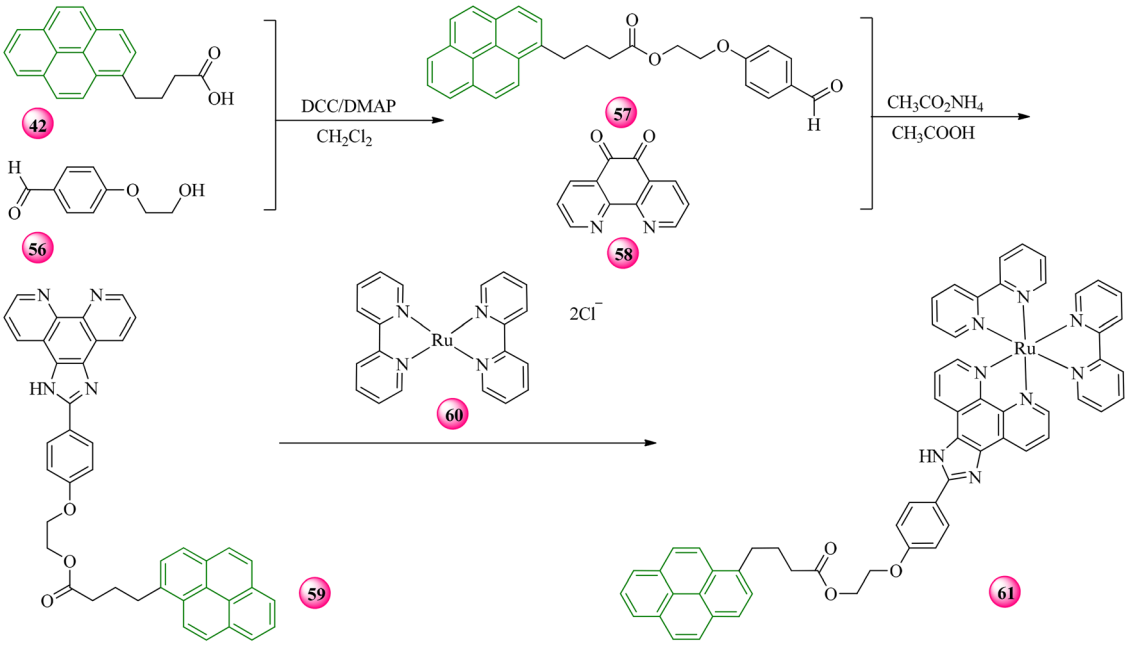

Fig. 21 Schematic of the synthesis of Ru(II) complexes. Reproduced with permission from ref. 44 copyright 2011, Elsevier.

the presence of *N*,*N*′-dicyclohexylcarbodiimide (DCC) and 4-dimethylaminopyridine (DMAP) in CH_2Cl_2, which resulted in **57**, and stirred under an argon atmosphere (Fig. 21). Then, **57**, 1,10-phenanthroline-5,6-dione (**58**), and ammonium acetate were dissolved in hot glacial acetic acid, leading to a pyrene-tagged phenanthroline ligand (**59**). Following this, compound **59** and $[Ru(bpy)_2Cl_2]\cdot 2H_2O$ (**60**) were sonicated in absolute ethanol, degassed with argon, and refluxed. After cooling, a saturated $NaClO_4$ solution was added, resulting in a reddish solid that was filtered, washed, and dried to yield the final product (**61**). In the next step, to prepare the B–Ru–P/GS nanohybrid, GSs were combined with **61** in anhydrous DMF. The mixture was centrifuged to eliminate excess compound and subsequently washed with DMF, deionized water, and ethanol before being dried under a vacuum. To evaluate catalyst efficiency, the stability of the B–Ru–P/GS nanohybrid and its interaction with ruthenium(II) complexes were analyzed using fluorescence emission spectra. The I_D/I_G ratios of the GSs and the B–Ru–P/GS nanohybrid were 0.25 and 0.28, respectively, reflecting the increasing trend and confirming the presence of donor molecules on graphene. Additionally, the electrochemiluminescent (ECL) sensor with photoinduced electron transfer properties was examined to assess potential applications in electrochemiluminescence and as a photosensor. Based on the obtained data, the analysis of the B–Ru–P/GS nanohybrid demonstrated successful immobilization of ruthenium(II) complexes on graphene sheets, confirmed by increased thickness in atomic force microscopy (AFM) measurements and distinct fluorescence emissions that confirmed strong π-stacking interactions. Electrochemical studies revealed significantly enhanced electron transfer capabilities, with a peak current much higher than that of the Ru(II) complexes alone. The efficient quenching of fluorescence indicated effective stacking of the Ru(II) complexes on the GSs. On the other hand, the B–Ru–P/GS nanohybrid exhibited a higher photocurrent response, attributed to enhanced charge carrier generation and multi-step vectorial photoinduced electron transfer. Furthermore, the porosity of the anode structure increases light scattering and promotes rapid electron transport, making it a promising candidate for optoelectronic applications.

In 2012, Ding, Cosnier, and their co-workers successfully immobilized a pyrene-functionalized bipyridine complex of Ru onto the SWCNTs' sidewalls thanks to π-stacking interactions.[45] To synthesize [(2,2′-bipyridyl)$_2$(4,4′-bis(4-pyrenyl-1-ylbutyloxy)-2,2′-bipyridyl]ruthenium(II) hexafluorophosphate (**62**), 4,4′-bis(4-pyrenyl-1-ylbutyloxy)-2,2′-bipyridine was first prepared by refluxing 4,4′-bishydroxy-2,2′-bipyridine with 1-(4-bromobutyl)pyrene and K_2CO_3 (Fig. 22). The resulting ligand was then refluxed with $[Ru(bpy)_2Cl_2]$ in DMF under argon. Following solvent removal, H_2O was introduced into the mixture, which was subsequently washed with CH_2Cl_2. Ammonium hexafluorophosphate was then introduced, and the product was extracted with CH_2Cl_2. In order to functionalize SWCNTs with complex **62** (pyrene–Ru/SWCNTs) through noncovalent π–π interactions, SWCNTs and complex **62** were mixed in THF, and subsequent work-up, including sonication and centrifugation, was performed. Finally, the pyrene–Ru/SWCNT-modified Pt electrode was produced by drop-casting this solution onto the Pt electrode, drying it in a desiccator, and storing it in the dark. To enhance a stable electrochemical signal, pyrene–Ru/SWCNT/Pt electrodes underwent pre-oxidation for further experiments. The effective immobilization of **62** on SWCNTs/Pt was indicated by two reversible peak systems in the 0–1.2 V range, reflecting stable electrochemical behavior and nearly zero peak potential separation at slow scan rates, confirming the attachment of the complex. Additionally, the stability of the electrochemical $Ru^{II/III}$ signal, with only a 5% decrease in peak currents after 200 cycles, confirmed the robustness of the

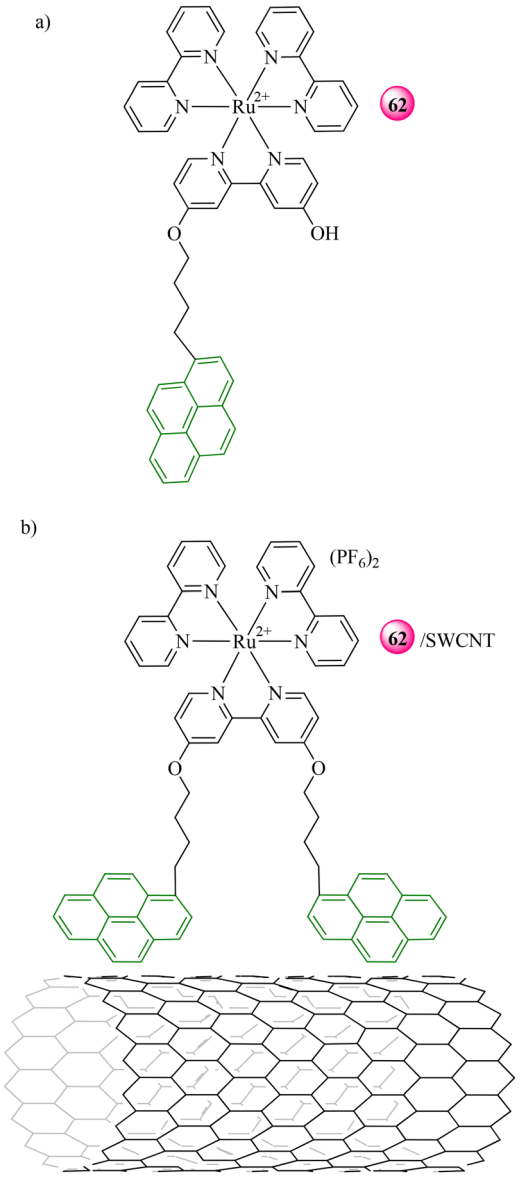

Fig. 22 Schematic representation of: (a) pyrene–Ru, **62** and (b) pyrene–Ru/SWCNTs. Reproduced with permission from ref. 45 copyright 2012, John Wiley and Sons.

functionalization. Moreover, the electrogenerated chemiluminescence (ECL) performance was also investigated in both organic (tripropylamine) and aqueous systems (using oxalate as a co-reactant). Based on the obtained results, the pyrene–Ru/SWCNT composite demonstrated effective oxidative-reductive ECL behavior, making it a suitable candidate for the utilization of solid-state ECL applications across different solutions.

In 2014, Mata, Peris, and co-workers synthesized an imidazole-based (NHC) ruthenium complex immobilized onto the rGO surface (Fig. 23).[5] NHC-based complexes are considered suitable catalysts due to the σ-donor character of NHC ligands and their high stability even under harsh conditions. In the first step, the imidazolium salt (**65**) was synthesized by the reaction of 1-(bromomethyl)-pyrene (**63**) and methylimidazole (**64**). Subsequently, imidazolium salt **65** was mixed with Ag_2O under light exclusion and refluxed in MeCN. Following this, $[RuCl_2(\eta^6\text{-}p\text{-cymene})]_2$ and KCl were introduced, and the resulting mixture was filtered. In the next step, the solvent was evaporated under reduced pressure, leading to the crude solid, which was then purified by column chromatography. The obtained ruthenium complex remained stable in the solid state and solution, even when exposed to air. The pyrene-tagged NHC–Ru complex (**67**) was then blended with sonicated rGO in dichloromethane (DCM) to form NHC–Ru–rGO (**69**). The decolorization of the solution color is the initial observation that the complexes have been immobilized. In order to evaluate the efficiency of **69**, several experiments on the oxidant-free dehydrogenation of alcohols were carried out, indicating that utilizing rGO as a support can significantly affect the progression of the reaction. Indeed, in the benzyl alcohol oxidation reaction, the supported catalyst exhibited higher activities than its homogeneous counterparts, and the heterogenized catalyst performed well in up to ten recycling cycles. According to the results, the Raman spectra of rGO revealed two noticeable peaks of D and G bands, and when NHC–Pd and NHC–Ru were incorporated, a slight upshift of the G band (lower defect density) was detected, which may be attributed to π–π stacking between the pyrene tag and the graphene surface. Notably, the surface area of the support is responsible for facilitating the interaction between the catalyst and the substrates, demonstrating that the larger the surface area, the higher the activity.

These researchers also employed π-stacking to immobilize the palladium and ruthenium complexes simultaneously with pyrene-tagged NHC ligands onto rGO, which results in a highly efficient and recyclable catalyst for hydrodefluorination (Fig. 24).[9] It is worth mentioning that the surface area of this co-immobilized catalyst increased from 164 to 221 $m^2\ g^{-1}$ after the catalyst's activation as a result of partial exfoliation. To prepare rGO–Ru–Pd, an equivalent molar mixture of metal complexes **67** and **68** and rGO were mixed in CH_2Cl_2, sonicated, and stirred, leading to a black solid, which was subsequently filtered and washed with CH_2Cl_2. A loss of color in the solution was the first sign of immobilization. After filtration and washing of the resulting product, rGO, along with the two catalysts, the filtrate was analyzed by ^1H NMR. The results demonstrate the absence of the corresponding signals for **67** or **68** in the spectrum of the filtrate, providing indirect evidence of the effective immobilization of the complexes onto the solid surface. The activity of the hybrid catalyst, rGO–Ru–Pd (**71**), was much higher than that shown by the Pd/rGO, verifying the crucial role of the synergistic effect of the two metals; indeed, Pd activates C–F bonds, and Ru enables hydrogen transfer. The hybrid catalyst has the potential to be reused over 12 times in the hydrodefluorination of fluorobenzene while maintaining its effectiveness and experiencing a minimal decrease in activity, which indicates that it has promising prospects for practical applications.

In 2014, Goff, Cosnier, and their co-worker reported the first instance of double functionalization of MWCNTs using a pyrene-tagged ruthenium molecular catalyst and a pyrene-tagged enzyme to accomplish an integrated electroenzymatic approach.[46] In order to synthesize the [(1,10-phenanthroline-5,6-dione)$_2$((4,4′-bis(4-pyrenyl-1-ylbutyloxy)-2,2′-bipyridine)Ru(II)] hexafluorophosphate

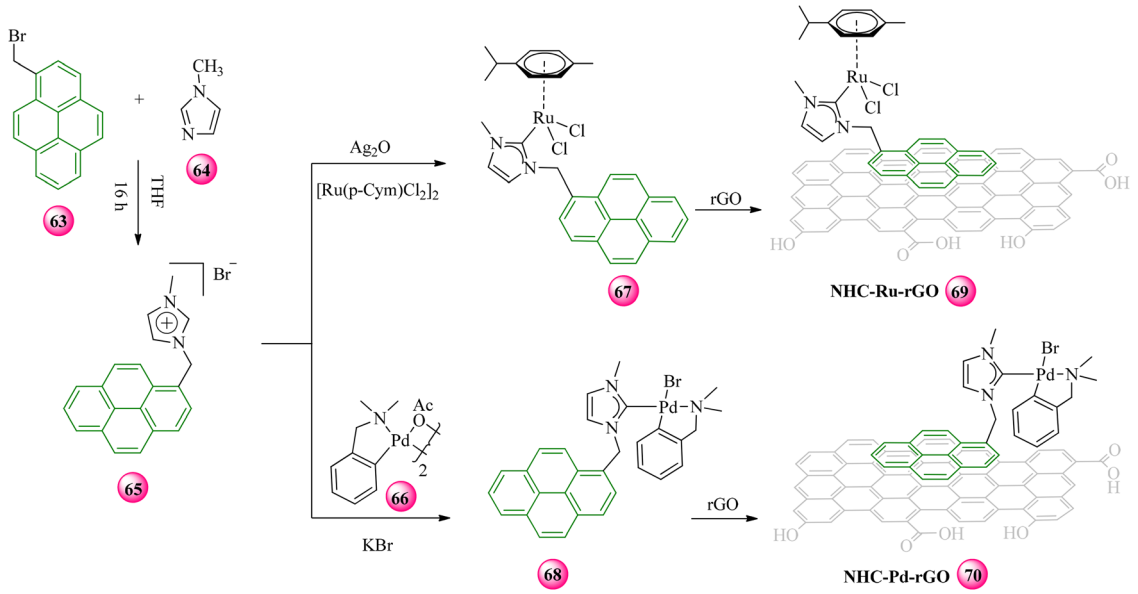

Fig. 23 Synthesis and immobilization of **67** and **68** complexes onto rGO. Reproduced with permission from ref. 5 copyright 2014, American Chemical Society.

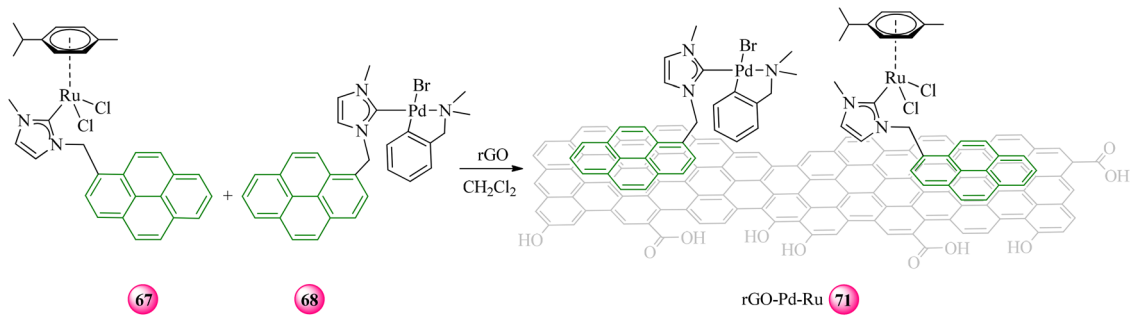

Fig. 24 Co-immobilization of pyrene-tagged palladium and ruthenium complexes bearing N-heterocyclic carbene ligands onto rGO. Reproduced with permission from ref. 9 copyright 2014, American Chemical Society.

complex (RuQ–pyrene) (**72a**), [Ru(1,10-phenanthroline-5,6-dione)$_2$-Cl$_2$] was refluxed with 4,4′-bis(4-pyrenyl-1-ylbutyloxy)-2,2′-bipyridine in ethylene glycol (Fig. 25). On the other hand, the modified MWCNT electrode was incubated in a RuQ–pyrene solution, followed by washing and characterization through CV analysis in a pure electrolyte. The electrode, in MeCN, exhibited the characteristic redox activity of immobilized RuQ–pyrene, along with non-reversible charge trapping peaks commonly seen in immobilized redox species. The formation of π–π stacking interactions between the pyrene fragments of the complex **72a** and the graphene layers of the MWCNT film enables physisorption on MWCNT electrodes. Indeed, the analysis of **72a**/MWCNTs revealed high maximum surface coverage, indicating effective functionalization. The electrodes achieved a maximum catalytic current of 2.5 mA cm^2 with NADH, demonstrating efficient electrocatalytic oxidation of NADH. Additionally, the electrochemical behavior of the RuQ–pyrene-functionalized electrodes remained stable over multiple scans, confirming good immobilization and stability of the Ru complex on the CNTs. On the

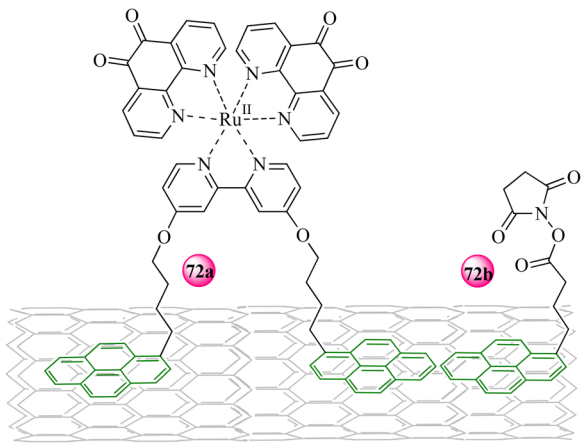

Fig. 25 Schematic representation of RuQ–pyrene (**72a**) and NHS–pyrene (**72b**) onto MWCNTs. Reproduced with permission from ref. 46 copyright 2014, Royal Society of Chemistry.

other hand, due to the straightforward self-assembly of pyrene molecules onto the sidewalls of MWCNT, researchers prepared doubly functionalized MWCNT electrodes using RuQ–pyrene (**72a**) and 1-pyrenebutyric acid *N*-hydroxysuccinimide ester (NHS–pyrene, **72b**), which performed well in glucose oxidation.

In 2015, Ozawa, Haga, and co-workers reported two new ruthenium complexes, one bearing two different groups, including two pyrene and four phosphonic acid moieties named a Janus-type complex (**75**), since it has double-faced properties, and the other one (**76**) possessing four pyrene fragments (Fig. 26).[47] Complex **75** was immobilized on HOPG (highly ordered pyrolytic graphite) *via* π–π interactions, leading to a hydrophilic surface with exposed phosphonic acid groups. In contrast, when the complex was attached directly to the ITO surface, it led to a hydrophobic surface with exposed pyrene groups (Fig. 27). In order to synthesize **75**, 2,6-bis(*N*-methylbenzimidazol-2-yl)-4-{3,5-bis[4-(1-pyrenyl)butyloxy]-phenyl}pyridine (**74**) was prepared by reacting a respective diol with 1-(4-bromobutyl)pyrene, which was then reacted with $[Ru(EtL)(CH_3CN)Cl_2]$ (for the EtL structure see Fig. 26) to form the complex $[Ru(EtL)(L1)](PF_6)_2$ (L1 = 74). Following this, deprotection of ethyl groups using trimethylsilyl bromide yielded **75**. Similarly, the symmetric complex $[Ru(L1)_2](PF_6)_2$ (**76**) was obtained by reacting $RuCl_3{\cdot}3H_2O$ with **74** in a DMF–glycerol mixture. Subsequently, both the ITO electrode and the HOPG were modified by immobilization through soaking in an aqueous DMF solution of **75**. Janus-type complex **75** served as a primer layer for developing the fabrication of advanced multilayers of redox-active Ru complexes on HOPG. The unbound phosphonic acid groups on the **75**-modified HOPG facilitated metal–phosphonate bonding. In this regard, the HOPG electrode was first soaked in a solution of **75** involving an aqueous DMF for several hours, rinsed thoroughly with ultrapure water, and then dipped in an aqueous solution of $ZrOCl_2$, followed by another rinse and re-immersion in the **75** solution (Fig. 27). On the other hand, to prepare layer-by-layer (LbL) films of Ru complexes separated by graphene, the **75**-modified ITO electrode was utilized. The LbL multilayer film, consisting of **75**, **76**, and graphene, was formed by first spin-coating a graphene suspension onto the **75**-modified ITO electrode and drying it in the flow of N_2. Subsequently, the graphene-modified electrode was soaked in a solution of DMF involving **76** and dried before being treated again with the graphene suspension through spin-coating. Several observations were made

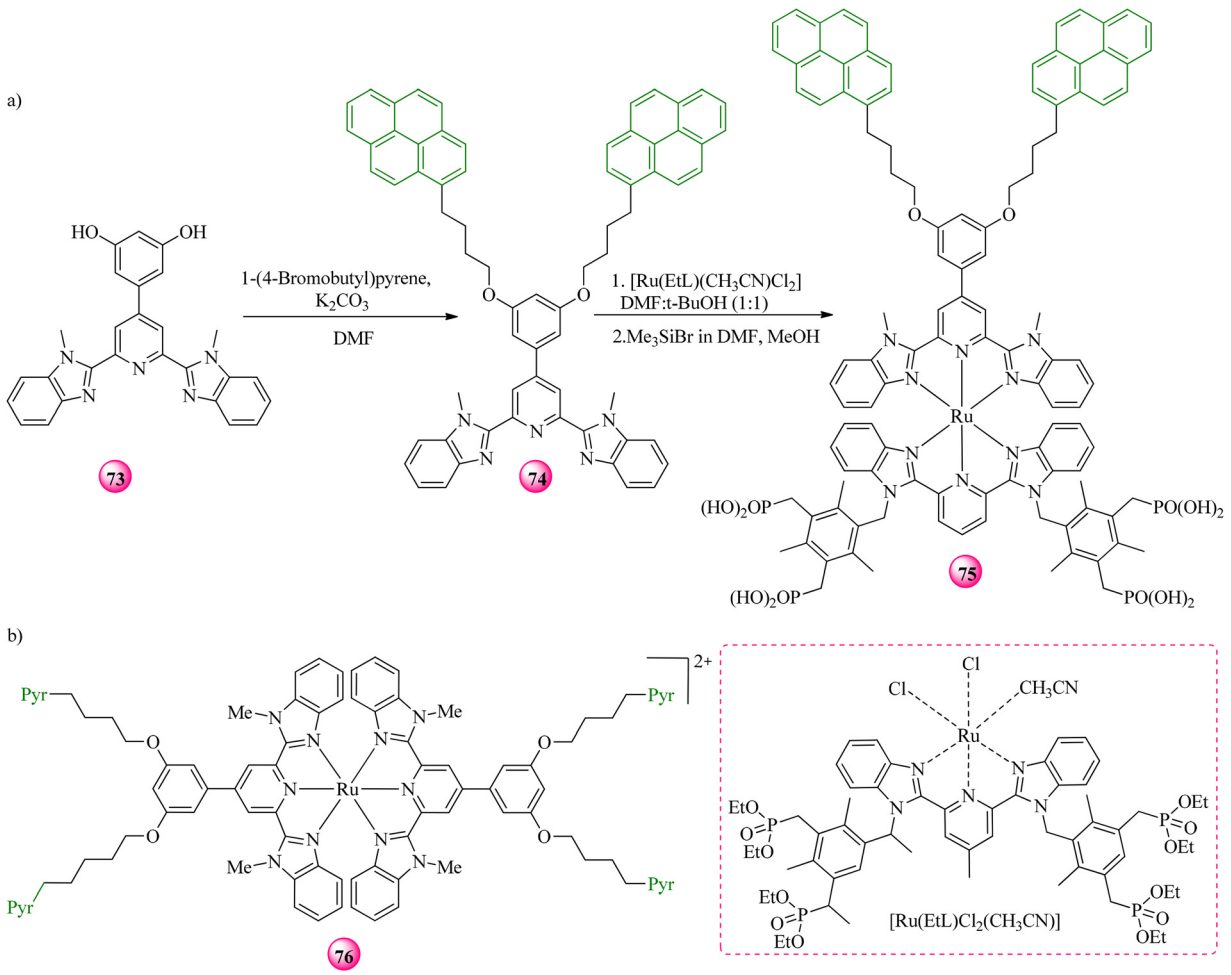

Fig. 26 The scheme of (a) the synthetic route of ligand **74** and Ru-**75** complex and (b) complex **76**. Reproduced with permission from ref. 47 copyright 2015, Chemical Society of Japan.

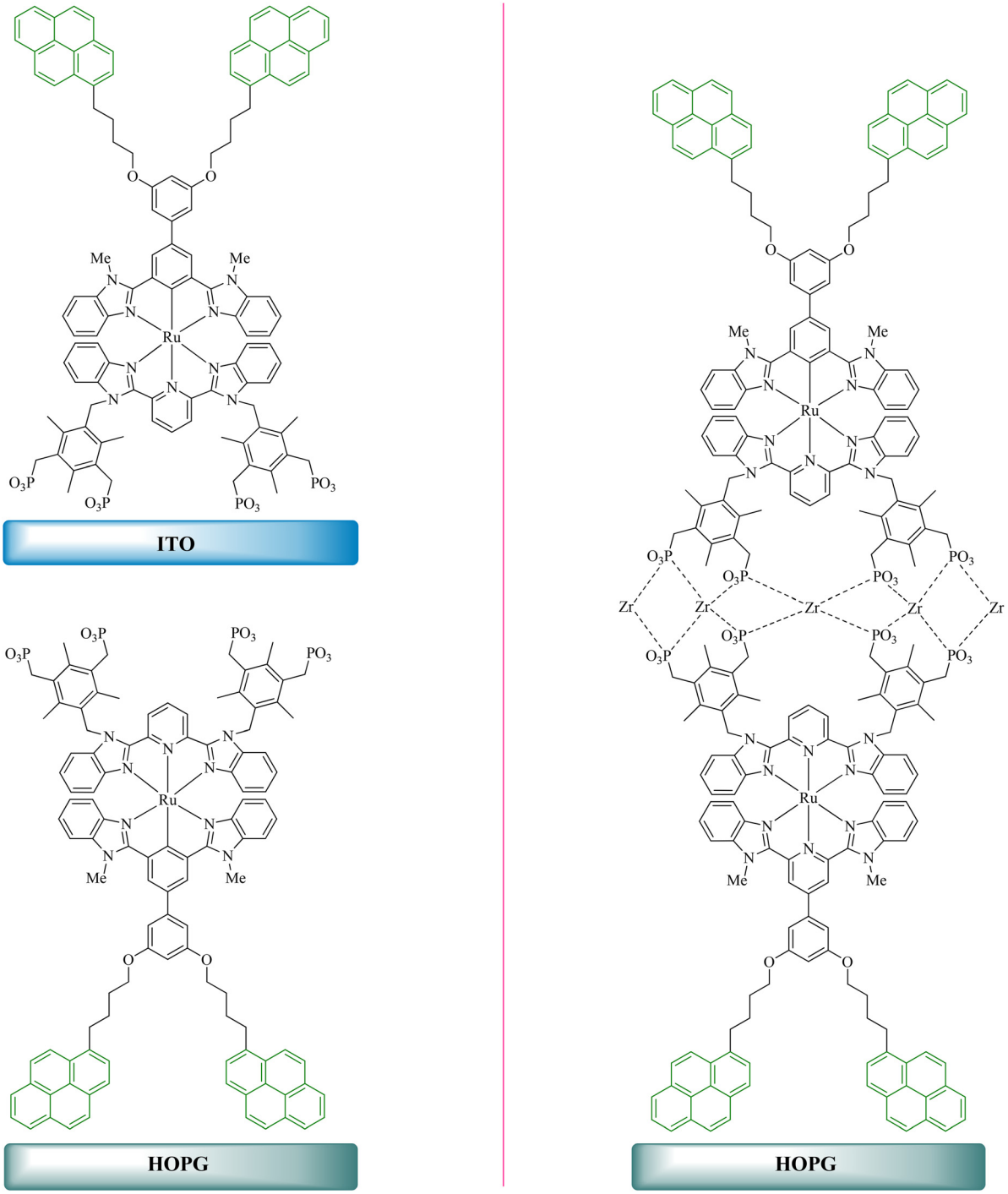

Fig. 27 Proposed surface-tethered structures for the **75** monolayer on ITO and HOPG and a bilayer connected by the Zr–phosphonate bond on HOPG. Reproduced with permission from ref. 47 copyright 2015, Chemical Society of Japan.

based on the various data for each type of immobilization of the pyrene-tagged Ru complex. Firstly, due to contact angles associated with water droplets in both the HOPG and ITO measurements, a remarkable change in hydrophilicity was shown, indicating an effective attachment of **75** onto these supports. Secondly, based on the CV results of the bilayer film at a specific oxidative wave, it was 1.5 times larger compared to that of the **75** monolayer on the HOPG surface. Thirdly, corresponding to the graphene absorption, the MLCT band of **76**, and CV data, the consistent increase in the absorption bands and oxidative peak current with additional layers indicates the formation of a consistent layer structure throughout the LbL process.

In 2016, Blondeau, Sala, Godard, Llobet, and their co-workers reported a hybrid solid-state system containing pyrene-tagged Ru complexes immobilized on MWCNTs.[48] These complexes serve as highly stable molecular anodes for water oxidation, achieving over

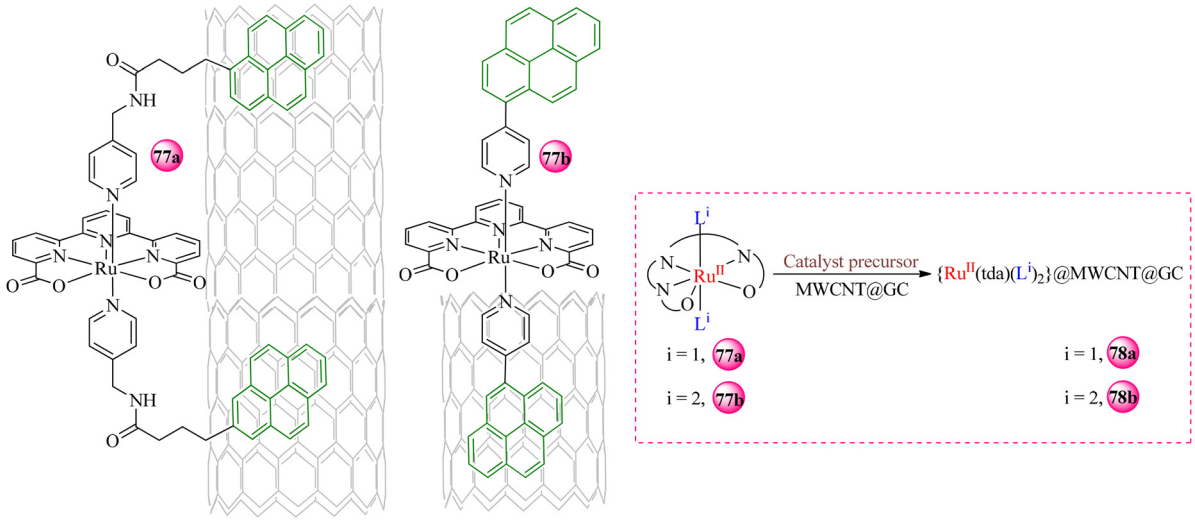

Fig. 28 Schematic representation of the anchoring of complexes **77a** (left) and **77b** (right) in MWCNTs. Reproduced with permission from ref. 48 copyright 2016, John Wiley and Sons.

a million turnover numbers at specific potentials without any signs of degradation, thanks to π-stacking interactions. These ruthenium complexes $\{Ru(tda)(L^1)_2\}$ (**77a**) and $\{Ru(tda)(L^2)_2\}$ (**77b**) (tda^{2-} = [2,2′:6′,2″-terpyridine]-6,6″-dicarboxylato, L^1 = (4-(pyrene-1-yl)-*N*-(pyridine-4-ylmethyl)butanamide and L^2 = (4-(pyrene-1-yl)pyridine)) were synthesized by reacting the ruthenium precursor with the respective ligands L^1 and L^2, which involve pyrenyl groups for effective anchoring *via* π-stacking interactions on MWCNTs (Fig. 28). To assess the efficiency of the pyrene-tagged Ru complex immobilized on MWCNTs (**77a** and **77b**), turnover numbers, CV analysis, and stability were analyzed, revealing values over a million, redox behavior and long-term stability. The performance of these heterogeneous catalysts was similar to their homogeneous counterparts, attributed to the "water nucleophilic attack" mechanism involved in the O–O bond formation step, which is common to both systems. This approach provides robust immobilization of the complexes onto the MWCNTs while preserving their intrinsic electronic properties, leading to stable hybrid materials that demonstrate impressive catalytic activity for water oxidation.

In 2016, Brunschwig, Gray, and their co-workers synthesized two new immobilized pyrene-tagged complexes involving a ruthenium tris(bipyridyl) (**79**) and an iridium bipyridine complex of [Cp*Ir] (**80**) (Cp* = penta-methylcyclopentadienyl) onto carbon electrodes (Fig. 29)[49] and studied their electrochemical properties at negative potentials since these conditions are essential for the majority of catalytic processes involved in fuel production. In order to synthesize these complexes, a

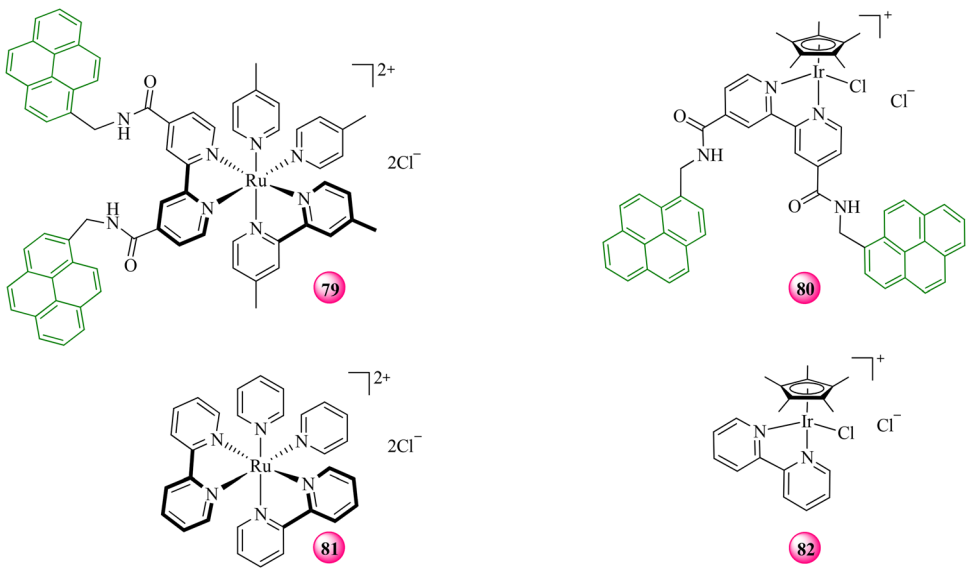

Fig. 29 Schematic structures of $[Ru(P)(4,4'\text{-dimethyl-}2,2'\text{-bipyridine})_2]Cl_2$ (**79**), $[(\eta^5\text{-}C_5Me_5)Ir(P)Cl]Cl$ (**80**), and their analogues with no pyrene fragments (**81** and **82**). Reproduced with permission from ref. 49 copyright 2016, Institute of Physics Publishing.

pyrene-appended bipyridine ligand (**P**) was prepared through the reaction of 1-pyrenylmethylamine hydrochloride and bipyridine dicarboxylic acid. On the one hand, complex **79** was obtained by metallating **P** with Ru(4,4′-dimethyl-2,2′-bipyridine)$_2$Cl$_2$ and purifying it through recrystallization. On the other hand, complex **80** was similarly derived by treating **P** with [Cp*IrCl$_2$]$_2$. In the subsequent step, functionalization of Ketjen black electrodes with complexes **79** or **80** was performed by immersing them in a dilute CH_2Cl_2 solution, followed by rinsing with CH_3CN to eliminate loosely bound complexes. The electrochemical investigations proved that noncovalent immobilization was suitable not only for achieving immobilized metal complexes but also for studying reductive electrochemical properties. Successful immobilization on carbon electrodes with high surface area was confirmed by X-ray photoelectron spectroscopy. According to electrochemical data, in CH_3CN, both complexes demonstrated reversible reduction behavior at distinct electrochemical potentials. Indeed, the pyrene-tagged ruthenium complexes (**79**) exhibited excellent stability, with reversible currents persisting for more than an hour. Meanwhile, it was indicated that the iridium complex has electrochemical characteristics, which can lead to ligand exchange and the emergence of various species on the surface. Nevertheless, the stability of these noncovalent interactions under negative electrode polarization declined.

In 2016, Mata and co-workers specifically investigated the stability of various immobilized ruthenium complexes containing NHC ligands, which were functionalized with varied polyaromatic groups, including pyrene (Pyr), pentafluorophenyl (PhF), and anthracene (Ant) on rGO, and also explored their recyclability (Fig. 30).[50] The synthesis procedure for pyrene-tagged Ru is mentioned earlier (see Fig. 23). According to the recycling experiment data, using (*p*-trifluoromethyl)benzyl alcohol as the model substrate for the dehydrogenation reaction, PhF–Ru–rGO (**85**) was effective for reuse up to five times, while Ant–Ru–rGO (**86**) was reused up to eight times, both showing no significant decline in activity. The system with the pyrene tag, the Pyr–Ru–rGO catalyst (**69**), proved to be the best in recyclability, being reused more than ten times without any notable loss in activity. The hybrid material **69** exhibits a heterogeneous catalytic behavior owing to the strong interaction between graphene and the pyrene tag, ensuring that the molecular complex remains firmly anchored to the surface. Thanks to this robust immobilization hindering the degradation of the ruthenium complex, catalytic activity was enhanced; therefore, lower catalyst loading is required. Moreover, based on hot filtration experiments, no desorption of the complex **67** is observed in contrast to **83** and **84**, possessing weak π–π interactions with graphene, underscoring the stability of this hybrid material in catalysis. It is deduced that, unlike pentafluorobenzyl or anthracene groups, pyrene fragments facilitate the process of immobilization onto the solid supports through π-stacking interactions.

In 2016, Crévisy, Schulz, and co-workers synthesized three Hoveyda-type ruthenium complexes involving pyrene-tagged NHC ligand (**87**), benzylidene moiety (**88**), or both (**89**) (Fig. 31).[14] It has been believed that the tag's position may significantly impact the properties of the obtained pre-catalysts. This new class of modified complexes have been immobilized non-covalently on graphene or rGO, and their recovery and activity have been studied for metathesis reactions. It is noticeable that, although the pre-catalyst immobilized *via* the benzylidene core (**88**) showed slower catalyst initiation, a lower loading of catalyst (100 ppm) was adequate to reach nearly complete conversion (compared to 250 ppm for the other pre-catalysts). These differences may be attributed to the use of different NHC ancillary ligands, specifically SIPr for **88** and SIMes-type for **87** and **89**. Indeed, the trifluoroacetamido moiety in **87** or the SIPr moiety in **88** is known to have some influence on different stability and activation phases of these three types of pre-catalysts.[51]

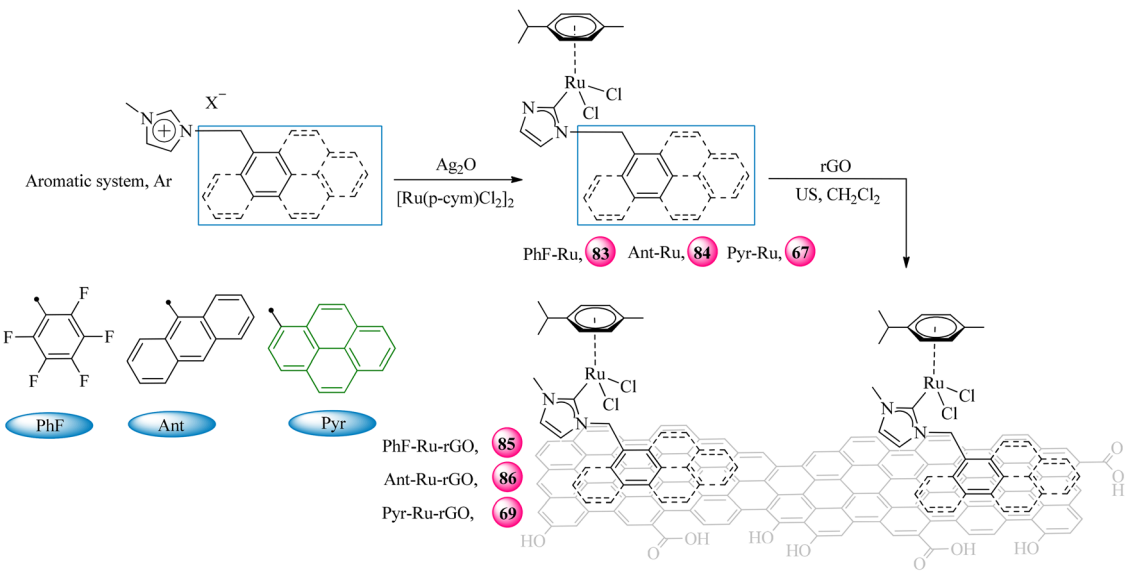

Fig. 30 The schematic procedure for immobilized Ru complexes, including **83**, **84**, and **67**, involves PhF, Ant, and Pyr fragments, respectively. Reproduced with permission from ref. 50 copyright 2016, Royal Society of Chemistry.

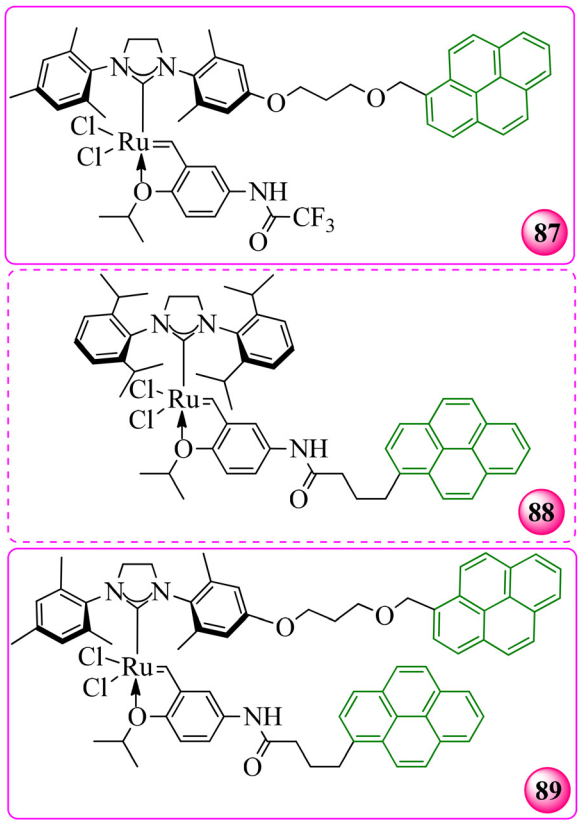

Fig. 31 Hoveyda-type pyrene-tagged ruthenium complexes involving pyrene-tagged NHC ligand (**89**), benzylidene moiety (**90**), or both (**91**). Reproduced with permission from ref. 14 copyright 2016, Elsevier.

To prepare compound **93**, which is necessary for the synthesis of **88** and **89**, a coupling reaction was performed between 4-(pyren-1-yl)butanoic acid and 4-isopropoxy-3-vinylaniline hydrochloride mediated by DCC and DMAP (Fig. 32). Complex **87** was obtained by treating Ru complex **90** with 2,2,2-trifluoro-*N*-(4-isopropoxy-3-vinylphenyl)acetamide and CuCl, followed by purification. Furthermore, complexes **88** and **89** were synthesized by reacting pyrene-tagged compound **93** with (SIPr)-$RuCl_2(PPh_3)$(Indenylidene) (**M_{23}**®) and **90**, respectively. For the immobilization of the Ru-catalysts on the rGO support, all defined compounds were dissolved in DCM, followed by the introduction of rGO. The immobilization of catalysts attributed to the pyrene-tagged Ru complexes on the solid surface was confirmed through UV-visible analysis, which involved the disappearance of their characteristic feature based on the amount of support added and the reaction duration (**88** < **87** < **89**). The recycling ability of ruthenium complexes has been attributed to the capability of the styrenylether ligand to re-coordinate with the $14e^-$ metal center, resulting in the formation of a stable species during the termination step. This phenomenon is commonly referred to as the boomerang effect. Within this context, ligand **94** (see Fig. 33) was synthesized using a similar method as described for the synthesis of compound **93**. The use of pyrene-tagged styrenyl-ether as an additional ligand immobilized on rGO improved catalytic results by facilitating a boomerang effect that made the species of active ruthenium stable. This effect was made possible due to the higher concentration of the benzylidene ligand on the support, which enhanced stability. Additionally, the presence of the extra ligand provided broader coverage of the rGO surface, protecting the Ru active species from potential damage caused by the support. The compound **88**/**94**@rGO was effectively used to facilitate metathesis reactions in a multi-substrate process (Fig. 33). The findings demonstrate that this catalyst has the potential to be recycled four times with no immediate loss of activity in diene and ene-yne RCM reactions.

In 2016, Haga and co-workers studied the adsorption of four redox-active ruthenium pyrene-tagged complexes (**100a**, **100b**, **100c**, and **100d**), showing that their adsorption varies according to the number of pyrene moieties (Fig. 34).[52] In the synthetic procedure of **100a** (possesses eight pyrene tags) and **100b** (possesses four pyrene tags), in the first step, **98** carrying four pyrene fragments was synthesized by reacting triphenylphosphine and tetrabromomethane with 3,5-bis[4-(1-pyrenyl)butoxy]benzenemethanol (**95**) to obtain **96** followed by reaction with K_2CO_3 and bis(benzimidazole)pyridine (**97**) (Fig. 35). Complex **100a** was prepared by further reaction of precursor complex **99** with another **98** ligand in a mixture of DMF and *t*-BuOH. Afterward, in a similar process, **100b** was prepared by the reaction of 2,6-bis(1-methylbenzimidazol-2-yl)pyridine (**101**) and **99** in DMF and *t*-BuOH. Complex **100c** (possessing two pyrene tags) was also synthesized similarly, starting from ligand **105** (possessing two pyrene tags) and precursor **106**. Finally, **100d** (possessing one pyrene tag) was prepared through the reaction of 2,6-bis(1-methylbenzimidazol-2-yl)pyridine and precursor **109** in ethylene glycol, heating with microwave radiation and purifying the resulting precipitate.

These complexes were subsequently immobilized onto HOPG, SWCNTs, and MWCNTs. It was verified that complex **100b**/HOPG showed a higher electron transfer rate than MWCNTs and SWCNTs. Additionally, complex **100a** (eight pyrene groups) exhibited a strong affinity to carbon surfaces, whereas **100b**, **100c**, and **100d** had weak interactions with glassy carbon (GC). Notably, all complexes successfully facilitated the transfer of electrons to the GC electrode *via* the pyrene fragment(s). Research on oxidative electropolymerization of pyrene derivatives on graphene oxide or CNTs using Ru or Os complexes showed that the number of pyrene groups influenced the polymerization rate and efficiency. Compound **100b** (four pyrene groups) polymerized electrochemically 60 times faster than **100c** and **100d**. It has been observed that multimodal pyrene anchor groups exhibit attractive efficiency as primers and adsorbents in electrochemical polymerization.

Solar energy is crucial for sustainable fuel production through water oxidation. Ruthenium complexes are highly active in this regard, and there is great interest in developing binuclear scaffolds to enhance their performance through an intramolecular mechanism. In 2020, Meyer and co-workers examined the impact of the number and position of pyrene fragments in the structure of diruthenium electrocatalysts immobilized on CNTs for water-oxidation.[53] Two synthetic strategies were employed to attach pyrene moieties to diruthenium water oxidation catalysts (WOCs) constructed *via* bis(bipyridyl)pyrazolate (bbp^-). (Fig. 36). The first

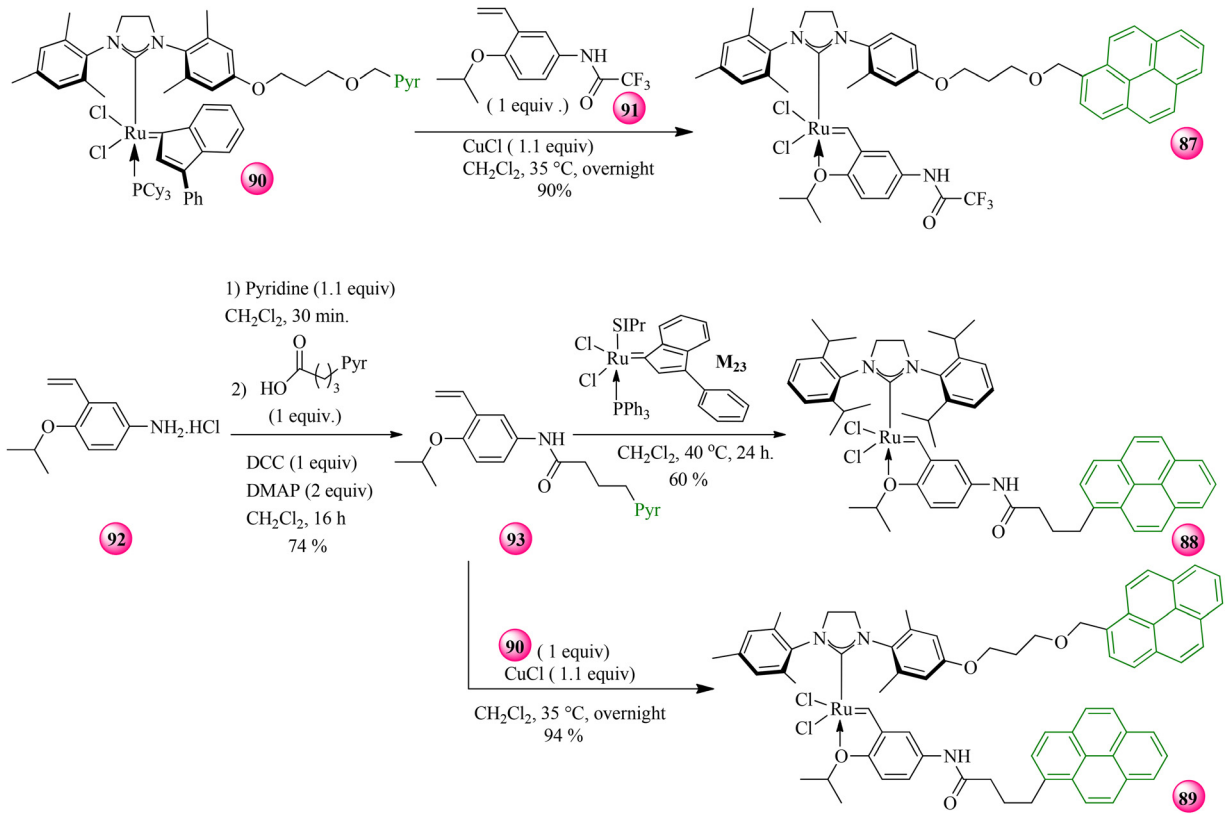

Fig. 32 The synthesis procedure of pyrene-tagged Ru complexes **87**, **88**, and **89**. Reproduced with permission from ref. 14 copyright 2016, Elsevier.

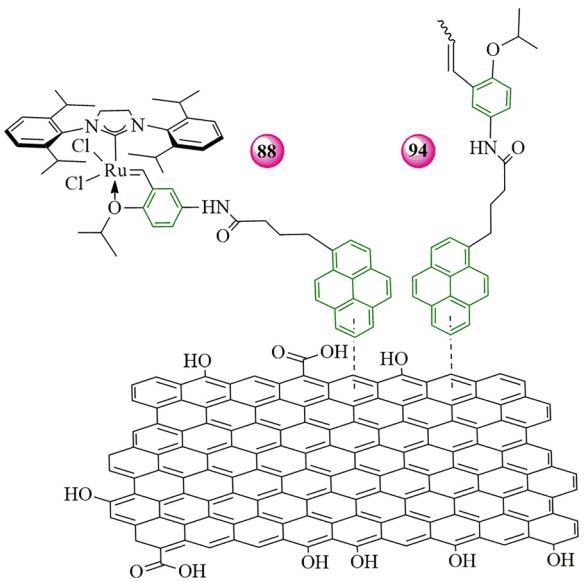

Fig. 33 Schematic illustration of the immobilization of **88** and **94** on rGO. Reproduced with permission from ref. 14 copyright 2016, Elsevier.

strategy involves the replacement of axial pyridines with pyrene-modified pyridine (py^{pyrene}), yielding complex $[(^{Me}bbp)Ru_2(OAc)(py^{pyrene})_4](PF_6)_2$ (**113**). In the second strategy, pyrene has covalently adhered to the pyrazolate backbone through a phenylene spacer as in complex $[(^{pyrene}bbp)Ru_2(OAc)(py)_4](PF_6)_2$ (**118**). Although the synthesis of complex **113** follows established protocols, complex **118** demands a Suzuki–Miyaura cross-coupling reaction. To synthesize complex **113**, the proligand ^{Me}bbpH is introduced into a solution of $RuCl_2(dmso)_4$ and NEt_3 in ethanol, forming a precursor, which was then treated with py^{pyrene} and NaOAc to produce the bridged precatalyst **113**, which was obtained through crystallization. In the case of complex $[(^{pyrene}bbp)Ru_2(OAc)(py)_4](PF_6)_2$ (**118**), the pyrene anchor was attached to the bbp^- ligand core at an earlier stage, using a MOM-protected iodo derivative (MOM = methoxymethylether), which underwent a Suzuki–Miyaura cross-coupling reaction to introduce the pyrene group. The new proligand ^{pyrene}bbpH was then used in a modified one-pot procedure established for complex **113** to synthesize complex **118.** In order to verify the successful immobilization of the complexes on the electrode surface, initial electrochemical measurements were conducted under non-catalytic conditions prior to the onset of the oxygen evolution reaction (OER). GC|MWCNT|**118** exhibited superior stability and activity due to the diruthenium catalyst immobilizing through the pyrene on the bbp^- backbone. Although some factors, including solvation, may contribute, it can be deduced that the substrate binding site in GC|MWCNT|**118** may be favorably oriented; on the other hand, GC|MWCNT|**113** likely experiences closer active site interactions and restricted access. The π-systems of pyrazolate and pyrene play a key role in the charge transfer in GC|MWCNT|**118.** It was supposed to have more stability and activity as well as less leaching with the increase in the number of immobilized pyrene fragments

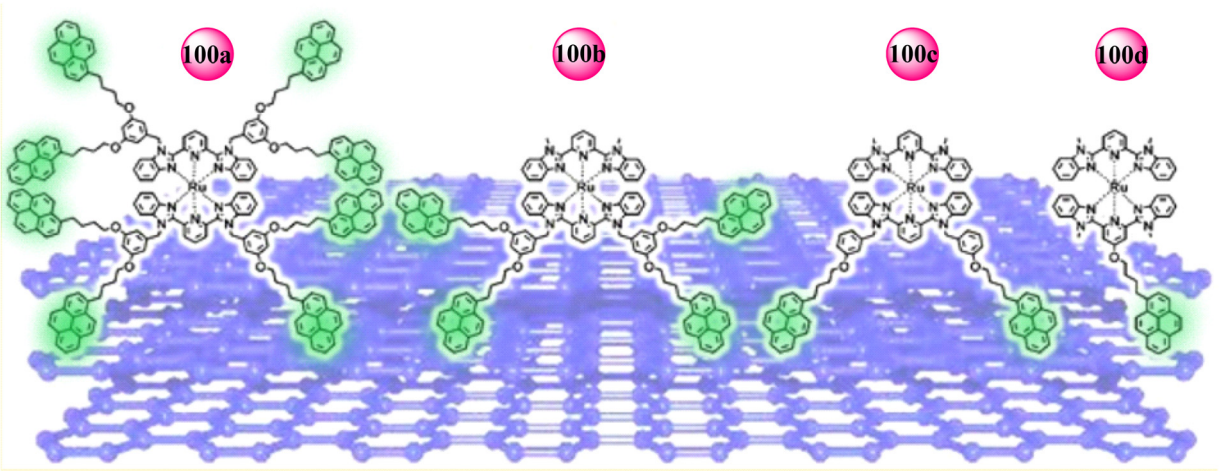

Fig. 34 Chemical structures of the immobilized Ru complexes **100a**, **100b**, **100c**, and **100d** containing different numbers of pyrene groups onto CNTs. Reproduced with permission from ref. 52 copyright 2016, American Chemical Society.

in GC|MWCNT|**113**; however, it was not observed experimentally. Despite higher turnover, GC|MWCNT|**118** exhibits more desorption, highlighting that a single pyrene is insufficient for strong attachment and preventing leaching.

In 2022, Teixidor, Romero, and co-workers found a suitable approach to synthesize and immobilize new pyrene-tagged ruthenium complexes with the bidentate pyridylpyrazol ligand, involving tridentate terpyridine (trpy) and 3-(2-pyridyl)-1-(pyrazolyl) methylpyrene (pypz–pyr) as a photoredox oxidation catalyst under aqueous conditions.[54] To synthesize the ligand pypz–pyr (**120**), the pyrazolic ligand 2-(3-pyrazolyl)pyridine (pypz-H) was reacted with 1-(bromomethyl)-pyrene, resulting in the preparation of Ru^{II} complexes **121** and **122**. Mixing [$RuCl_3$(trpy)] (**119**) and **120** in an ethanol–water solution at reflux with Et_3N led to substituting two chlorido ligands after the introduction of NH_4PF_6 to yield a mixture of *cis*- and *trans*-isomers for complex **121** (Fig. 37). Indeed, the non-symmetric nature of the pypz–pyr ligand facilitates the formation of these isomers. Isolated Ru–Cl complexes through column chromatography demonstrated a challenging process of obtaining pure *cis* isomers, and by reducing the reflux time to two hours, the *trans*-isomer was produced. In the next step, the Ru–OH_2 complex (*trans*-**122**) can be accomplished from the Ru–Cl complex using $AgPF_6$ or by dissolving complex **121** in heated water, demonstrating the probable pyrene group's essential role in enhancing the lability of the Cl ligand. In order to obtain the immobilized *trans*-**121** complex, rGO was dispersed in CH_2Cl_2 and sonicated, followed by the addition of the *trans*-**121** complex to prepare the immobilized complex, rGO@*trans*-[RuCl(trpy)(pypz–pyr)](PF_6) (Fig. 37). On the other hand, the rGO@*trans*-**122** complex was subsequently obtained by stirring rGO@*trans*-**121** in a water/acetone mixture at high temperature. It is noticeable that ruthenium loading in rGO@*trans*-**122** was determined using inductively coupled plasma atomic emission spectrometry (ICP-AES) and characterization involved scanning electron microscopy (SEM), UV-vis, and differential pulse voltammetry (DPV). However, due to strong absorption from rGO, the IR spectrum did not reveal precise signals for the immobilized complex. Based on the obtained data, rGO–*trans*-**122** indicated negligible leaching, and its photoredox catalytic activity was observed within the heterogeneous phase. Additionally, since the hybrid materials resemble the electrochemical behavior of homogeneous complexes, the immobilized complexes preserve the electrochemical properties of their molecular precursors. Additionally, according to the other obtained results, which highlight the catalyst's maintaining adequate yields and high selectivity, the heterogeneous rGO@*trans*-**122** demonstrated excellent performance in the photooxidation of various primary and secondary alcohols, especially benzylalcohol and 1-phenylethanol, outperforming the homogeneous *trans*-**122**. The potential recyclability of these catalysts leads to achieving reusable catalysts for practical applications, which were evaluated over five cycles during the photooxidation of benzyl alcohol reaction in water with no requirement of an additional photosensitizer since they have the ability to act as a catalyst and photosensitizer at the same time.

Besides, in 2024, these researchers reported the immobilized pyrene-tagged ruthenium complexes onto GO supports through π-stacking interactions in order to utilize them in aqueous environments as photoredox catalysts.[55] The general synthesis of these catalysts relies on the addition of bpea-pyrene (1-[bis-(pyridine-2-ylmethyl)amino]methylpyrene, **126**) to $RuCl_3$, leading to the preparation of [$RuCl_3$(bpea-pyrene)] (**127**) (Fig. 38). This complex was reacted with 2,2′-bipyridine in a mixed solvent at reflux with Et_3N, followed by the introduction of saturated NH_4PF_6 solution and purification, yielding *trans*–*fac*-**128**. In the subsequent step, the Ru–OH_2 complex *trans*–*fac*-**129** was obtained by reacting the Ru–Cl (**128**) complex with $AgNO_3$ in a water/acetone (3 : 1) or by refluxing in a water/acetone mixture, without Ag^+ ions. Finally, *trans*–*fac*-**129** was then immobilized onto GO by treating a sonicated dispersion of GO in water, followed by the addition of *trans*–*fac*-**129**, resulting in the GO@*trans*–*fac*-[Ru(bpea-pyrene)(bpy)OH_2](PF_6)$_2$, which was filtered, washed, and dried. It is noticeable that synthesis with CH_2Cl_2 as a solvent is also possible; however, it produces lower yields of product compared to water (Fig. 39). In order to

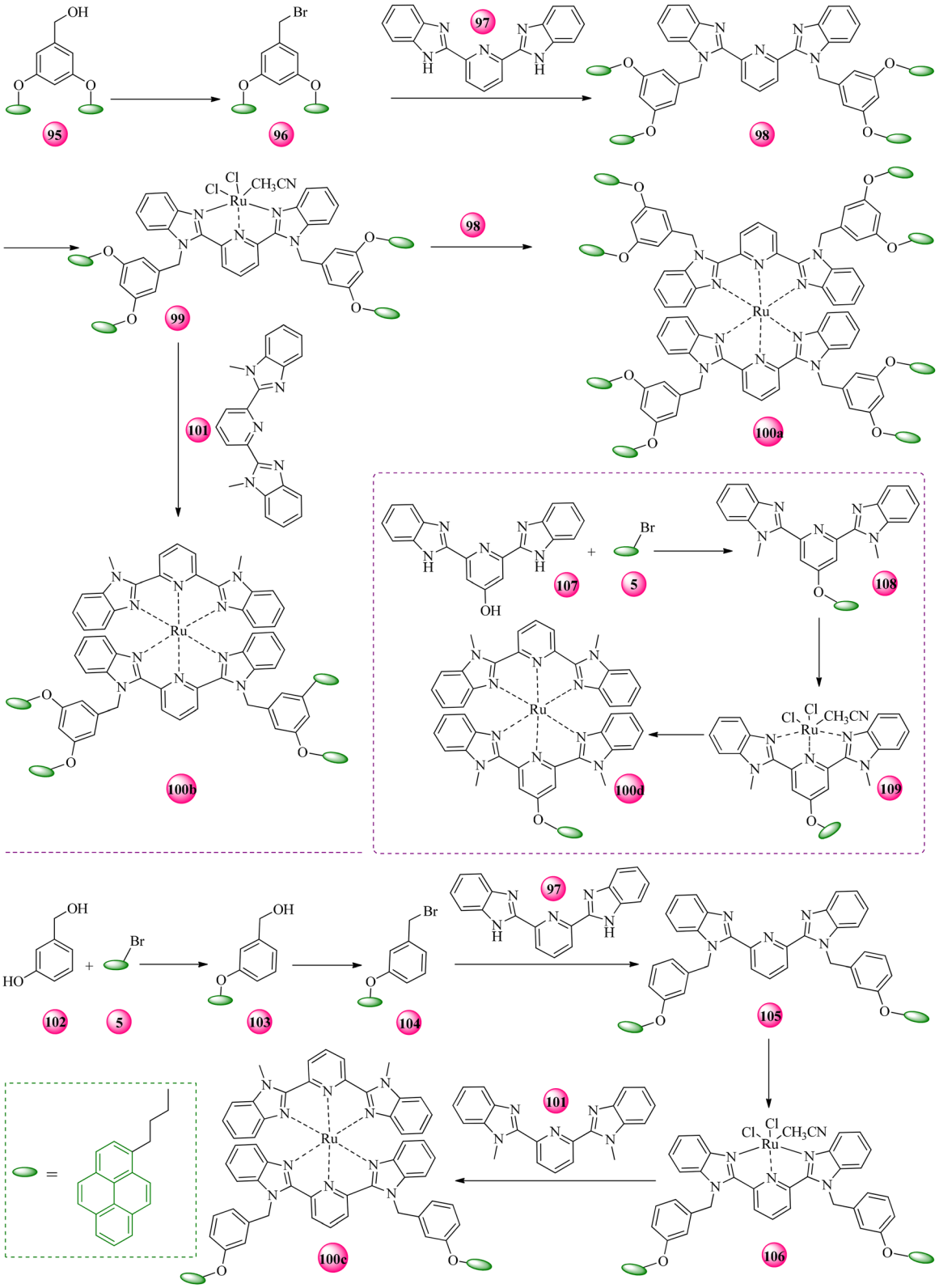

Fig. 35 The procedure for the synthesis of four different types of pyrene-tagged ruthenium complexes (**100a**, **100b**, **100c**, and **100d**). Reproduced with permission from ref. 52 copyright 2016, American Chemical Society.

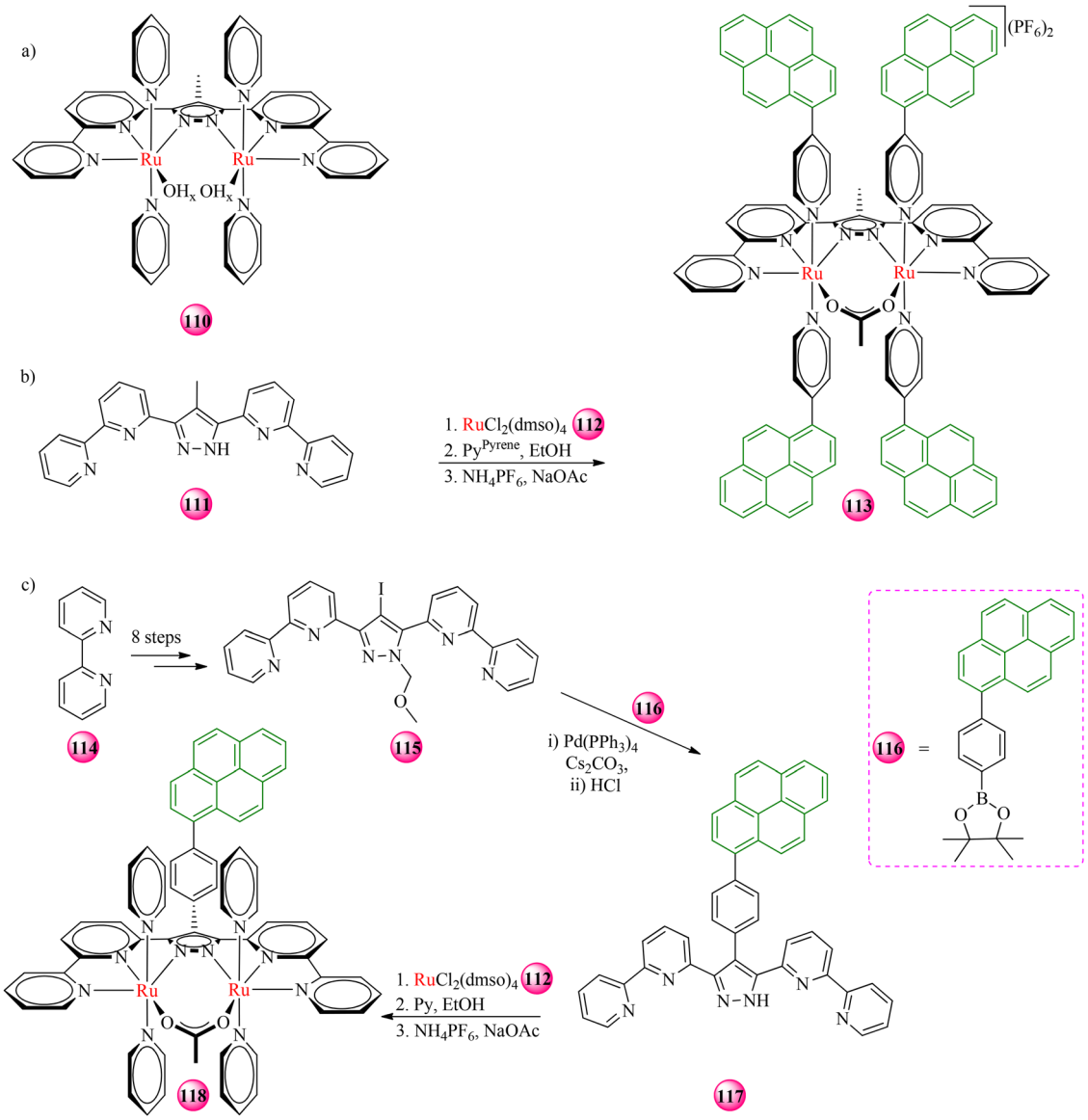

Fig. 36 (a) [(Mebbp){Ru(OHx)}2(py)4]-type diruthenium WOC. (b) Synthesis of [(Mebbp)Ru2(OAc)(pypyrene)4](PF6)2 (**113**). (c) Synthesis of ligand pyrenebbpH with pyrene modification and complex [(pyrenebbp)Ru2(OAc)(py)4](PF6)2 (**118**). Reproduced with permission from ref. 53 copyright 2020, American Chemical Society.

confirm the consistent distribution of ruthenium in the functionalized support, various techniques, including TEM, SEM, XPS, UV-vis, and DPV, were investigated. According to the results, the heterogeneous GO@*trans–fac*-**129** performed better than the homogeneous *trans–fac*-**129** in the photooxidation of aromatic alcohols. This enhancement can be attributed to better electron transfer and hindered recombination of hole–electron pairs during light excitation. Another hypothesis is that the catalyst may undergo diminished deactivation after immobilization onto GO. These hybrid materials are effortlessly recyclable and reusable to avoid the utilization of heavy metals, which can cause pollution and high costs. Moreover, an experiment in water based on the oxidation of 4-methylbenzyl alcohol maintained high conversion efficiency and selectivity over at least five uses with no notable loss of activity. Notably, it showed the highest TON among the other reported values for the heterogeneously catalyzed photooxidation of alcohols.

4.6. Pyrene-tagged osmium complexes

In 2013, Cosnier and co-workers reported an immobilized pyrene-tagged tris(bipyridine)osmium(II) complex (**130**) onto GO, chemically reduced graphene oxide (c-rGO), and electrochemically reduced graphene oxide (e-rGO) electrodes as a redox probe and compared them with GC and MWCNTs (Fig. 40).[56] Pyrene fragments facilitate the nanostructured graphitic carbon electrodes to be functionalized through two distinct methods: either electropolymerization by the irreversible pyrene-oxidizing or supramolecular binding by π–π interactions. The synthesis procedure of **130** is similar to tris(bispyrene-bipyridine)iron(II) which is explained before (Fig. 8). In order to synthesize

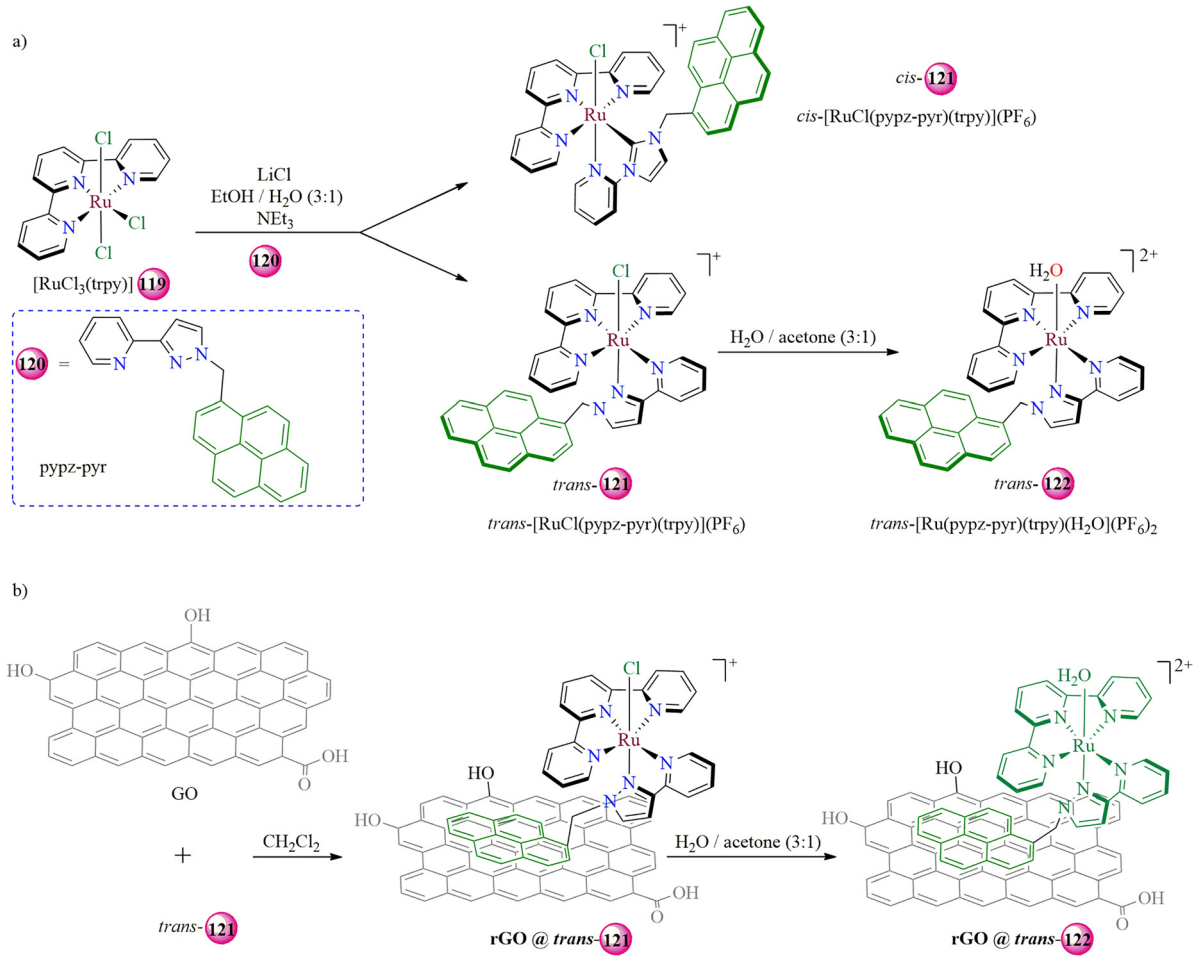

Fig. 37 (a) Synthetic procedure of complexes **121** and **122** and (b) the immobilization of *trans*-**121** and *trans*-**122** onto rGO. Reproduced with permission from ref. 54 copyright 2022, Royal Society of Chemistry.

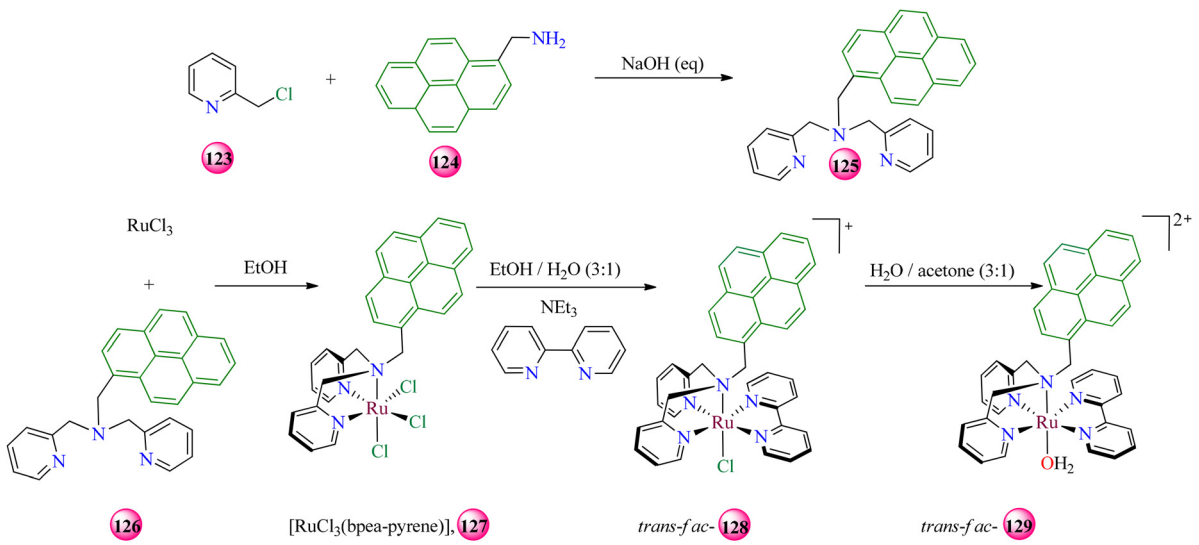

Fig. 38 Synthesis procedure for the preparation of **127**, *trans*–*fac*-**128**, and *trans*–*fac*-**129** complexes. Reproduced with permission from ref. 55 copyright 2023, American Chemical Society.

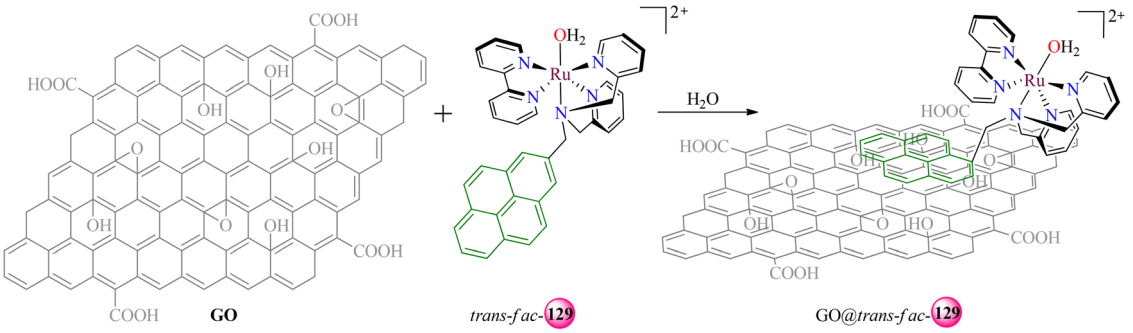

Fig. 39 The procedure for the immobilization of *trans–fac*-**129** onto GO. Reproduced with permission from ref. 55 Copyright 2024, American Chemical Society.

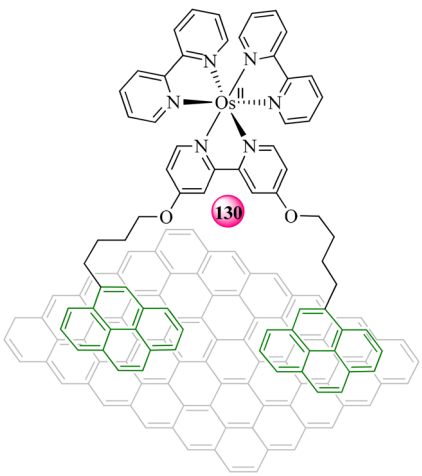

Fig. 40 Schematic structure of an immobilized pyrene-tagged Os complex (**130**) onto rGO. Reproduced with permission from ref. 56 copyright 2013, American Chemical Society.

[bis(2,2′-bipyridine)(4,4′-bis(4-pyren-1-ylbutyloxy)-2,2′-bipyridine]-osmium(II) hexafluorophosphate (**130**), a mixture of 4,4′-bis(4-pyren-1-ylbutyloxy)-2,2′-bipyridine and $[Os(bpy)_2Cl_2]$ was heated in ethylene glycol. Subsequently, a saturated aqueous $Na_2S_2O_8$ solution was introduced, and the resulting product was precipitated with an aqueous NH_4PF_6 solution to obtain the Os(II) complex (**130**) after filtering and washing with water and diethyl ether. In order to enable the supramolecular binding of **130**, electrodes were incubated in a solution of acetonitrile involving the Os(II) complex, followed by rinsing thoroughly with acetonitrile and acetone. In order to evaluate and compare the properties of these immobilized pyrene-tagged complexes (**130**) onto various supports, several experiments, such as calculating surface concentrations *via* measuring the charge under the oxidation peak, electrosynthesis, and polymerization through chronoamperometric experiments, were carried out. Based on the obtained data, the GC electrode demonstrated no adsorption, while e-rGO surfaces had weak adsorption for **130**. Surface concentration data from e-rGO electrodes indicated partial coverage, proving limited intercalation between graphene layers, which is similar to the behavior of HOPG. Reducing the GO film, which removes oxides, strengthens e-rGO nanosheet interactions and further hinders complex insertion into the graphene structure. Additionally, based on the electrosynthesis procedure regarding c-rGO and MWCNTs, the enhancement in current following each scan is higher than those observed for GC and e-rGO electrodes. On the other hand, in chronoamperometric experiments, e-rGO and GC electrodes led to polymerization with lower yield compared to MWCNT and c-rGO electrodes. Moreover, the greater quantity of complex **130** immobilized through electropolymerization, in contrast to the π–π interaction approach, highlights that π-stacking interactions are appropriate for the formation of a single layer, whereas electropolymerization results in the aggregation of multiple layers. The pyrene-tagged Os(II) complex (**130**) proved to be an effective redox probe for evaluating rGO surfaces in organic solvents. It highlights the significant role of π-stacking in the electrochemical behavior of various advanced carbon electrodes.

In 2016, Goff and co-workers reported a non-covalent method to synthesize pyrene-tagged Os^{II}–NHC (**135**) on a graphene surface through π–π interactions, which act as a redox intermediary for oxygen bioelectrocatalytic reduction *via Myrothecium verrucaria* (M_VBOD) (Fig. 41).[57] In the first step, a dimeric $[Ag^{I}(bis\text{-}NHC)]_2^{2+}$ starting complex (**131**) and the metal precursor, in this case $[OsCl(\mu\text{-}Cl)(\eta^6\text{-}p\text{-cyment})]_2$, participate in a well-known carbene transfer reaction. The osmium complex, $[OsCl(bis\text{-}NHC)(\eta^6\text{-}p\text{-cymene})]PF_6$ (**132**), possessing a chelating bis-NHC and *p*-cymene ligand, was formed by transmetalation and chloride substitution. The Os^{II}–NHC complexes **134** and **135** were prepared through the reaction of this complex with bipyridine or chemically pyrene-modified bipyridine. Subsequently, it was immobilized onto the surface of MWCNTs *via* straightforward immersing of the MWCNT electrode in a MeCN solution of **135**, followed by successive washing with MeCN and acetone.

Since NHC ligands can be modified based on their electronic properties, they could be an innovative substitute for other two-electron donors, such as imidazoles or pyridines. The higher electron-donating characteristics of these ligands than the more well-known pyridine ligands facilitate fine-tuning the osmium center's redox potentials while maintaining the stability of osmium complexes in various redox states. Not only can they produce a high fuel cell voltage, but they also reduce overpotentials toward the specific electrocatalytic reaction on

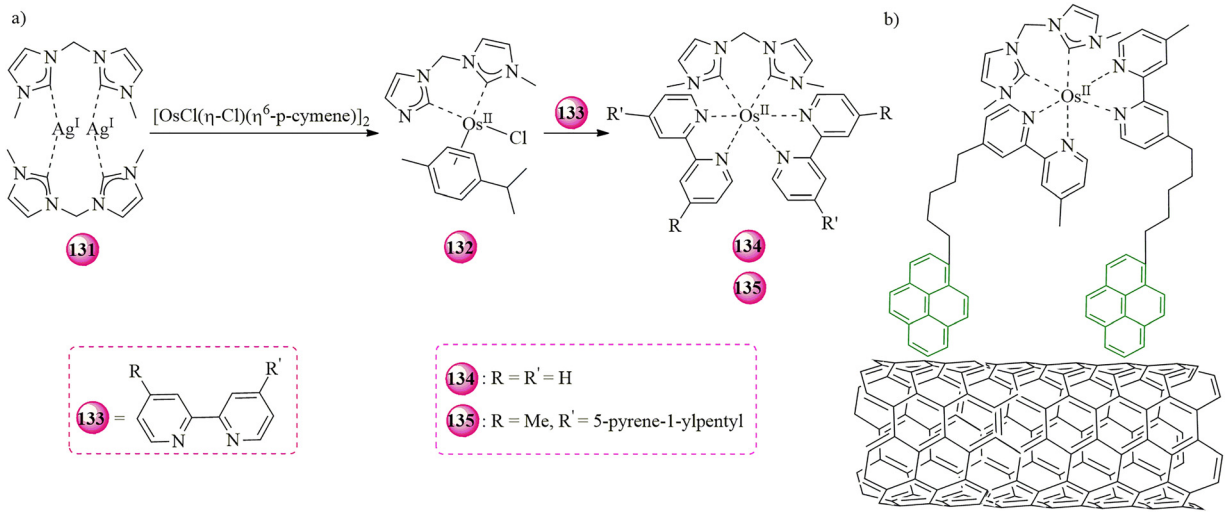

Fig. 41 (a) Synthesis of complexes **134** and **135**, (b) the immobilization of complex **135** onto CNTs. Reproduced with permission from ref. 57 copyright 2016, American Chemical Society.

the electrode. To investigate how well Os^{II}–NHC complexes interact with MWCNT electrodes, a metallopolymer was developed by electropolymerizing the pyrene fragments on GC electrodes, and nanostructured redox electrodes based on these complexes were fabricated. The results demonstrate that the redox properties of the Os^{II}–NHC complex (**135**) are adequate to promote electron transfer with the bilirubin oxidase of M_VBOD and reach high potential electroenzymatic oxygen reduction, which can open up new opportunities for bio-prospects.

4.7. Pyrene-tagged cobalt complexes

In 2009, Goldsmith and co-workers reported a pyrene-tagged cobalt complex immobilized onto SWCNTs and employed electrochemical analysis to evaluate the *in situ* immobilization (adsorption) process (Fig. 42).[58] To synthesize $[Co(tpy\sim py)_2](PF_6)_2$ (**136**), 4-pyren-1-yl-*N*-[5([2,2′;6′,2″]terpyridin-4′-yloxy)-pentyl]-butyramide (tpy ~ py) and $CoCl_2{\cdot}6H_2O$ were refluxed in absolute ethanol, yielding a yellow-orange solution. After cooling, it was mixed with deionized (DI) water and washed with CH_2Cl_2 to eliminate excess ligands. Afterward, ammonium hexafluorophosphate was then introduced to precipitate the product, resulting in a brown powder after passing through several steps.[59] For functionalizing SWCNTs with $[Co(tpy\sim py)_2]^{2+}$, a platinum working electrode was used in a three-electrode cell. In this regard, a suspension of SWCNTs was placed onto the Pt surface, leading to the dispersion of the nanotubes after evaporation of water. The efficiency of immobilized $[Co(tpy\sim py)_2]^{2+}$ was evaluated through CV on the SWCNT-coated electrode, and the anodic peak currents were studied before and after immobilization. Additionally, surface coverage was calculated using the Randles–Sevcik equation, and results were compared with those obtained from a bare platinum electrode to assess specificity. Based on the collected results, the anodic peak currents for the Co(II/III) redox process indicated that the electrochemically active surface area of the platinum electrode coated with SWCNTs was about eight times larger than that of the bare electrode due to the significant presence of SWCNTs.

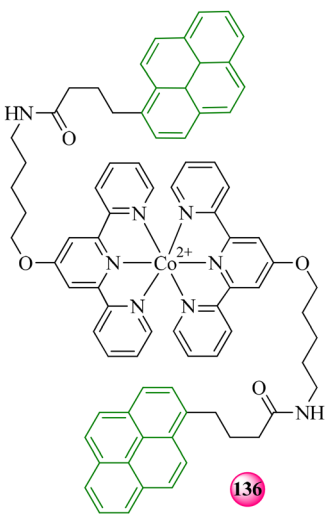

Fig. 42 Bis(4-pyren-1-yl-*N*-[5-([2,2′;6′,2″]terpyridin-4′-yloxy)-pentyl]-butyramide)cobalt(II) ion ($[Co(tpy\sim py)_2]^{2+}$), complex **136**. Reproduced with permission from ref. 58 copyright 2009, American Chemical Society.

In 2011, Dichtel and co-workers synthesized a redox-responsive pyrene-tagged cobalt(II) bis-terpyridine complex bearing a tripodal binding unit that reacts with graphene using three pendent pyrene units (Fig. 43).[60] In order to synthesize the tetrahedral core, ethynylmagnesium bromide was substituted with tris(*p*-methoxyphenyl)methyl chloride. The terminal alkyne group was then transformed into a terpyridyl ligand *via* a Sonogashira cross-coupling reaction, and the methoxy moieties were demethylated *via* the reaction with BBr_3. The resulting triphenol was alkylated with pyrene tosylate utilizing Williamson etherification conditions. Finally, the tripodal ligand was metalated by reacting with excess $Co(tpy)Cl_2MeCN$, forming **141**. These researchers integrated a Co(II) bis-terpyridyl complex ($[Co\text{-}(tpy)_2]^{2+}$) into the graphene-binding tripod to study its binding strength and

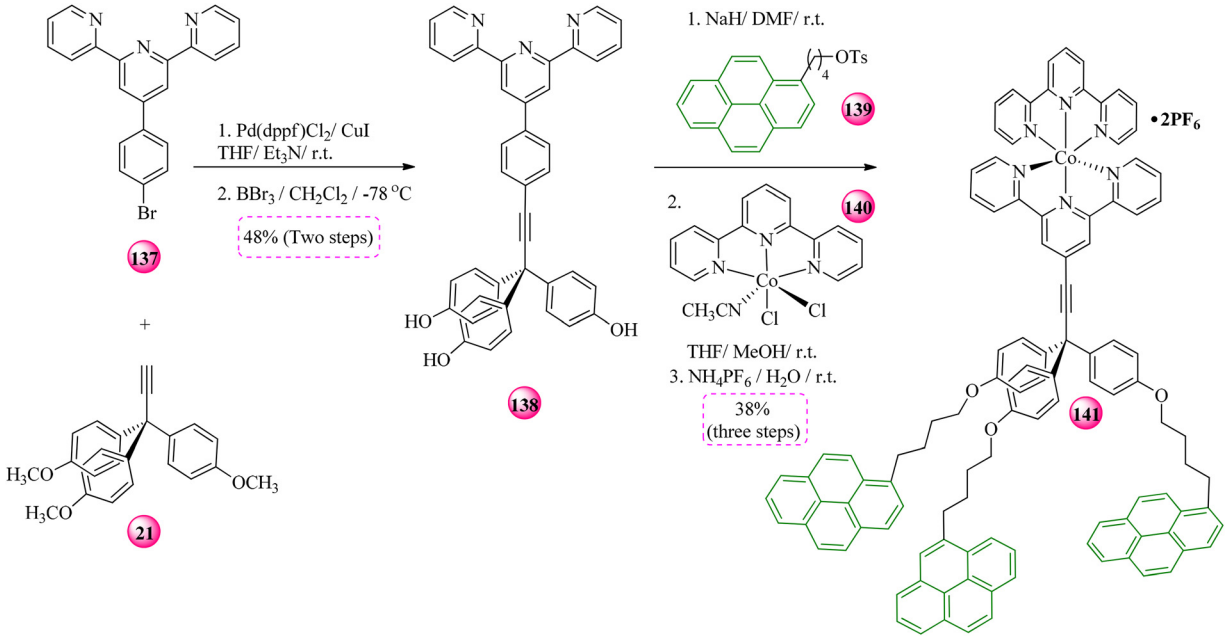

Fig. 43 The synthesis procedure of tripodal graphene binder **141**. Reproduced with permission from ref. 60 copyright 2011, American Chemical Society.

surface coverage through electrochemically observing the $Co^{2+/3+}$ redox couple. Based on kinetic experiments, the individual pyrene fragments can effortlessly desorb from the graphene surface when exposed to organic solvents. However, the tripodal binding motifs form stable monolayers on the graphene, exhibiting significantly slower desorption in fresh electrolytes than model compounds featuring a single pyrene fragment.

In 2014, Chen and co-workers reported three cobaloxime complexes (**142a**, **142b**, and **142c**) and immobilized them onto photoactive g-C_3N_4 as an eco-friendly and stable nanomaterial for hydrogen generation (Fig. 44).[19] In order to synthesize [Co(dmgH)$_2$-(4-COOH-py)Cl] (**142a**) ($dmgH_2$ = dimethylglyoxime), [Co(dmgH)-($dmgH_2$)Cl_2] was suspended in acetonitrile, followed by the addition of isonicotinic acid (4-COOH-py) and subsequent heating, stirring, filtration, and crystallization, leading to dark red crystals of **142a**. On the other hand, to synthesize [Co(dmgH)$_2$(*N*-pyren-1-ylmethyl-isonicotinamide)Cl] (**142b**), in the first step, triethylamine was introduced into a green suspension of [Co(dmgH)($dmgH_2$)Cl_2] in methanol, resulting in a brown solution and finally yielding brown crystals after the introduction of *N*-pyren-1-ylmethyl-isonicotinamide. Additionally, for the immobilization of **142a**, **142b**, or **142c** onto g-C_3N_4, a solution of each complex in acetonitrile was mixed with g-C_3N_4. After centrifugation, the clear solution was analyzed using UV-visible absorption spectroscopy to determine the amount of the adsorbed complex based on absorbance differences before and after immobilization. Based on the obtained data, increasing the concentration of cobaloximes did not improve the adsorption, and no significant differences were noted among them, indicating similar behavior. To assess the impact of the COOH, pyrene-tagged, and H groups on the photocatalytic activity of the Co complex, the TONs of hydrogen evolution of the **142a**, **142b**, and **142c**/g-C_3N_4 systems were studied. The results demonstrated that the **142a**/g-C_3N_4 system performed appropriately in contrast to **142c**/g-C_3N_4, highlighting the carboxyl group's effectiveness as a linkage for H_2 evolution. Notably, the **142b**/g-C_3N_4 system exhibited the highest activity compared to **142a**/g-C_3N_4 and **142c**/g-C_3N_4, indicating that **142b** serves as the superior co-catalyst for H_2 production, likely due to π-stacking interactions with g-C_3N_4. It is noticeable that the photocatalytic performance of these systems was associated with the effective charge separation in the excited g-C_3N_4, as indicated by steady-state photoluminescence spectroscopy. Moreover, the fluorescence quenching sequence (**142b** > **142a** > **142c**) aligns with their photocatalytic activity.

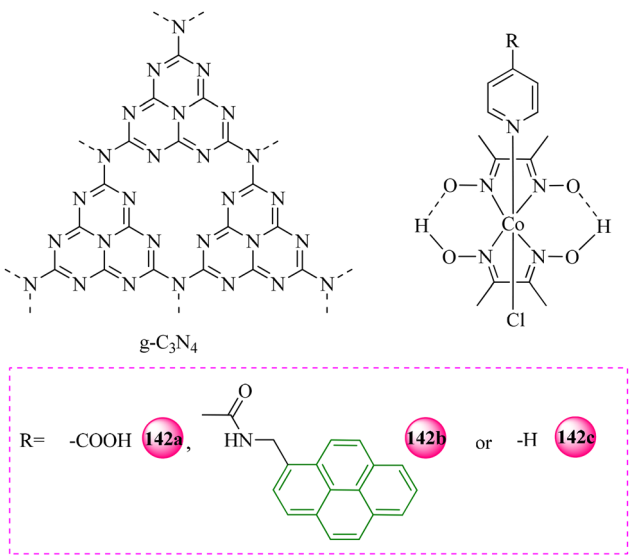

Fig. 44 The scheme of g-C_3N_4 and Co **141a**, **141b**, and **141c** complexes. Reproduced with permission from ref. 19 copyright 2014, Royal Society of Chemistry.

In 2016, Reisner and co-workers reported the synthesis and immobilization of a pyrene-tagged cobaloxime copolymer (pPyCo, **147**) and pyrene-tagged cobaloxime (PyCo, **148**) onto MWCNTs through π-stacking interactions to develop a functional buckypaper (BP) for catalytic hydrogen evolution (Fig. 45).[61] Indeed, cobaloximes offer several advantages, including easy synthesis, customizable catalytic properties through ligand modification, high proton-reduction activity at low overpotential, and effective performance in aqueous solutions. In order to synthesize **147** and **148**, $[Co(dmgH)(dmgH_2)Cl_2]$ was used as a starting material in both processes, but with different solvents and conditions. In order to obtain **148**, triethylamine was added to a green suspension of the cobalt complex in methanol, resulting in a color change to brown before heating and adding 4-(pyren-1-yl)-*N*-(pyridin-4-yl)butanamide. In contrast, the synthesis of **147** involved dissolving $[Co(dmgH)(dmgH_2)Cl_2]$ in a methanol–chloroform mixture, followed by the addition of the multifunctional copolymer (pPy, **146**). The obtained poly(cobaloxime) (**147**) was precipitated with hexane and washed extensively, yielding a light-brown powder. Next, GC/MWCNT electrodes were modified with **147** and **148** to characterize their electrochemical behavior on MWCNT surfaces. The GC/MWCNT electrodes were prepared *via* drop-coating a dispersion of MWCNTs in NMP onto the GC disk electrode. Following vacuum drying, a homogeneous MWCNT film was formed. The electrodes were then incubated in a solution of **147** or **148** in DMF, followed by rinsing with DMF and water. On the other hand, BP-**147** and BP-**148** were prepared through filtration of a dispersion of MWCNTs and molecular catalysts onto a polytetrafluoroethylene membrane in DMF, yielding consistent and stable MWCNT disks. To assess the effectiveness of immobilized **147**, a comparative study was conducted with a similar monomeric pyrene-tagged cobaloxime (**148**). Accordingly, cyclic voltammetry (CV), turnover number (TON), controlled-potential electrolysis, and faradaic yield were examined. Turning to the details, CV analysis indicated vigorous electrochemical activity with a reversible redox wave at a specific potential, and TONs indicated a significantly higher number for **147** in comparison with **148**. Moreover, based on data from controlled-potential electrolysis, **147** exhibited stable current densities and higher faradaic yield, which was up to 90%, than BP-**148**. Besides, it has good stability under aerobic conditions, generating significant hydrogen and highlighting its enhanced catalytic performance. Indeed, the polymeric hybrid material demonstrates

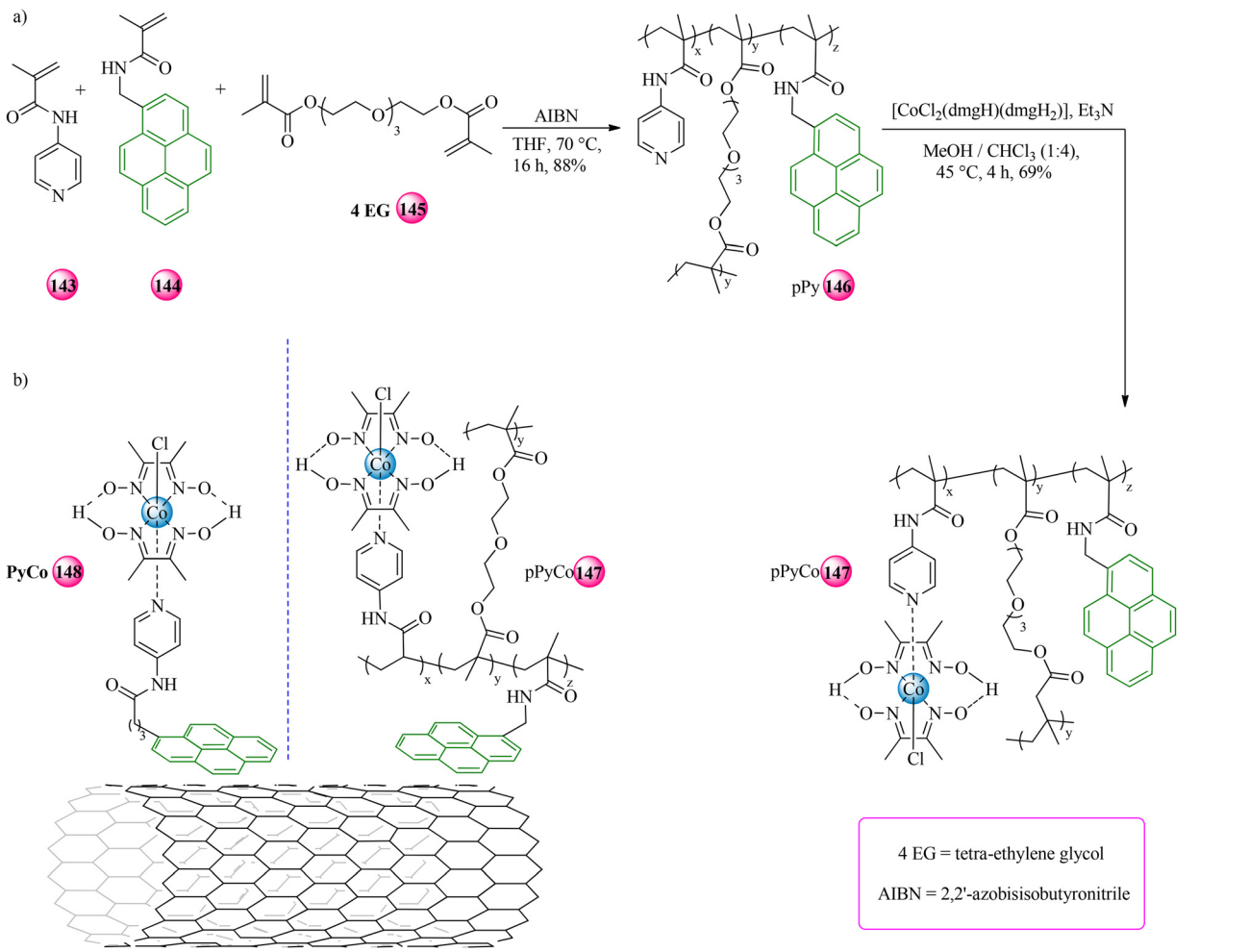

Fig. 45 Schematic of (a) the synthetic procedure for pPyCo (**147**) and (b) the immobilization of **147** and **148** onto the MWCNT. Reproduced with permission from ref. 61 copyright 2016, John Wiley and Sons.

four times greater catalytic activity and twice the stability of its monomeric counterpart, effectively acting as an activating and protective environment for the cobaloxime catalyst, akin to the role of enzymes within a protein matrix.

In 2017, Zheng and co-workers used a straightforward two-step process to synthesize an immobilized pyrene-tagged cobalt salophen complex (**154**) onto MWCNs through π–π interactions (Fig. 46).[62] In order to synthesize **154**, initially, a $Pd(PPh_3)_4$ catalyzed coupling reaction between 4-bromobenzene-1,2-diamine (**149**) and 1-pyreneboronic acid (**150**) was performed. Subsequently, the obtained aromatic amine (**151**) reacted with two moles of salicylaldehyde to produce ligand **153**. Under reflux conditions in ethanol, ligand **153** and $CoCl_2{\cdot}6H_2O$ underwent a reaction, forming brown powder of complex **154**. In order to prepare **154**/MWCNTs/GC, the immobilization of **154** on MWCNTs was initially performed through the soaking of MWCNT powder in DMF containing **154**. In the next step, a homogeneous ink of **154**/MWCNT was applied onto the surface of the GC electrode using a drop-casting technique. The electrochemical behavior of immobilized **154** was investigated using cyclic voltammetry under neutral conditions. The outcomes demonstrated high activity in electrocatalytic water oxidation and verified the preservation of **154** activity even after the immobilization process. Additionally, the **154**/MWCNTs/GC electrode exhibited a low overpotential of 530 mV at 10 mA cm^{-2}, a practical current for synthesis of solar fuel; however, neither the pure MWCNTs/GC, the bare GC, nor the **153**/MWCNTs/GC electrode indicated any catalytic response under the same conditions, revealing that complex **154** was crucial for electrocatalytic water oxidation. The Raman spectra of **154**, MWCNTs, and the **154**/MWCNT composite revealed that **154** preserved its initial molecular structure on the surface of the solid support. In order to assess the activity and durability of the composites of **154**/MWCNTs, bulk electrolysis was carried out after dropping the composite ink onto carbon cloth (CC), resulting in **154**/MWCNTs/CC through the same method that was utilized for the preparation of **154**/MWCNTs/GC. The obtained results indicated a high TON, faradaic efficiency (more than 90%), and durability for oxidizing water, in contrast to the pyrene-free systems, make it an attractive option as a heterogeneous catalyst for the oxidation of water.

In 2016, Cao and co-workers synthesized pyrene-tagged cobalt corrole on MWCNTs *via* a straightforward method to obtain highly efficient electrocatalysts in aqueous solutions for both the OER and the ORR (Fig. 47).[63] The reaction between 5,15-bis(pentafluorophenyl)-10-(4)-(1-pyrenyl)phenylcorrole and $Co(OAc)_2$ in pyridine eventually yielded red crystals of **161**. In order to immobilize **161** onto an MWCNT-coated electrode, the MWCNT was added to DMF, leading to a mixture that was sonicated and then dropped on top of the ITO, GC disk, or GC electrodes. Subsequently, a solution of **161** or **162** in CH_3CN was introduced dropwise into the MWCNT-coated electrodes. The results from fluorescence quenching experiments indicated that complex **161** was emissive, and adding MWCNTs caused quenching of its emission, revealing strong non-covalent interactions between the pyrene fragment of the complex and the MWCNTs. The **161**/MWCNT composite exhibited high stability and activity preservation for the OER and the ORR, while **162**/MWCNTs lost its activity by washing with dichloromethane, highlighting the key role of π–π interactions between the pyrene fragment of **161** and MWCNTs. Indeed, it facilitates the transfer of electrons and increases the adhesion of **161** on carbon supports to improve the performance of this catalyst for O_2 reduction. Additionally, the catalytic current of the as-prepared **161**/MWCNT was higher than that of the **162**/MWCNT, again verifying the massive impacts of π-stacking on the surface stability and OER activity of **161**.

In 2020, Zhu, Liang, and co-workers developed a novel approach for constructing a metalloporphyrin@MWCNT nanocomposite, an alternative to the traditionally used Pt-based, using a pyrene–pyridine (Pyr–Py) hybrid ligand as a bridge to immobilize Co(II)tetraphenylporphyrin onto CNTs through π–π interactions for oxygen reduction and evolution (Fig. 48).[64] The MWCNT/pyrene–pyridine hybrid compound was prepared by mixing Pyr–Py and MWCNT in an isopropyl alcohol (IPA) Nafion solution, followed by sonication, stirring, filtration, washing, and drying. Subsequently, **164**/MWCNT/Pyr–Py was obtained by mixing a portion of complex **164** with modified MWCNTs in isopropyl alcohol (IPA), followed by filtering, washing, and drying. Notably, unfunctionalized MWCNTs were mixed with Co(II)porphyrin to produce **164**/MWCNT. On the other hand, GC/MWCNT/Pyr–Py was obtained by drop-coating the MWCNT/Pyr–Py composite onto a GC electrode, immersing it in a CH_2Cl_2

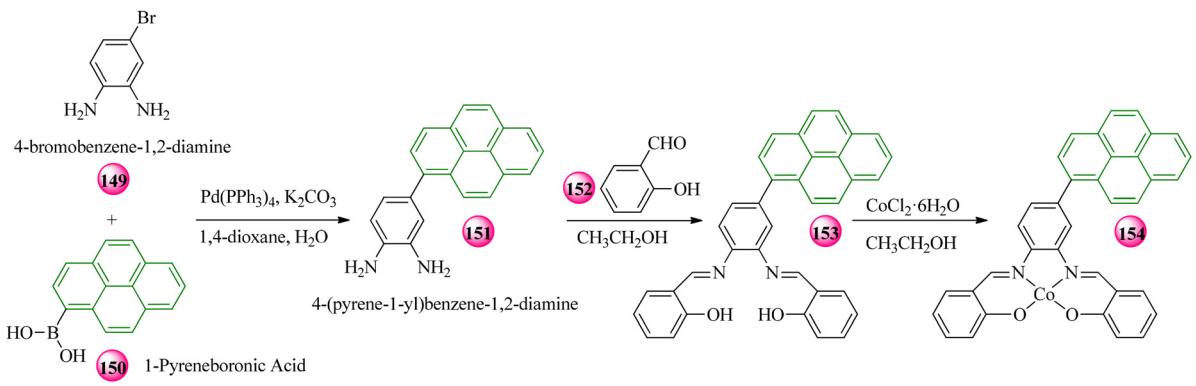

Fig. 46 Synthesis of pyrene-tagged Co salophen complex **154**. Reproduced with permission from ref. 62 copyright 2017, Royal Society of Chemistry.

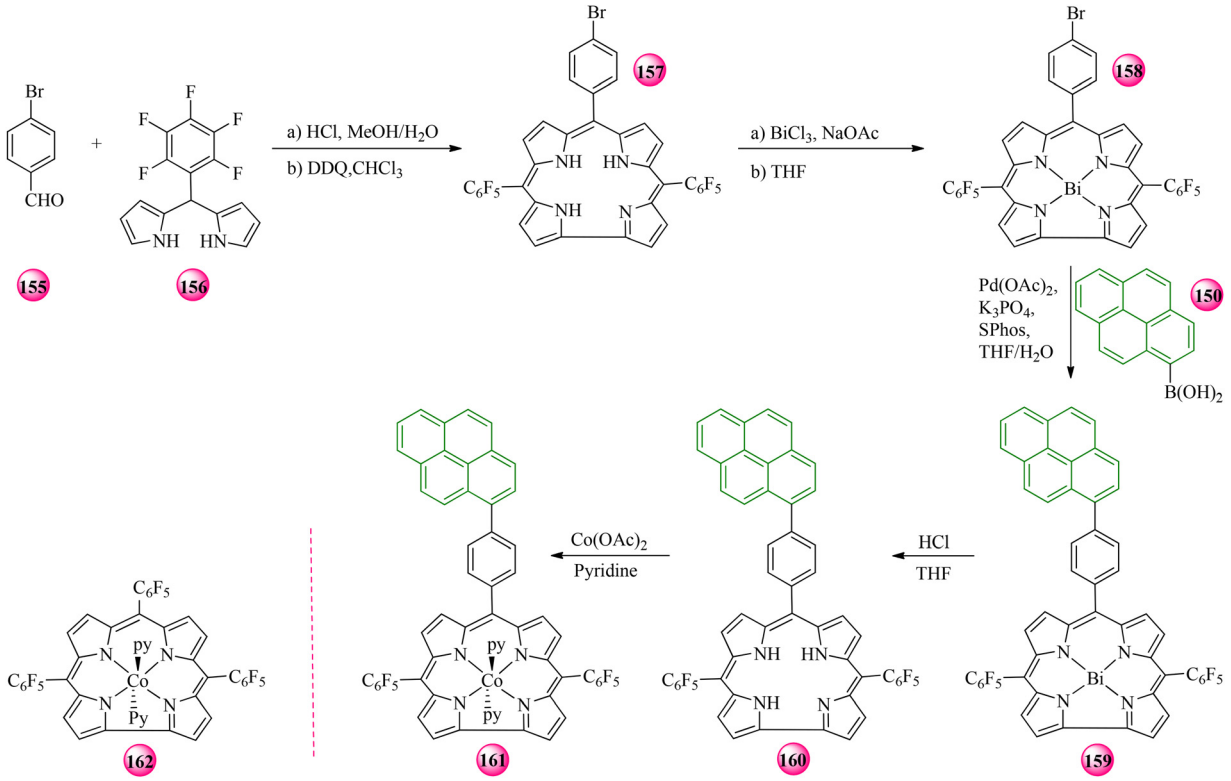

Fig. 47 The molecular structures of Co corroles include **161** and **162** complexes. Reproduced with permission from ref. 63 copyright 2016, American Chemical Society.

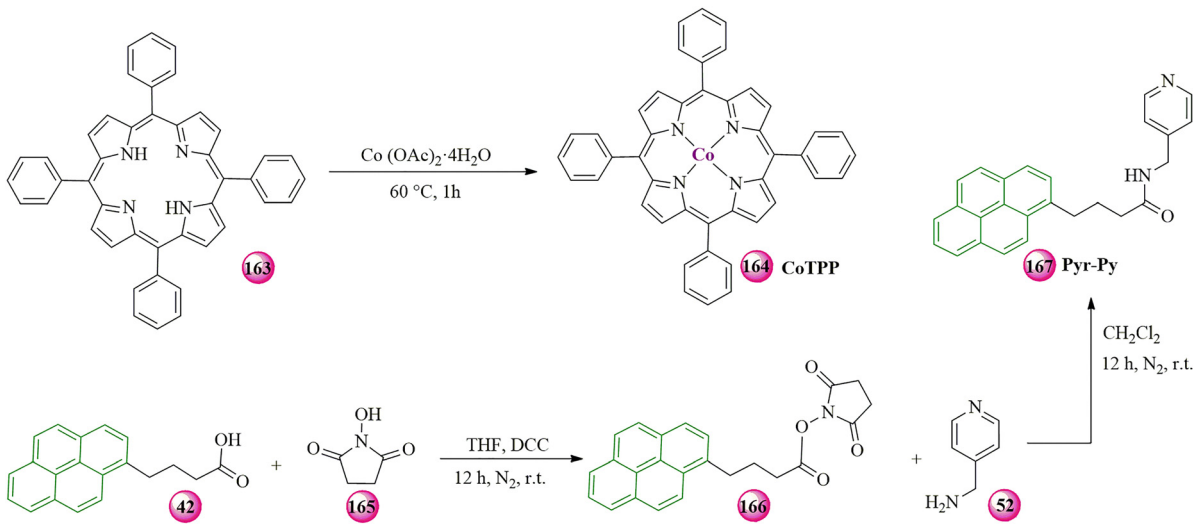

Fig. 48 Synthesis procedure for Co(II) porphyrin (**164**) and the pyrene–pyridine hybrid (Pyr–Py). Reproduced with permission from ref. 64 copyright 2020, Royal Society of Chemistry.

solution of Co(II) porphyrin for coordination to the center of the Co(II)porphyrin. A similar process without the Pyr–Py moiety was used, leading to GC/MWCNTs with Co(II) porphyrin, immobilized onto MWCNTs (**164**/MWCNT). According to the collected data, first, the **164**/MWCNT/Pyr–Py catalyst exhibits a 140 mV lower onset overpotential for the oxygen evolution reaction compared to **164**/MWCNT, implying improved OER activity owing to the presence of the Pyr–Py moiety. Secondly, the current densities of **164**/MWCNT/Pyr–Py were significantly higher compared to **164**/MWCNTs, with **164**/MWCNT/Pyr–Py exhibiting over 5 times greater current density. Thirdly, in controlled-bulk electrolysis experiments in phosphate-buffered saline (PBS), **164**/MWCNT/Pyr–Py showed much higher oxygen evolution compared to **164**/MWCNTs. Indeed, the axial coordination of the Pyr–Py linker

enhanced electrocatalytic performance in the ORR and the OER by increasing π-stacking interaction on the carbon support.

In 2024, Robert, Odobel, and their co-workers introduced two immobilized pyrene-tagged cobalt pyridyldiimine complexes (**172** and **179**) on CNTs to be utilized in an aqueous carbonate buffer while enhancing CO_2 reduction activity (Fig. 49).[65] In order to synthesize complexes **172** and **179**, substituted carboxylic esters **168** and **175** were the key intermediate ligands. Methyl-2,6-diacetylisonicotinate (**168**) and chloro-2,6-diacetylpyridine (**173**) were prepared *via* a Minisci reaction, and ligand **175** was prepared through a Suzuki cross-coupling reaction between **173** and **174**. The ester groups of these ligands were subsequently saponified to prepare the respective carboxylic acids, which were converted to *N*-hydroxysuccinimide esters (**170** and **177**) using NHS and *N*-ethyl-*N*′-(3-dimethylaminopropyl)carbodiimide (EDC). Subsequently, these compounds were reacted with pyrenemethylamine to prepare the corresponding amides (**171** and **178**). Finally, condensation of diamine on pyridyldiimine, templated *via* cobalt ions, resulted in the formation of complexes **172** and **179**. To investigate the use of these catalysts, CPE experiments utilized **172**/MWCNT and **179**/MWCNT inks deposited on carbon paper. The complexes and MWCNTs were mixed in a 1 : 10 ratio with ethanol and sonicated for 30 minutes. Subsequently, Nafion was added, and sonication continued for another 30 minutes. The ink was kept overnight under magnetic stirring before being applied to the carbon paper surface by drop casting. To evaluate the chemical properties of **172** and **179**, several CPE analyses, such as selectivity towards CO, faradaic efficiency, TON, and stability, were performed. Based on the obtained results, both **172**/MWCNTs and **179**/MWCNTs showed high selectivity towards CO with modest stability and faradaic efficiency. However, after the immobilization, not only did they maintain their CO selectivity at over 97% and activity for up to 5 hours, but they also demonstrated remarkable stability, activity, TONs, and catalytic rates. These catalysts have the potential to be used as electro- or photo(electro)-catalysts.

4.8. Pyrene-tagged rhodium complexes

In 2008, Zhou and co-workers reported a new method for the synthesis of recyclable chiral pyrene-tagged pyrphos rhodium catalysts immobilized onto carbon nanotubes through π-stacking interaction for asymmetric hydrogenation of α-dehydroamino esters.[66] The synthesis of the pyrene-modified pyrphos ligand (*R*,*R*)-**181** was a straightforward approach involving the reaction of (3*R*,4*R*)3,4-bis(diphenylphosphino)pyrrolidine (pyrphos, *R*,*R*-**180**) with 1-pyrenebutyric acid in DCC and DMAP, yielding the (*R*,*R*)-**181** ligand in high yield (Fig. 50). In order to obtain an immobilized pyrene-tagged Rh complex onto CNTs, Rh-$(COD)_2BF_4$

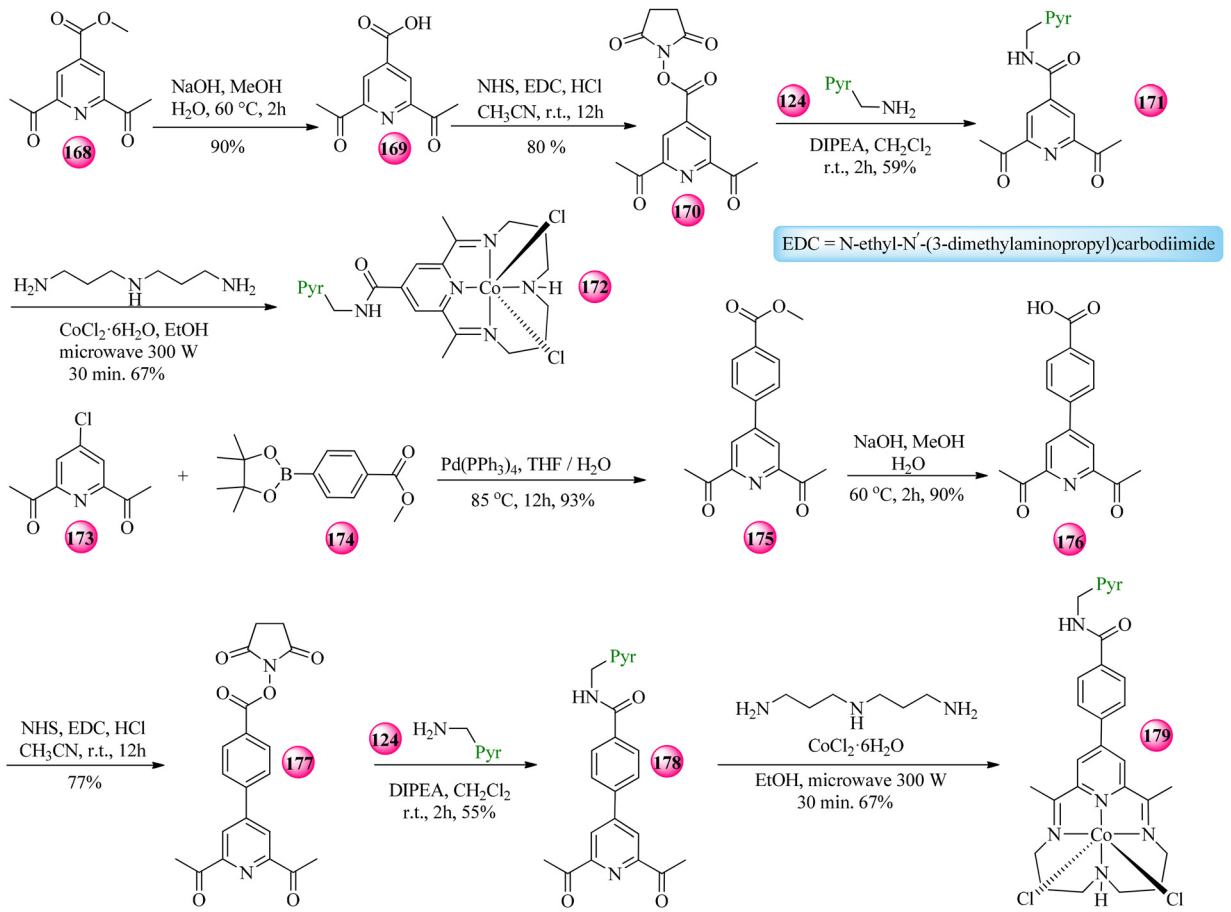

Fig. 49 Synthesis procedure for complexes **172** and **179**. Reproduced with permission from ref. 65 copyright 2024, Royal Society of Chemistry.

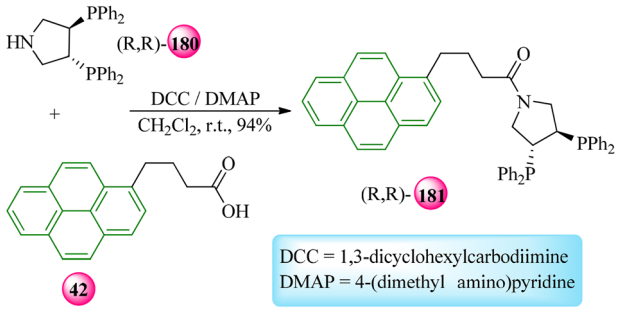

Fig. 50 Synthesis of pyrene-modified pyrphos ligand **181**. Reproduced with permission from ref. 66 copyright 2008, John Wiley and Sons.

(COD = 1,5-cyclooctadiene) was reacted with (*R*,*R*)-**181**, which was then treated with CNTs in different solvents. Subsequently, another process for hydrogenation reaction and CNT-assistant catalyst recycling was performed. In this process, a mixture of $[Rh(COD)_2]BF_4$ and ligand (*R*,*R*)-**181** was stirred in CH_2Cl_2 under nitrogen. Based on the asymmetric hydrogenation of α-dehydroamino esters' results, the catalyst could be successfully recycled and reused without obviously losing enantioselectivity or activity for nine cycles. Notably, the extent of catalyst immobilization onto CNTs varied depending on the solvents. Indeed, this method holds significant potential for various applications in organic synthesis.

In 2015, Minteer and co-workers reported the preparation of a pyrene-tagged rhodium complex involving the phenanthroline ligand (pyr–Rh) and developed an electrode setup utilizing this pyr–Rh complex, which was then immobilized onto MWCNTs through π–π stacking to regenerate nicotinamide adenine dinucleotide (NADH) from NAD^+.[67] To synthesize **186**, initially, **42** and a drop of DMF were dissolved in benzene, followed by the addition of oxalyl chloride, leading to the crude product of **182** after several steps. Subsequently, **182** and 1,10-phenanthrolin-5-amine **183** were each dissolved in DCM followed by gradual mixing, resulting in the precipitate of **184**. Next, **184** was dissolved in EtOH/$CHCl_3$ and reacted with the pentamethylcyclopentadienylrhodium(III) chloride dimer (**185**). The mixture was stirred under nitrogen, followed by the evaporation of the solvent under reduced pressure and dispersing the yellow solid in dry ethyl ether. Finally, an orange solid of **186** was achieved after another stirring and filtration (Fig. 51). In order to obtain the pyr–Rh/MWCNT modified electrodes, MWCNTs were dispersed thoroughly in NMP, sonicated, and vortexed. Subsequently, a portion of MWCNTs was applied to a GC electrode, followed by immersing in a pyr–Rh complex solution (Fig. 52). Based on obtained data from hydrodynamic amperometry, which was considered to assess the efficiency and reusability of the Rh pyrene-tagged catalyst, and UV-vis spectroscopy for measuring the concentration of NADH generation, the activity of the Rh complex in the absence of pyrene fragments significantly declined after five cycles. However, the pyrene-tagged Rh complex exhibited stable catalytic activity and acceptable reusability. Furthermore, the rate constant of NADH regeneration demonstrated the stability and durability of the pyrene-tagged rhodium complex in contrast to the bare rhodium complex, which indicated a dramatic decrease due to the leaching of the catalyst from the modified electrodes. In this system, Rh(I) is oxidized to Rh(III) *via* the transfer of a hydride ion to NAD^+; then, by accepting two electrons from the electrode, Rh(III) can be reduced at the electrode surface again. On the other hand, the MWCNTs and pyr-phen only act as a support and an anchor, respectively, to immobilize the rhodium redox centers onto the surface of the electrode. Notably, pyr–Rh has the potential to be utilized in a biocatalytic setting in the presence of malate dehydrogenase (MDH) to reduce oxaloacetic acid enzymatically.

In 2015, Kim and co-workers reported a cyclopentadienyl pyrene-tagged rhodium complex and its immobilization on rGO through π–π interactions for hydrogen photoproduction under controlled visible light in the presence of Pt nanoparticles and formate.[68] To synthesize pyrene-tagged Rh complex (**188**), the pentamethylcyclopentadienyl rhodium(III) chloride dimer and pyr-phen (**187**) were mixed up in ethanol at ambient temperature,

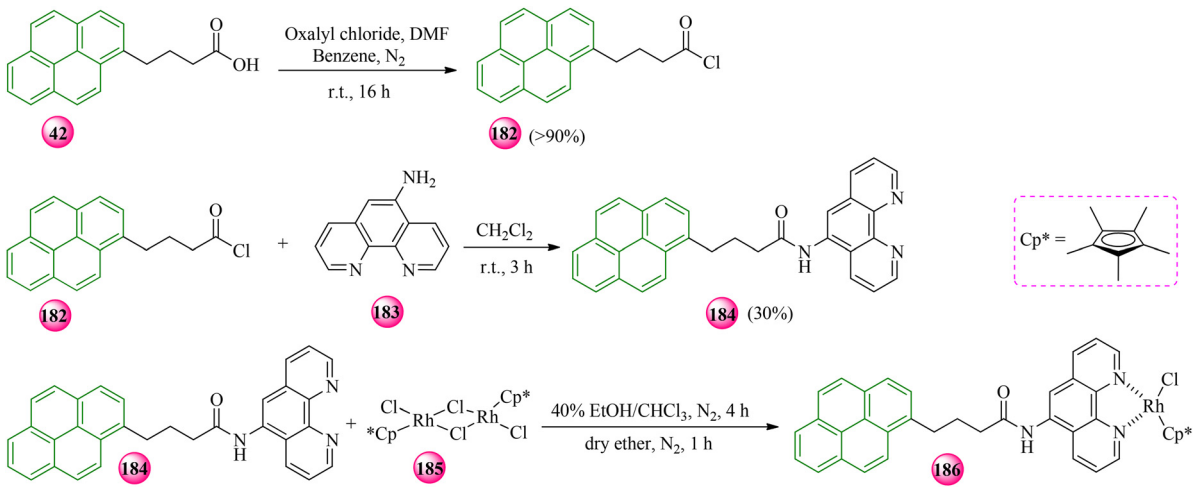

Fig. 51 Synthesis of pyrene-tagged rhodium complex **186**. Reproduced with permission from ref. 67 copyright 2015, The Electrochemical Society.

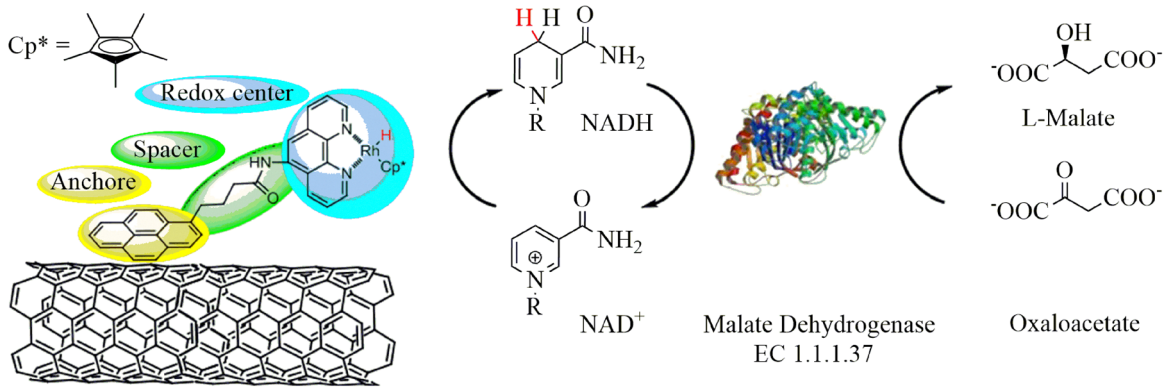

Fig. 52 Schematic illustration of the immobilized pyrene-tagged Rh redox complex onto MWCNTs. Reproduced with permission from ref. 67 copyright 2015, The Electrochemical Society.

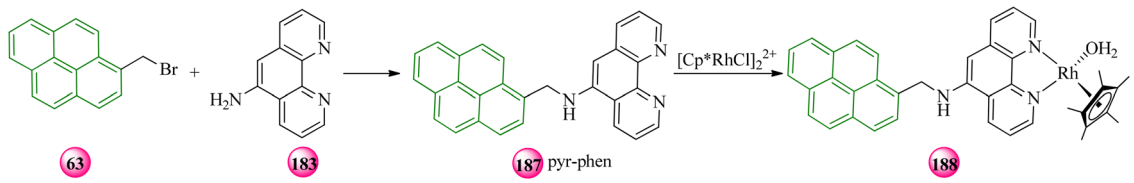

Fig. 53 Synthesis of pyrene-tagged Rh complex **188**. Reproduced with permission from ref. 68 copyright 2015, Elsevier.

leading to a change in the initial color of the solution from red to orange (Fig. 53). Finally, the powder of **188** was obtained *via* the evaporation of solvent, followed by recrystallization in methanol, and then immobilized onto rGO (Fig. 54). The results from **188** indicated a significantly enhanced rate of hydrogen production, much higher TON than the respective bare Rh catalyst, and considerably increased catalytic stability after immobilization onto rGO for the photocatalytic reaction process. Indeed, the tight immobilization of the catalyst onto rGO signifies the highest rate of hydrogen production, owing to a faster rate of electron transfer from the Rh–H ($[Cp^*(phen)Rh^{III}–H]^+$) species to rGO and then to Pt nanoparticles. Furthermore, in a comparison experiment, GO was used instead of rGO to produce hydrogen, revealing that, in contrast to **188** alone, **188** with the GO did not significantly increase hydrogen generation, showing that GO's electrical conductivity was markedly lower than rGO's. These findings highlight the pivotal role of rGO in transferring electrons efficiently to the platinum nanoparticles from the Rh(III)-hydrides.

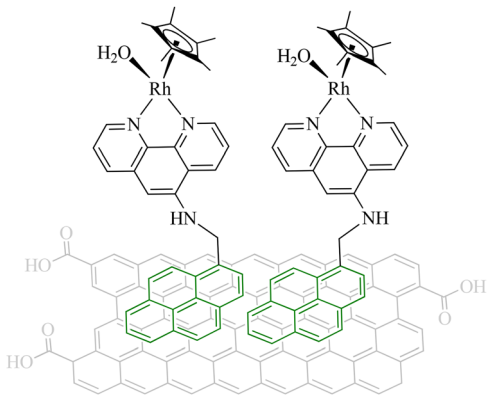

Fig. 54 The schematic illustration of the π-stacking interaction between complex **188** and rGO. Reproduced with permission from ref. 68 copyright 2015, Elsevier.

In 2018, Peris and his co-workers prepared two types of pyrene-tagged rhodium NHC complexes to evaluate the efficiency of these structures (**191** and **192**) (Fig. 55).[69] In order to obtain **191** and **192**, the imidazolium or bisazolium salts, **189** or **190**, were reacted with $[RhCl(COD)]_2$ (COD = cyclooctadiene) in a THF/DMF mixture. The addition of KBr promotes the formation of the bromide involving **191** and **192** complexes. These complexes were then immobilized onto rGO by mixing them with rGO in DCM, sonicating, and stirring, leading to a black solid followed by filtration and washing with CH_2Cl_2 (Fig. 56). The disappearance of the solution color can be visually evident for the immobilization of the catalysts onto the solid surface. The effectiveness of these complexes was evaluated by 1,4-addition of arylboronic acids to cyclohexene-2-one and the hydrosilylation of alkynes at the terminal position. According to the results from the first experiment, rGO-**191** lost 30 percent of its rhodium after five cycles, while rGO-**192** maintained its metal content throughout the nine cycles. It was found that the dimetallic complex involving two pyrene fragments was more active and recyclable than the catalyst with just one pyrene tag in both catalytic reactions, and leaching was reduced considerably after the immobilization of the metal complex onto the solid surface through more than one pyrene fragment. These results showed that the efficiency of the immobilization relies on the number of anchoring pyrene fragments on the catalyst structure. Additionally, not only does the immobilization of the

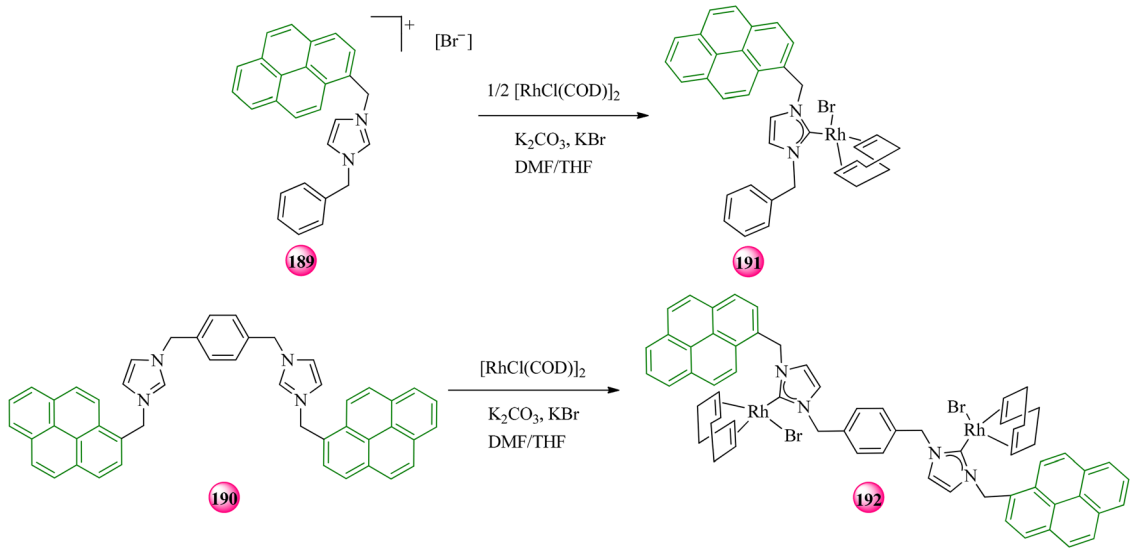

Fig. 55 Preparation of **191** and **192** complexes. Reproduced with permission from ref. 69 copyright 2018, John Wiley and Sons.

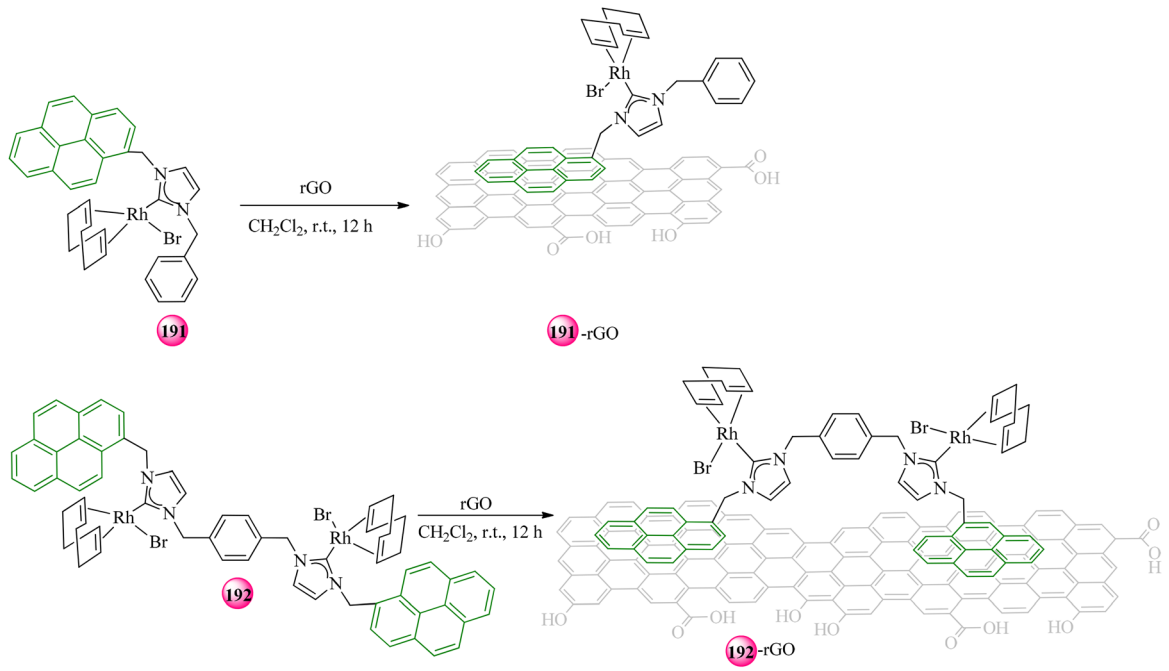

Fig. 56 The immobilization of pyrene-tagged Rh catalysts **191** and **192** onto rGO. Reproduced with permission from ref. 69 copyright 2018, John Wiley and Sons.

catalyst onto rGO make the catalysts be reused effectively, but it also enhances selectivity. The interaction of the pyrene fragments with rGO results in an effective immobilization, and the hybrid materials and their homogeneous analogues showed the same catalytic activity in the first cycle.

In 2019, Godard and co-workers reported the synthesis and immobilization of pyrene-tagged rhodium complexes onto three solid supports: rGO, MWCNTs, and carbon beads (CBS), and assessed these catalysts in the asymmetric hydroformylation (AHF) of norbornene.[70] The synthesis of two pyrene-tagged diphosphite ligands (**202** and **203**) was reported, starting with the reaction of 1,2,5,6-di-isopropylideneglucofuranose (**193**) with *N*-bromosuccinimide and triphenylphosphine, leading to the preparation of the corresponding 6-bromo derivative (**194**) and subsequently the alcohol derivatives (**195**) after treating with $NaNO_2$ (Fig. 57). The alkylation of **195** with either 1-(bromomethyl)pyrene or 4-(pyren-2-yl)butyl trifluoromethanesulfonate yielded **196** and **197**, which then underwent 3,5-acetal deprotection. The resulting diols, **198** and **199**, were then reacted with freshly synthesized phosphochloridite to provide the desired pyrene-tagged diphosphites **200** and **201**. Subsequently, the cationic complexes **202** and **203** were synthesized

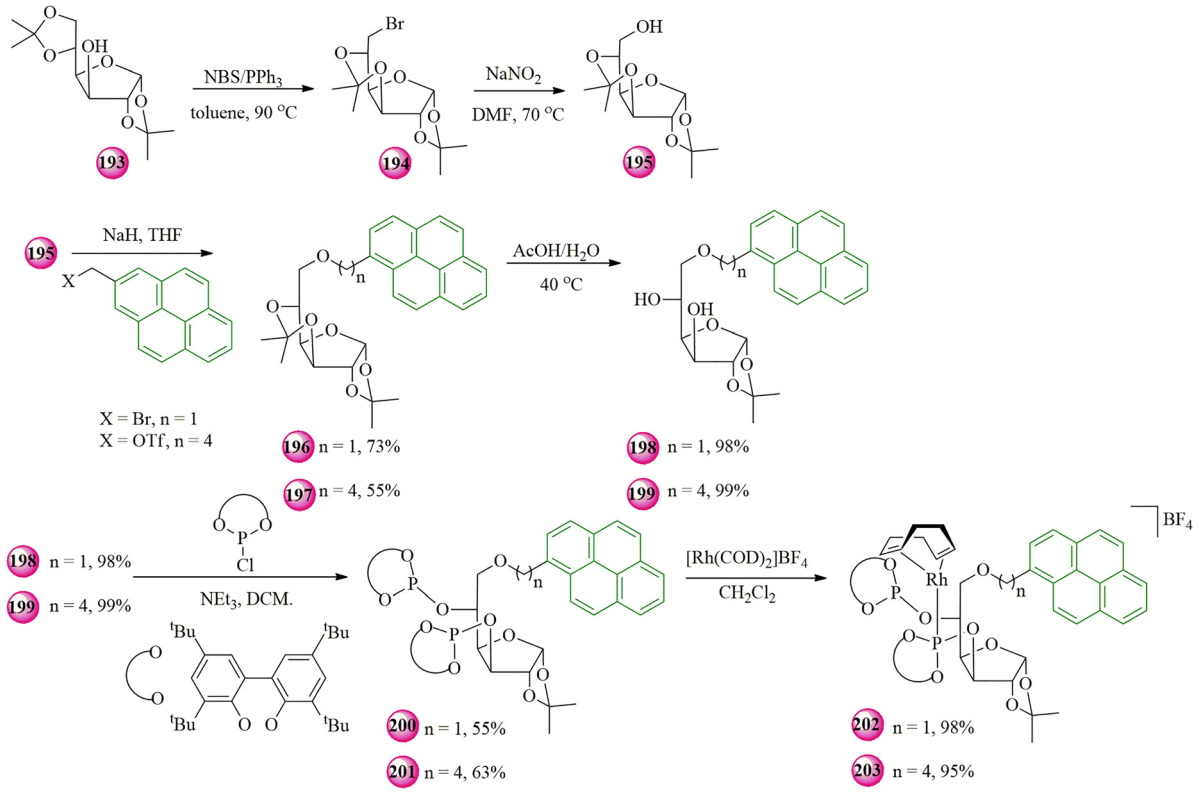

Fig. 57 Synthesis procedure for pyrene-tagged rhodium complexes **202** and **203**. Reproduced with permission from ref. 70 copyright 2019, John Wiley and Sons.

through the reaction of $[Rh(COD)_2]BF_4$ with ligands **200** and **201**. The immobilization of **202** and **203** complexes onto MWCNTs was performed by dispersing the MWCNTs in ethyl acetate, followed by adding the complexes and stirring the mixture (Fig. 58). The effect of these solid supports on the efficiency of the catalysts was studied *via* AFH experiments. Based on the obtained data under batch conditions, **203**@MWCNTs showed a higher activity than **202**@MWCNTs due to the presence of a longer chain length between the ligand backbone and the pyrene fragment; however, both of them showed lower conversion and ee's compared to their homogeneous counterparts. Nevertheless, under continuous flow conditions, **203**@MWCNTs exhibited a higher enantioselectivity than the respective homogeneous catalyst, which may be owing to an enhanced gas–liquid mass transfer. Furthermore, **203**@MWCNTs displayed lower loss in activity than rGO and CBs, possibly due to the greater surface area of rGO and CBs than MWCNTs and the strength of ligand's interactions with the solid support.

In 2020, Shi and co-workers designed a pyrene-tagged Rh complex catalyst to be *in situ* immobilized onto graphene through π–π stacking interactions to catalyze asymmetric hydrogenation of dehydroamino acid esters, allowing for high catalytic reactivity and enantioselectivity without additional chemical modifications for both solid supports and metal complex catalysts.[71] In this regard, a pyrene-tagged MonoPhos ligand (**207**) was synthesized through the straightforward reaction of 1-pyrenebutyric acid and (*R*)-[1,1′-binaphthalene]-2,2′-dimethoxy-6-butanol (**204**) and subsequent

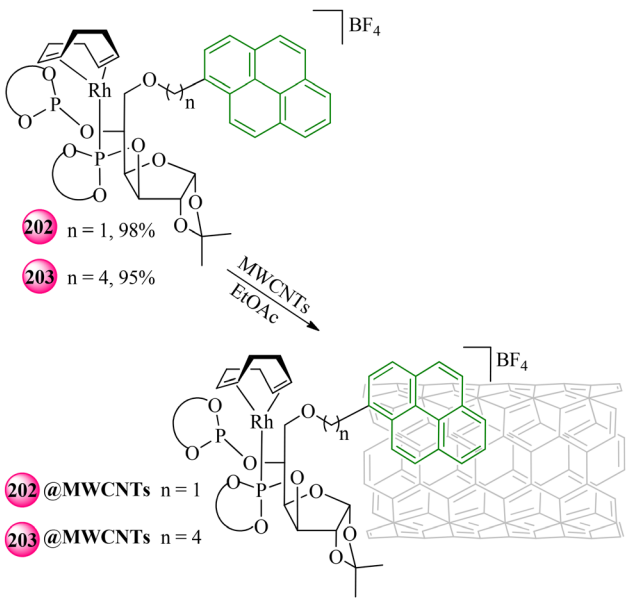

Fig. 58 The immobilization of pyrene-tagged complexes **202** and **203** onto MWCNTs. Reproduced with permission from ref. 70 copyright 2019, John Wiley and Sons.

hydroxyl deprotection and reaction with hexamethyltriamidophosphite (Fig. 59). Next, the π–π interactions between a rhodium(I) complex (**208**) and graphene were established by

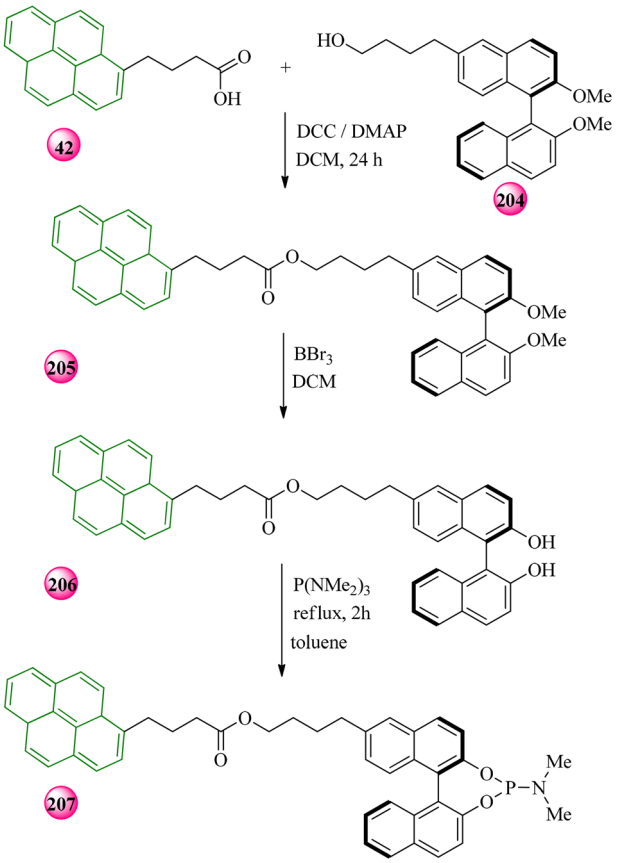

Fig. 59 Synthesis procedure of **207**. Reproduced with permission from ref. 71 copyright 2020, Royal Society of Chemistry.

first mixing the pyrene-tagged ligand (**207**) with the rhodium precursor, forming complex **208**, which was then immobilized onto the graphene surface after mixing with graphene and stirring, as indicated by the loss of the solution's original orange color (Fig. 60). The hybrid material **208**@graphene effectively catalyzes the asymmetric hydrogenation of α-dehydroamino acid derivatives under standard conditions, obtaining high conversion, enantioselectivity and activity, demonstrating its comparable performance to the homogeneous system. Additionally, the hybrid **208**@graphene material led to easy reusability and recovery, which can be separated from the reaction solution through simple cannula filtration and recharging with solvent and substrates. It has the potential to be utilized for at least 13 cycles with consistent catalytic activity and enantioselectivity. It is noteworthy that after 13 recycling reactions without releasing toxic metal ions into the products, the total Rh leaching was measured as negligible compared to its homogeneous catalyst.

4.9. Pyrene-tagged iridium complexes

Iridium complexes have been recognized as CO_2 reduction electrocatalysts since the late 1990s.[72] In 2014, Meyer, Brookhart, and co-workers synthesized a highly efficient, selective, durable, and selective catalyst for reducing CO_2 into formate electrochemically, accomplished by using π–π interactions. Accordingly, an iridium pincer catalyst tagged with pyrene (**209**) was immobilized onto CNT-modified gas diffusion electrodes (GDEs) to improve mass transfer at the gas–liquid interface (Fig. 61).[73] The immobilization of **209** was achieved by drop-casting onto GC/CNT or FTO/CNT (fluorine-doped tin oxide) electrodes. The CNT surface was then coated with a polyethylene glycol (PEG) overlayer to make it hydrophilic while retaining the electroactive surface area. The non-covalent immobilization strategy facilitates the reloading of the fresh Ir catalyst on the CNT electrode, promoting reusability. Based on the results, the catalyst showed high faradaic efficiencies, TON, and long-term performance while maintaining stability over 50 times under CO_2, proving its robust performance.

In 2015, Peris and his co-worker reported the synthesis and immobilization of two pyrene-tagged NHC iridium complexes (**214** and **216**) onto rGO surfaces that can be suitable heterogeneous catalysts for the process of borrowing hydrogen (Fig. 62).[74] Iridium complexes **214** and **216** were synthesized using similar procedures. The mixtures of either **189** or **190**, $\{IrCl(COD)\}_2$, K_2CO_3, and KBr were stirred in THF/DMF under N_2. Complex **214** was isolated by precipitation from CH_2Cl_2/hexane, while complex **216** was purified and isolated by washing with CH_2Cl_2/EtOAc. Immobilization of **214** and **216** was obtained by mixing the complexes and rGO in CH_2Cl_2, forming black solids (**214**-rGO and **216**-rGO), which was verified by the first sign of immobilization: loss of the color of the solution (Fig. 63). In order to assess these heterogeneous catalysts, β-alkylation of secondary alcohols using primary alcohols was carried out. By comparing catalysts **214** and **216** to evaluate the influence of their mono- or di-metallic nature and pyrene fragments for immobilization, it was exemplified that **216** remained active with superior recyclability over 12 runs, while **214** was deactivated after seven runs.

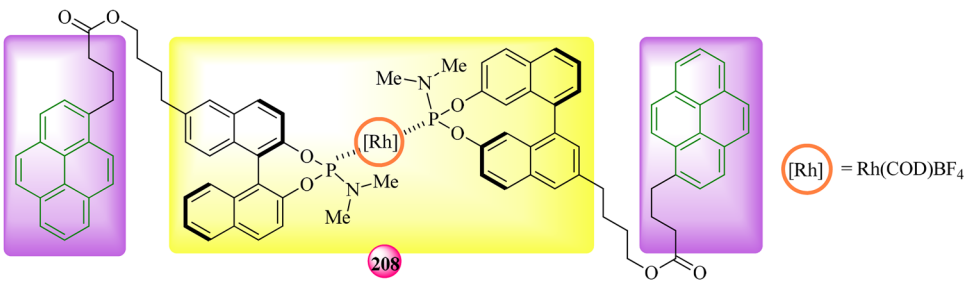

Fig. 60 Schematic structure of pyrene-tagged Rh complex **208**. Reproduced with permission from ref. 71 copyright 2020, Royal Society of Chemistry.

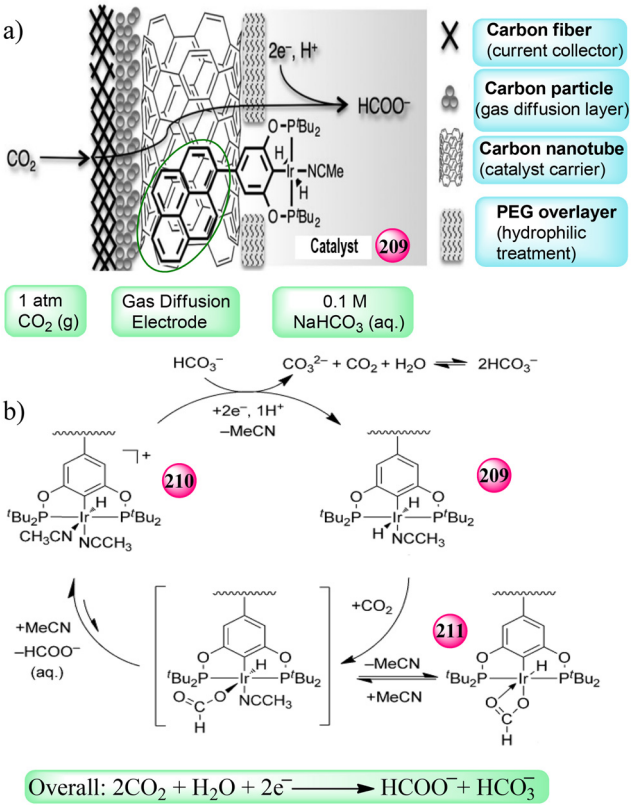

Fig. 61 (a) Representation of a carbon nanotube-coated gas diffusion electrode with surface-bound Ir pincer dihydride catalyst **209** for electrochemical reduction of CO_2 to formate. (b) Illustration mechanism for interfacial reduction of CO_2 to formate. Reproduced with permission from ref. 73 copyright 2014, John Wiley and Sons.

Notably, the extent of leaching was significant for **214** bearing one pyrene fragment; however, it was considered negligible for **216** bearing two pyrene groups.

In 2016, Reek and co-workers reported immobilized pyrene-tagged NHC $IrCp^*Cl_2$ ($Cp^* = C_5Me_5$) (**224**) onto MWCNTs and FTO surface anodes to serve as a water oxidation catalyst (Fig. 64).[75] In order to synthesize compound **224**, first, 3-dimethylamino-1-propanol (**218**) was converted to the corresponding chloride (**219**), leading to a white solid after workup, which was then deprotected under basic conditions, yielding the free amine (**220**). Subsequently, the amine was reacted with *N*-methylimidazole to prevent intermolecular reactions. After washing the reaction mixture with Et_2O, a viscous ionic liquid was obtained (**221**), which was then treated with Ag_2O in DCM, forming the silver carbene complex, followed by reaction with $\{IrCp^*Cl_2\}_2$. Finally, the hygroscopic NHC $IrCp^*Cl_2$ complex (**222**) was dissolved in anhydrous THF and reacted with 1-(bromoacetyl)pyrene (**223**), preparing compound **224** as a yellow solid. The pyrene-tagged iridium complex (**224**) was then immobilized onto MWCNTs through a typical experiment, including stirring of **224** in the presence of MWCNTs, followed by ultrasonication of the mixture, leading to a dispersed and stable MWCNT in water. The successful immobilization of compound **224** on the MWCNT surface was confirmed by reacting the modified MWCNT with the cerium ammonium nitrate in a Clark-type electrode reaction chamber (Fig. 65). Compared to unmodified MWCNTs with the same cerium ammonium nitrate concentration, a rapid visible release of oxygen (O_2) was recognized. Indeed, the MWCNT/Pyr^+ assembly was deposited onto FTO substrates and assessed as a working electrode for the electrocatalytic oxidation of water. According to the results, nanotubes containing precursor **224** exhibited initial high current densities at pH 2.0, attributed to water oxidation. In spite of promising current density, the FTO/MWCNT/Pyr^+ anode degraded at potentials exceeding 1.4 V *vs.* NHE due to oxidation of the pyrene anchoring group; therefore, for future related systems, a more stable anchoring moiety is recommended to withstand the oxidative conditions.

In 2017, Lu and co-workers reported the synthesis of a cyclometalated pyrene-tagged iridium complex (**227**), which

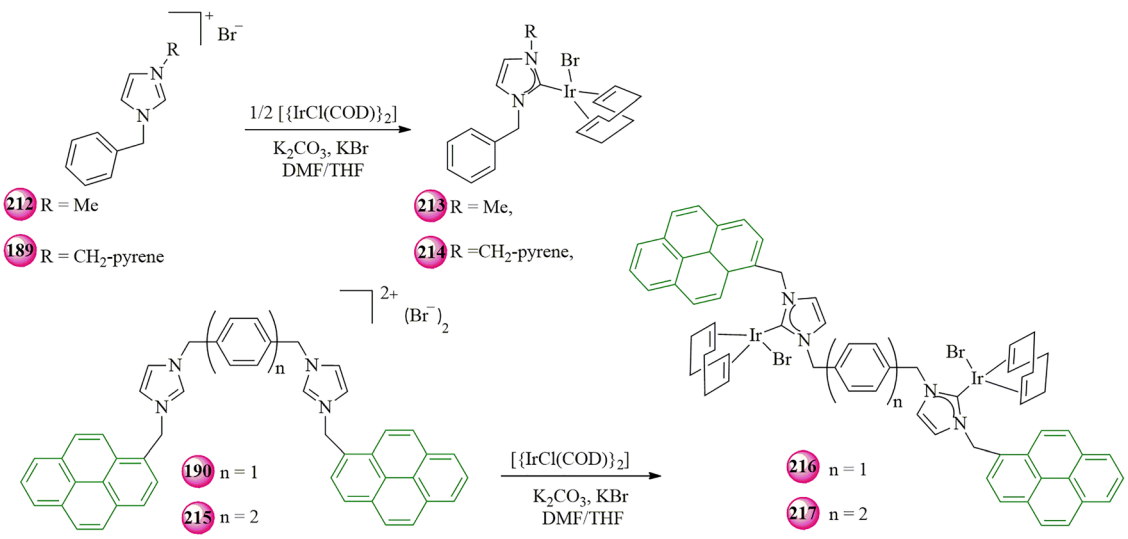

Fig. 62 The representation of the synthesis of pyrene-tagged Ir complexes. Reproduced with permission from ref. 74 copyright 2015, John Wiley and Sons.

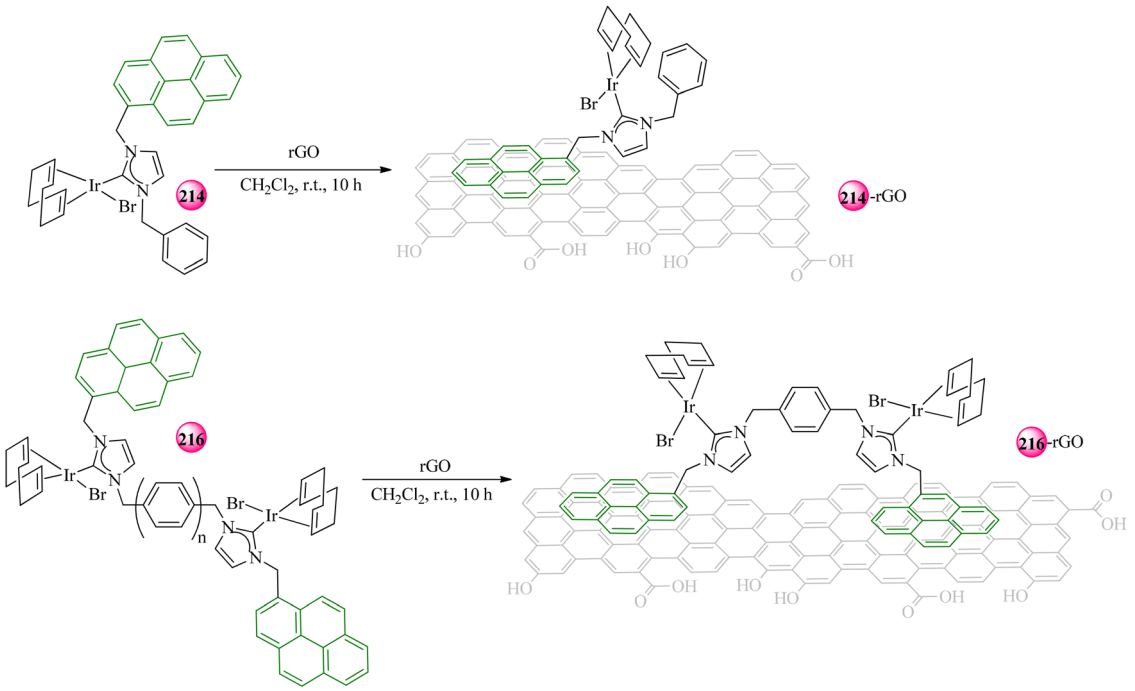

Fig. 63 The immobilization of pyrene-tagged Ir catalysts **214** and **216** onto rGO surfaces. Reproduced with permission from ref. 74 copyright 2015, John Wiley and Sons.

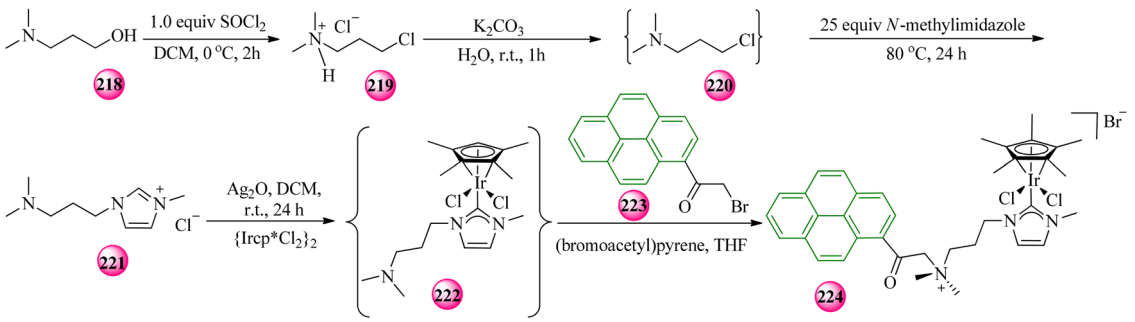

Fig. 64 The synthetic procedure for pyrene-functionalized catalyst **224**. Reproduced with permission from ref. 75 copyright 2016, John Wiley and Sons.

was then immobilized on MWCNTs by π–π stacking interactions to dehydrogenate indolines in aqueous solution (Fig. 66).[8] Iridicycle **225** was synthesized by reacting $[Cp^*IrCl_2]_2$, NaOAc, and an imine ligand in CH_2Cl_2 under an inert atmosphere. This iridicycle was then reacted with 1-pyrenesulfonyl chloride (**226**), Et_3N, and THF under an inert atmosphere and stirring under reflux, eventually leading to an orange solid of iridicycle **227**. To immobilize **227** onto MWCNTs, the pyrene-tagged compound was dissolved in THF, followed by adding MWCNTs, treating with water, centrifuging, and drying the collected catalyst. Since the choice of solvent may be essential for immobilizing iridicycle **227** onto MWCNTs, water was added to the THF solution, improving polarity, decreasing solubility, and strengthening MWCNT stacking, effectively facilitating the immobilization of iridicycle **227** on MWCNTs. In order to evaluate the performance of **227**-rGO in an aqueous solution, a reaction of indoline catalytic dehydrogenation (CDH) using H_2O/trifluoroethanol was carried out. Based on the obtained results, the **227**-rGO catalyst, as a heterogeneous catalyst, demonstrated high activity and performed successfully and repeatedly for at

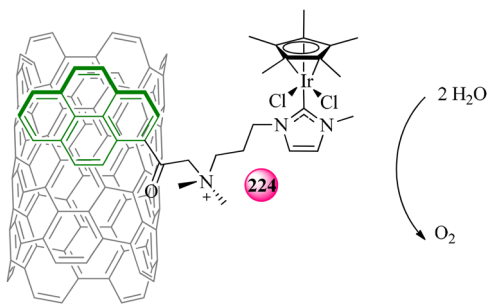

Fig. 65 The representation of immobilization of pyrene-tagged iridium complex **224**. Reproduced with permission from ref. 75 copyright 2016, John Wiley and Sons.

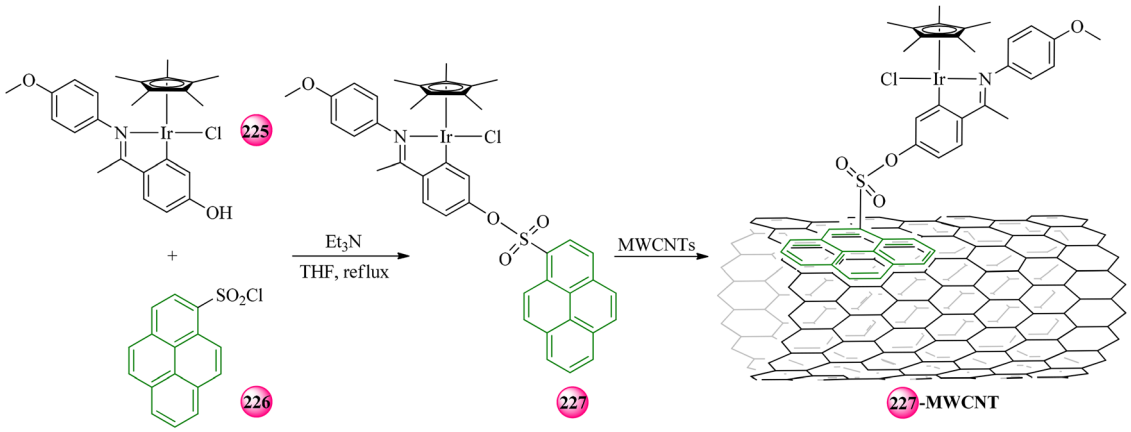

Fig. 66 The synthesis procedure for the immobilization of iridicycle **227** onto MWCNTs. Reproduced with permission from ref. 8 Copyright 2017, American Chemical Society.

least seven cycles during the CDH process, with minimal loss; therefore, an effective catalyst system was achieved thanks to this immobilization technique. Additionally, the fluorescence spectroscopy technique was applied to monitor the immobilized **227**, revealing the extent of **227**'s leaching from the surface of MWCNTs, which was considered negligible.

In 2023, Koepf, Gennari, and co-workers found a strategy to immobilize a pyrene-tagged iridium pincer catalyst onto MWCNTs *via* non-covalent π–π stacking for CO_2 reduction to $HCOO^-$ with a dramatically low overpotential in aqueous solution.[76] In order to synthesize a pyrene-tagged Ir complex (**234**), 1-(4-bromobutyl)pyrene (**5**) was reacted with diethyl 4-hydroxypyridine-2,6-dicarboxylate (**228**) to form derivative **229**, linking the pyrene and pyridine moieties through an ethereal bond *via* a Williamson-type reaction (Fig. 67). Subsequent selective reduction of the ethyl esters with $LiBH_4$ and tosylation of the resulting diol produced the reactive electrophile **231**, which can engage in nucleophilic substitution with bis-*tert*-butyl

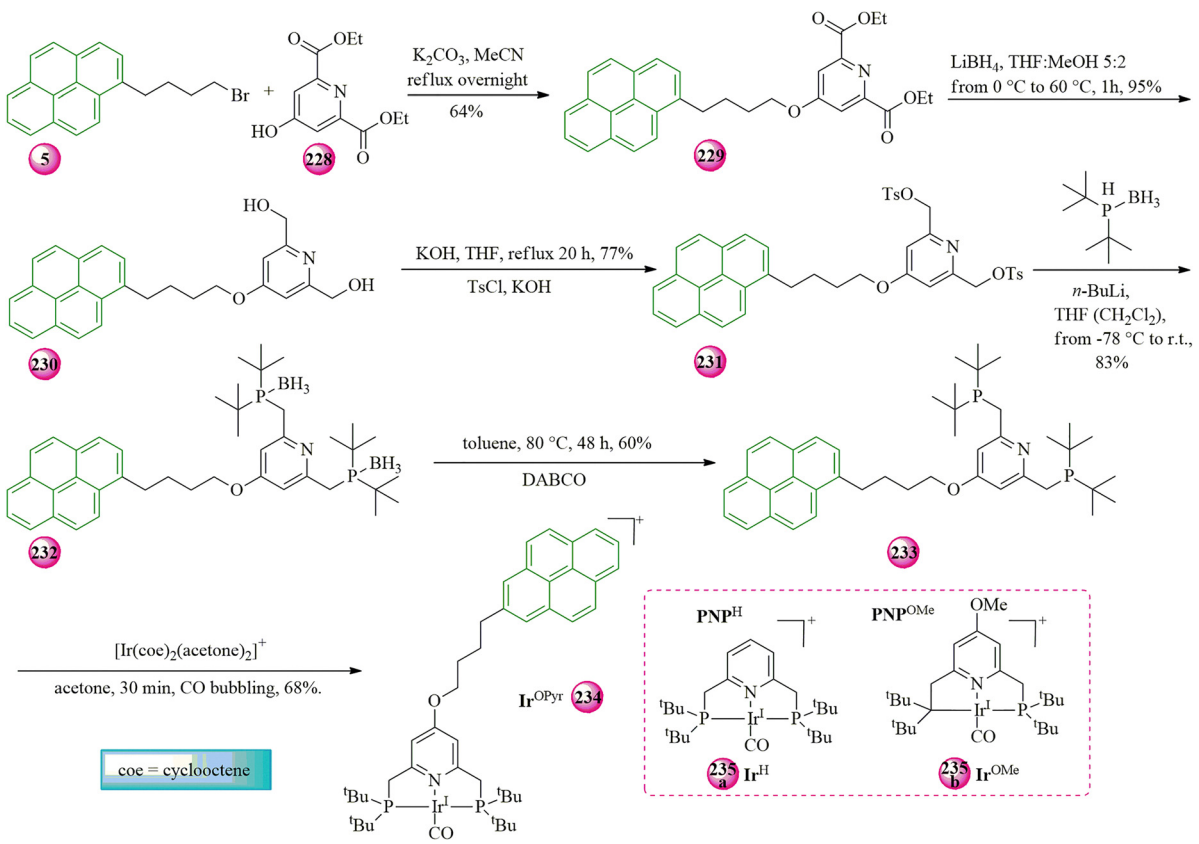

Fig. 67 The synthesis procedure for the ligand PNP^{OPyr} (**233**) and the schematic structure of Ir^{H} (**235a**) and Ir^{OMe} (**235b**). Reproduced with permission from ref. 76 copyright 2023, John Wiley and Sons.

phosphine, leading to **232**, followed by isolation of **233** after deprotection of the phosphines. Next, $[Ir(coe)_2(acetone)_2]PF_6$ (coe = cyclooctene) was introduced into the solution of **233** in acetone to obtain **234**. The immobilized **234** was obtained by adding **234** and Nafion to pre-sonicated MWCNTs in CH_3CN, leading to an ink, which was subsequently deposited on the GC electrode. Electrochemical properties of **234** were examined through CV in DMF with $^nBu_4NPF_6$ using a GC working electrode under an Ar atmosphere. The reference complexes Ir^H (**235a**) and Ir^{OMe} (**235b**), lacking the pyrene fragment, showed an irreversible reduction peak for Ir^H corresponding to the first monoelectronic reduction of the {(PNP)Ir} (PNP = phosphorus–nitrogen–phosphorus) unit. In contrast, **235b** exhibited a more cathodic potential due to its methoxy group. Additionally, **234** displayed two irreversible cathodic potential peaks followed by a reversible one, indicating a diffusion-controlled process, along with a reversible peak assigned to one-electron reduction of the pyrene moiety, respectively. Moreover, CV analysis of electrodes coated with **234**@MWCNTs revealed slightly higher cathodic currents under CO_2 than bare MWCNTs, suggesting moderate CO_2 reducing reaction (CO_2RR) activity of the hybrids in water. Notably, following immobilization, selective $HCOO^-$ production was preserved even in pure water, along with a noticeable CO_2RR overpotential reduction, while demonstrating high stability under turnover conditions.

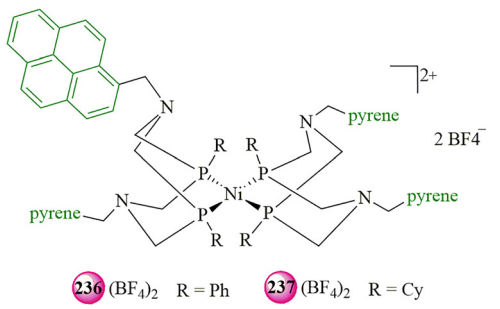

Fig. 68 Schematic representation of pyrene-tagged Ni complexes (**236** and **237**). Reproduced with permission from ref. 77 copyright 2011, John Wiley and Sons.

4.10. Pyrene-tagged nickel complexes

In 2011, Jousselme, Artero, and their co-workers reported the immobilization of two types of pyrene-tagged nickel complexes (**236** and **237**), which function as CO tolerant and robust catalysts for hydrogen evolution and uptake.[77,78] To synthesize $[Ni(P_2^{Ph}N_2^{CH_2Pyrene})_2](BF_4)_2$ (**236**$(BF_4)_2$), $[Ni(MeCN)_6](BF_4)_2$ was stirred in MeCN with $P_2^{Ph}N_2^{CH_2Pyrene}$, resulting in an orange powder after filtration and washing with Et_2O (Fig. 68). $Ni(P_2^{Cy}N_2^{CH_2Pyrene})_2](BF_4)_2$ (**237**$(BF_4)_2$) was prepared using the same nickel complex, yielding a red powder, upon similar processing. In the next step, a solution of either **236**$(BF_4)_2$ or **237**$(BF_4)_2$ in dichloromethane was filtered over a prepared MWCNTs/GDL electrode (GDL = gas diffusion layers) (Fig. 69). The electrode was then washed with acetonitrile to eliminate any unimmobilized nickel complexes and underwent air-drying, leading to **236**$(BF_4)_2$ or **237**$(BF_4)_2$/MWCNTs/GDL. These molecularly engineered materials maintained their activity in the presence of CO, which is essential for overcoming a major challenge for H_2 fuels to improve the technology of Nafion-based proton-exchange membrane (PEM) fuel cells. Additionally, these catalysts exhibited no activity loss after 6 hours. They showed high TONs as well, confirming these catalysts' robustness and lack of leaching, confirmed by chronoamperometric measurements at −0.3 V *vs.* NHE. Notably, the material from **237**$(BF_4)_2$ was found to be slightly more efficient for H_2 oxidation than that from **236**$(BF_4)_2$, verified by the study of solutions.

In 2020, Li, Fontecave, and co-workers developed an efficient and selective electrocatalyst for the reduction of CO_2 into CO under specific conditions using functionalized CNTs by pyrene-tagged nickel cyclam (cyclam = 1,4,8,11-tetraazacyclotetradecane) $[Ni(cyclam)]^{2+}$ through π–π interactions.[79] In order to synthesize $[Ni^{II}(Cl)(L)]Cl$ (**242**) (L = **241**), initially, **239** was prepared by dissolving 1-aminopyrene and NEt_3 in CH_2Cl_2, followed by the addition of chloroacetyl chloride (Fig. 70). Subsequently, **239**, cyclam (**240**), K_2CO_3, and KI were reacted

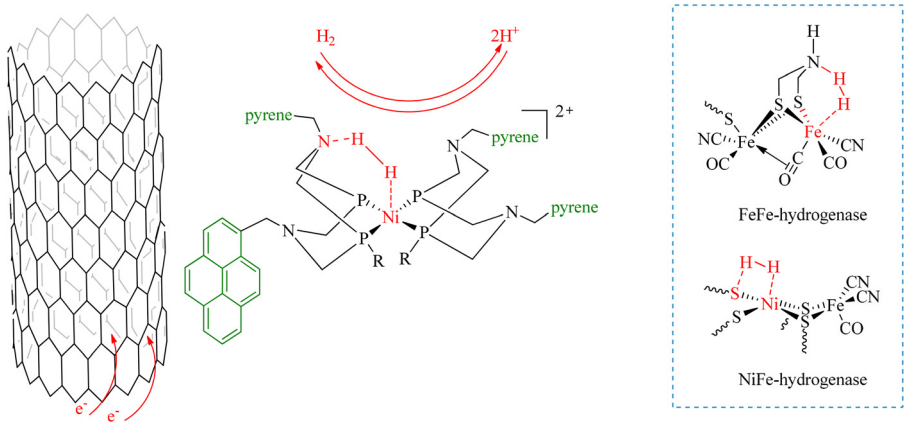

Fig. 69 Structure of the Ni–CNT H_2 oxidation reaction (HOR) catalyst based on a synthetic nickel bisdiphosphine complex inspired by the structures of the active sites of FeFe and NiFe hydrogenases. Reproduced with permission from ref. 78 copyright 2015, John Wiley and Sons.

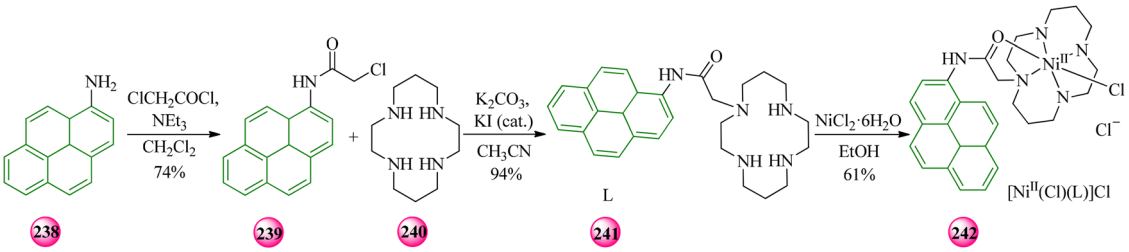

Fig. 70 The synthesis of pyrene-tagged Ni complex **242**. Reproduced with permission from ref. 79 copyright 2020, John Wiley and Sons.

together in CH_3CN, leading to off-white powder of **241**. Then, a solution of **241** was introduced into a $NiCl_2{\cdot}6H_2O$ solution in ethanol, and it was observed that the pale green solution quickly shifted to orange, then dark pink, and finally a pink–purple **242** complex after evaporation, dissolution, and ether diffusion. The immobilization process started with sonication of MWCNTs in ethanol and Nafion, followed by drop casting onto a GDL, made of carbon fiber cloth coated with a microporous Teflon layer. The obtained MWCNT/GDL electrode was subsequently immersed in a solution of complex **242** in DMF. The electrochemical results of **242** revealed a distinct one-electron reduction of Ni(II) to Ni(I), emphasizing its enhanced electron-enriched state owing to further electron-donating ligands. The complex was selective for CO_2 reduction while possessing weak activity. On the other hand, compared to its homogeneous counterpart, **242**/MWCNT/GDA exhibited better activity, current density, and TON while maintaining its selective feature, leading to one of the best systems for the electroreduction of CO_2 through the $[Ni(cyclam)]^{2+}$ catalyst.

In 2022, Cavazza, Goff, and co-workers designed an immobilized pyrene-tagged triazacyclononane Ni complex onto CNT electrodes as a practical and stable catalyst for the CO_2 reducing reaction (Fig. 71).[80] Initially, compound **243** reacted with 1-pyrenylmethyl bromide, and the resulting compound (**244**) was hydrolyzed to obtain the formyl derivative (**245**), which was then reacted with ethylbromoacetate to prepare **246** as an ester derivative. The obtained product was deprotected by losing formyl and ester groups and led to an insoluble green solid, 1-acetato-4-(1-pyrenyl)-1,4,7-triazacyclononane (AcPyTACN) (**247**). Next, MWCNTs were functionalized *via* an incubation process with a solution of pyrene in DMF and $NiCl_2$, leading to immobilized Ni-AcPyTACN on MWCNT. The final modification of MWCNT electrodes was performed by another incubation process in the presence of His-tagged recombinant carbon monoxide dehydrogenase from *Rhodospirillum rubrum* (Rec-*Rr*CODH^{His}). Notably, the Ni-**247**/MWCNT electrode, lacking immobilized CODH, demonstrated no electrocatalytic response. The results highlight the superior performance of Ni-**247** in immobilizing Rec-*Rr*CODH^{His} and indicate the involvement of the His-tag in enzyme immobilization. Indeed, the high-performance CODH enzyme associated with a pyrene anchor enabled efficient and stable CO_2 reduction with improved O_2 tolerance as well. Moreover, the stability of different kinds of electrodes was evaluated under constant potential. Based on the obtained results, nonmodified MWCNTs, MWCNTs modified with pyrene^{ADA}, and immobilized Rec-*Rr*CODH on AcPyTACN-modified electrodes retained their residual activity of 22%, 29%, and 43%,

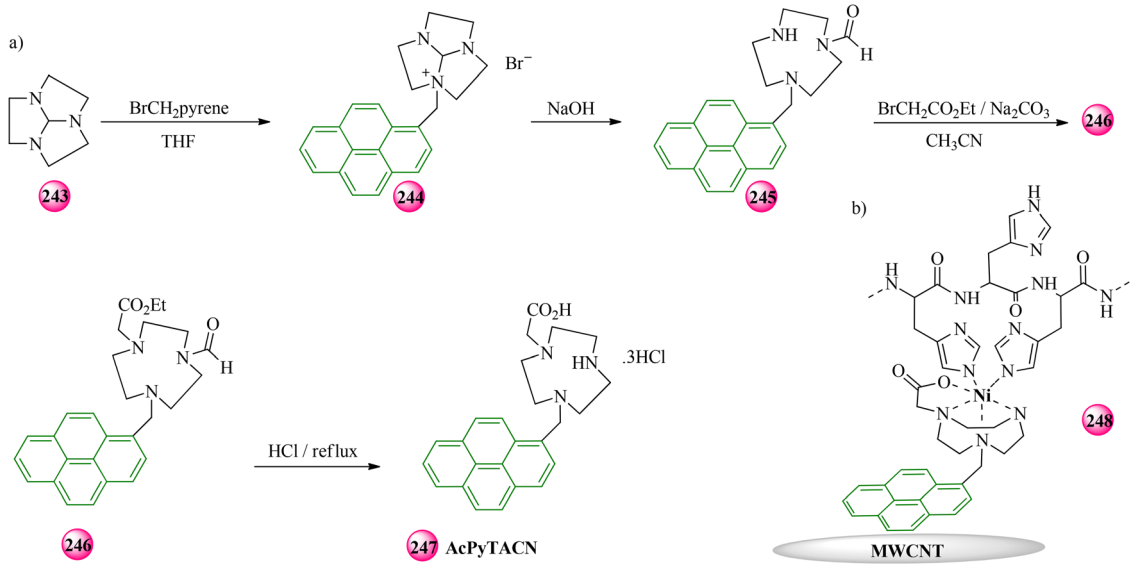

Fig. 71 The illustration of (a) the synthesis procedure for AcPyTACN and (b) Ni complexes formed from AcPyTACN/MWCNTs for the binding of histidine-tagged enzymes. Reproduced with permission from ref. 80 copyright 2022, John Wiley and Sons.

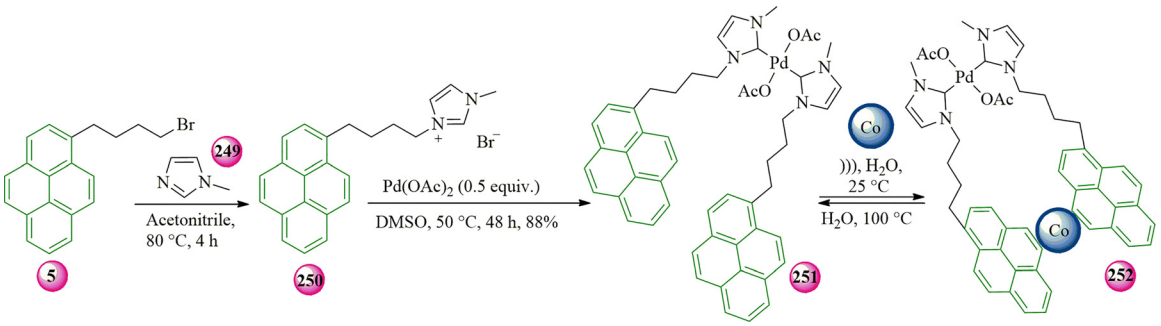

Fig. 72 Synthesis of pyrene-tagged palladium NHC complex **251** and reversible immobilization on Co/C-nanomagnets. Reproduced with permission from ref. 81 copyright 2010, John Wiley and Sons.

respectively. However, immobilized Rec-*Rr*CODH^{His} onto Ni-AcPyTACN-modified MWCNTs indicated a high residual activity (85%) and high TON, revealing outperforming stability compared to the other configuration and opening new prospects of immobilized enzymes for electrocatalysis applications.

4.11. Pyrene-tagged palladium complexes

In 2010, Reiser and co-workers reported a pyrene-tagged palladium complex, which was further immobilized on the graphene layer of the Co/C nanoparticles *via* π–π stacking interaction and used for the hydroxycarbonylation of aryl halides in water at 100 °C under atmospheric CO pressure.[81] In order to synthesize the pyrene-tagged palladium NHC complex (**251**), 1-(4-bromobutyl) pyrene (**5**) was first fused with 1-methylimidazole (**249**) to form a ligand precursor (**250**) and subsequently respective complex, **251** (Fig. 72). Next, the immobilization of the complex (**251**) onto cobalt nanoparticles was successfully achieved by dispersing Co/C nanoparticles in water and sonicating them with excess complex (**251**), leading to the immobilized catalyst (**252**). The catalyst (**252**) exhibited high activity throughout 16 reaction cycles of hydroxycarbonylation of 4-iodophenol and varied aryl halides with CO in water. Notably, since this noncovalent immobilization is temperature-sensitive in polar solvents, the "boomerang"-type catalyst may undergo dissociation from its heterogeneous support to the homogeneous phase at higher temperatures.

In 2013, Caminade, Majoral, Ouali, and their co-workers reported the immobilization of pyrene-tagged dendritic Pd catalysts onto MNPs involving Co/C for drug synthesis.[82] In order to synthesize the pyrene-tagged Pd–phosphine, initially, **42** and tyramine **253** were reacted, leading to a derivative **254** (**254** = ROH), which subsequently reacted with $N_3P_3Cl_6$ (**255**) and Cs_2CO_3 to form **256** (Fig. 73). Indeed, this dendron growth involved the reaction of P–Cl bonds with the phenolic group of 4-OH–C_6H_4–CHO and subsequent condensation with $H_2NNMeP(S)Cl_2$ to yield the first-generation of dendron (**259**). The Cl-terminated dendrons, including **256** and **259**, reacted with phosphine HO–C_6H_4–PPh_2 to produce pyrene-tagged multivalent phosphines (**258** and **260**). Finally, monomeric pyrene-tagged phosphine **263** was synthesized from **261** and phosphine **262**. In order to evaluate the efficiency of the catalyst and its recyclability, $Pd(OAc)_2$, Co/C NP, and **258**, **260**, and **263** ligands were added under argon to a Radley tube, followed by several processes. Based on the obtained Suzuki coupling reaction data, pyrene-tagged Pd complexes demonstrated good to excellent yields, with product yields of 70% to 98%. Regarding recyclability, a dendritic effect was noted, with the most effective catalyst, possessing ligand **258**, having the potential to be easily recovered by magnetic decantation and reused for at least 12 cycles without losing activity. Notably, Pd leaching met pharmaceutical industry limits for metal residues (<5 ppm Pd)

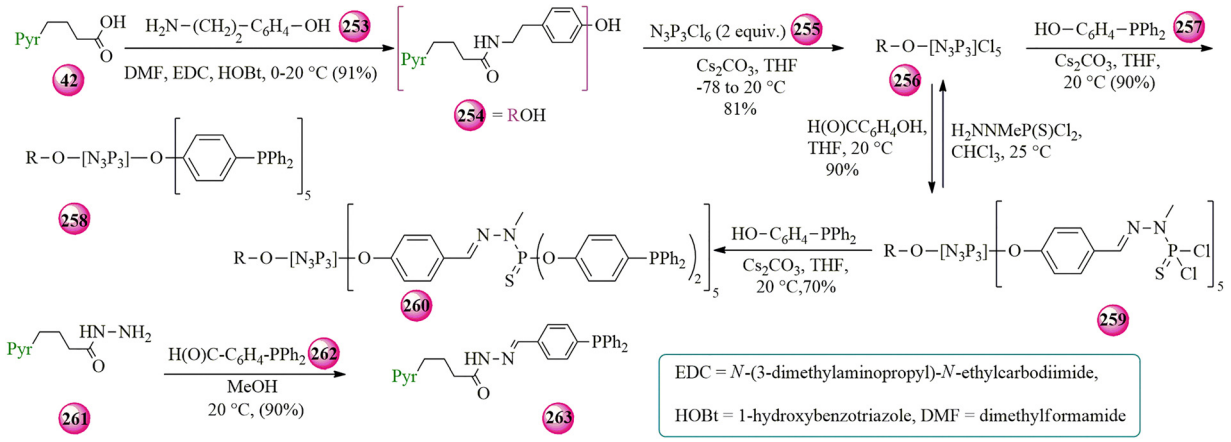

Fig. 73 Synthesis of pyrene (Pyr)-tagged phosphines **258**, **260**, and **263**. Reproduced with permission from ref. 82 copyright 2013, John Wiley and Sons.

after simple extraction with CH_2Cl_2 without the need for chromatographic purification attempts. Ultimately, the ligand's immobilization through reversible π-stacking interactions allows the catalysts to be practical in a solvent/water mixture at 60 °C, broadening their application to non-water-soluble substrates.

In 2014, Mata, Peris, and their co-worker reported a pyrene-tagged NHC–palladium complex, which was then immobilized onto rGO, as depicted in Fig. 23.[5] When **65** reacted with $[Pd(dmba)OAc]_2$ (dmba = cyclo-orthometalated *N*,*N*-dimethyl benzylamine) in the presence of KBr, it led to NHC–Pd(II) complex **68**, which was then immobilized onto rGO to yield NHC–Pd–rGO (**70**). The ^1H NMR spectrum of the filtrate revealed the absence of any trace of **68** in the solution as the initial proof of the quantitative deposition of **68** onto rGO. Catalyst **70** was tested using molecular hydrogen to investigate catalyst activity in the hydrogenation of unsaturated organic substrates, which verified **70** as a highly effective catalyst for various substrates. Additionally, in another evaluation experiment, **70** showed efficient catalytic performance (in low H_2 pressure and short time) in nitroarene reduction, which is a beneficial process in pharmaceutical and fine chemical synthesis. Furthermore, the recyclability of catalyst **70** was evaluated by using styrene as the model substrate, demonstrating that catalyst **70** could be recycled up to ten times without reducing activity. However, the slight loss of metal content percentage could be a result of mass gain during the several cycles owing to the adsorption of substances from the reactions; thus, it may not be attributed to the leaching or desorption of the metal complex.

As explained in Section 4.5, these researchers have developed a way to co-immobilize palladium and ruthenium complexes onto rGO using pyrene-tagged NHC ligands (Fig. 24).[9] In order to evaluate the activity of the hybrid material, palladium (**68**) and ruthenium (**67**), the hydrodefluorination of the fluoroarenes reaction was carried out. Notably, the supported catalysts required activation through a 24-hour refluxing process in iPrOH with *t*BuONa before their utilization in catalytic reactions. The results indicate that, although rGO–Pd exhibits a much lower activity in hydrodefluorination than rGO–Ru–Pd (**71**), the superior performance of **71** with even lower palladium loading confirms the essential synergistic role of the two metals. On the one hand, palladium nanoparticles facilitate the activation of C–F, which may be attributed to the catalyst activation during the progress of the reaction, potentially caused by the gradual formation of the palladium nanoparticles. On the other hand, the ruthenium heterogenized complex promotes hydrogen introduction through transfer hydrogenation, which can highlight their collaborative effect on the catalyst's exceptional performance. Recycling experiments of hydrodefluorination of fluorobenzene in the presence of catalyst **71** were conducted to determine whether catalyst **71** could be reused without losing its catalytic activity. The findings verify that the catalyst has the potential for practical applications due to being reused for up to 12 cycles without significant activity loss.

In 2019, Karami and co-workers synthesized a compound of pyrene-tagged ($[Pd\{(C,N)C_6H_4CH_2NH(Et)\}(Imd\text{-}P)Br]$) (NHC)Pd–rGO (**268**) through a straightforward process, based on π–π interactions to be used as a heterogeneous catalyst (Fig. 74).[83] In order to synthesize **267**, initially, the imidazolium salt (**266**) was synthesized through the alkylation of methylimidazole with 1-(bromoacetyl)pyrene (**223**), which was subsequently converted into the (NHC)Pd complex by reacting it with a palladacycle dimer $[Pd\{(C,N)C_6H_4CH_2NH(Et)\}(\mu\text{-}OAc)]_2$ (**265**). The reaction occurred in the presence of KBr, facilitating the formation of a bromide-containing complex **267**, which was entirely stable when exposed to air and moisture. In the next step, **267** was immobilized onto the surface of rGO by mixing the respective complex and rGO in dichloromethane, leading to the loss of the

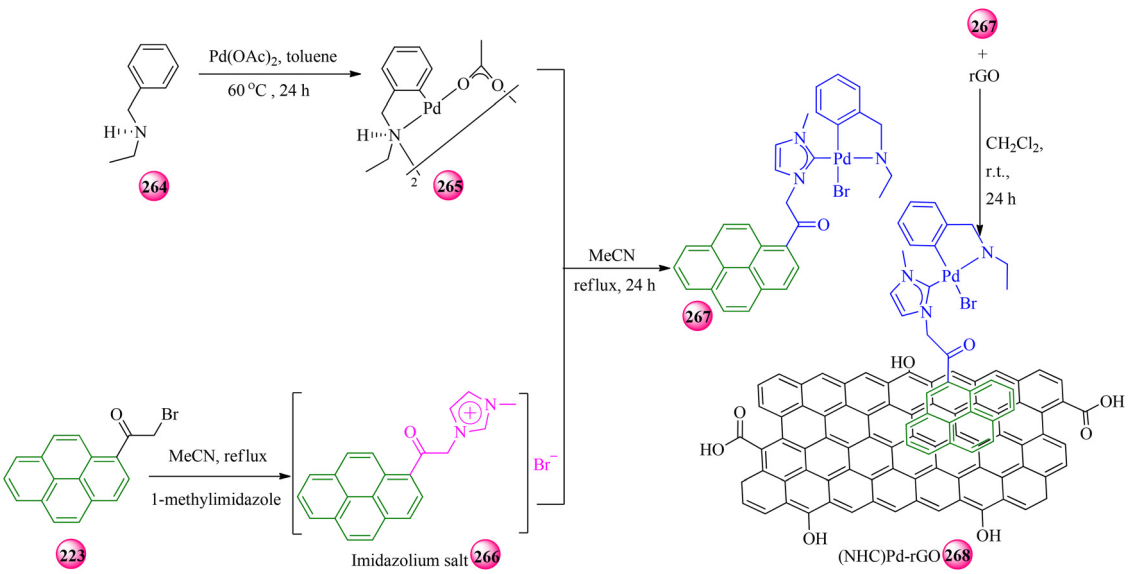

Fig. 74 Synthetic procedure of the ($[Pd\{(C,N)C_6H_4CH_2NH(Et)\}(Imd\text{-}P)Br]$) (NHC)Pd–rGO hybrid material. Reproduced with permission from ref. 83 copyright 2019, John Wiley and Sons.

solution color, which was the first sign that the (NHC)Pd complex had immobilized on the rGO surface and led to the preparation of the hybrid (NHC)Pd–rGO catalyst (**268**). The two-dimensional structure of graphene promotes complete accessibility to all catalytically active centers. To investigate the efficiency, activity, stability, and recyclability of **268**, Suzuki–Miyaura cross-coupling reactions of several aryl halides with phenylboronic acid were carried out. In addition to its high efficiency, it was determined that this reaction produced a nontoxic boronic acid as a by-product and high functional groups tolerance. Based on the obtained results, **268** can be reused for up to six cycles while maintaining its activity. Indeed, the stability and reusability of **268** may be attributed to the non-covalent interactions between the pyrene moiety and the solid support. In the other experiment, the catalytic activities of **267** and **268** catalysts were also evaluated in the reduction of *p*-nitrophenol to *p*-aminophenol using $NaBH_4$ in an aqueous medium at room temperature. Based on the obtained results, not only did **268** play a vital role in facilitating the surface reduction of *p*-nitrophenol to *p*-aminophenol, but **267** also had a positive effect on the catalyst system through Pd nanoparticles, as no reduction was observed in their absence.

In 2023, Guisado-Barrios, Mata, and co-workers reported the synthesis of a pyrene-tagged (NHC)Pd (**270**), its immobilization onto rGO (**270**-rGO), and its decomposition in the presence of H_2 to form Pd nanoparticles **270**-rGO–NPs (Fig. 75).[84] It was then used as a catalytic system for the hydrogenation and dehydrogenation of N-heterocyclic compounds. In order to synthesize **270**-rGO and then **270**-rGO–NPs, an imidazolium salt **269** was initially mixed with palladium(II) bromide, K_2CO_3, and 3-chloropyridine in a Schlenk flask. Subsequently, rGO was suspended in CH_2Cl_2, followed by ultrasonication, adding **270**, and stirring the mixture, which was isolated and washed with CH_2Cl_2 to form the hybrid material **270**–rGO. Finally, the reaction of **270**-rGO, Cs_2CO_3, and toluene, and introducing hydrogen gas into the system, afforded **270**-rGO–NPs. According to data from Raman spectroscopy, the incorporation of the molecular complex **270** or the formation of PdNPs does not change the relative intensity of the graphitic and defect bands. The efficiency of the **270**-rGO–NP catalyst was evaluated in the (de)hydrogenation of N-heterocyclic compounds. The Pd nanoparticles serve as active sites for hydrogenation by H_2, while rGO functions as both a carbocatalyst in acceptorless dehydrogenation and a support for palladium nanoparticles, enhancing their interaction with molecular hydrogen. Based on the obtained results, the stabilization of Pd nanoparticles *via* NHC ligands, along with the use of graphene for support, allows for the reuse of **270**-rGO–NPs in up to eight (de)hydrogenation cycles. Moreover, hot filtration experiments confirmed the heterogeneous nature of the process, which demonstrated a strong interaction between palladium nanoparticles and graphene, assisted by π-interactions of the ligand and the support.

4.12. Pyrene-tagged copper complexes

In 2013, Schulz and co-workers reported an immobilized pyrene-tagged Cu complex involving a bis(oxazoline) ligand onto different carbon supports, including charcoal, fullerene, and SWCNTs, to improve the asymmetric copper catalyst's ability.[85] It can be attributed to the pyrene moiety enabling π–π interactions with carbon supports for enhancing hybrid asymmetric Henry and ene reactions. The synthesis of the pyrene-tagged complex started from the deprotonation of bis(oxazoline) compound **271**, followed by the addition of a mesylate derivative **272** (derived from 4-(pyren-1-yl)butan-1-ol), which formed the intermediate compound **273**. Further deprotonation of compound **273** then enabled the introduction of a methyl group, consequently leading to the final targeted ligand **274** (Fig. 76). In the next step, to immobilize ligand-**274** onto the solid supports, ligand **274** was dissolved in DCM and added to $Cu(OTf)_2$, followed by introduction into charcoal, C_{60}, or SWCNT containing tubes. The ene reaction between ethyl glyoxylate and α-methyl styrene was chosen as an experiment to assess the catalytic systems. According to the results, all three supported catalysts showed high yields of the intended product in the first run. However, the selectivity of the transformations is different, *i.e.*, **274**-$Cu(OTf)_2$@charcoal had lower enantioselectivity compared to **274**-$Cu(OTf)_2$@fullerene, probably due to the fullerene structure modifying the complex intermediate. Ultimately, SWCNTs were found to be the best support among the others, offering consistently high yield and enantioselectivity values through all catalytic cycles, even in comparison with a fresh promoter.

In 2016, Thomas, Goff, and co-workers reported the synthesis of a bio-inspired mononuclear pyrene-tagged copper phenolato complex (**277**), which has the potential to mimic the

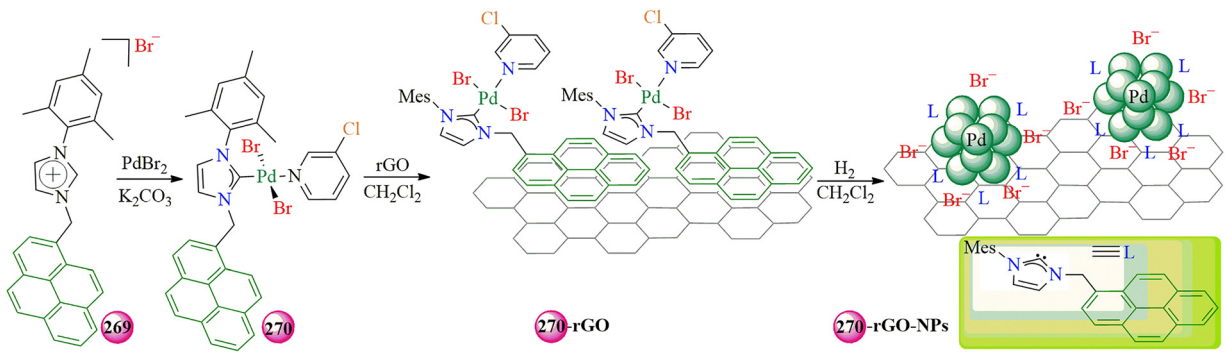

Fig. 75 Bottom-up synthetic procedure of pyrene-tagged palladium nanoparticles immobilized onto graphene. Reproduced with permission from ref. 84 copyright 2023, Elsevier.

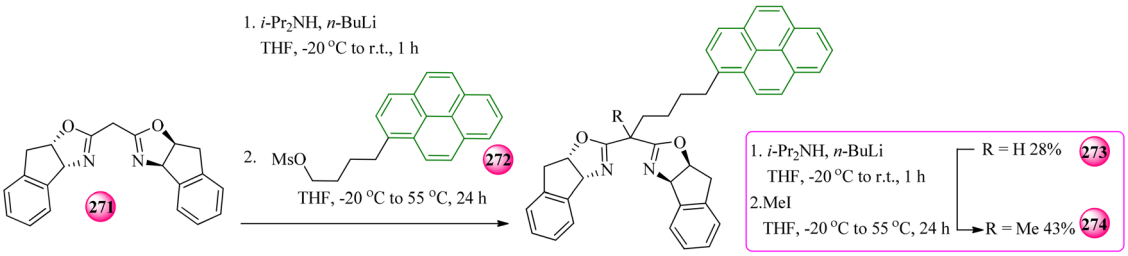

Fig. 76 Synthesis of the pyrene-tagged complex with bis(oxazoline) ligand **274**. Reproduced with permission from ref. 85 copyright 2013, Elsevier.

center of galactose oxidase (Fig. 77).[86] It was subsequently immobilized onto a MWCNT-modified glassy carbon electrode *via* π–π interactions and evaluated through an oxygen reduction reaction (ORR). In order to obtain complex **277**, the ligand (2-*tert*-butyl-6-{[(6-methyl-pyridin-2-ylmethyl)-pyridin-2-ylmethyl-amino]-methyl}-4-({4-[(pyren-1-ylmethyl)-amino]-butylamino}-methyl)-phenol) (**276**) was initially synthesized in a two-step process. First, it involved a Mannich reaction between (6-methylpyridin-2-yl)-*N*-(pyridin-2-ylmethyl)methanamine, 3-*tert*-butyl-4-hydroxy-benzaldehyde, and paraformaldehyde, leading to **275** (^{CHO}**LH**), followed by a reductive amination reaction with N^1-(pyren-1yl-methyl)butane-1,4-diamine (PBDI), leading to **276**. The resulting compound was subsequently dissolved in CH_3OH and then reacted with $CuCl_2{\cdot}2H_2O$, in the presence of Et_3N, to prepare

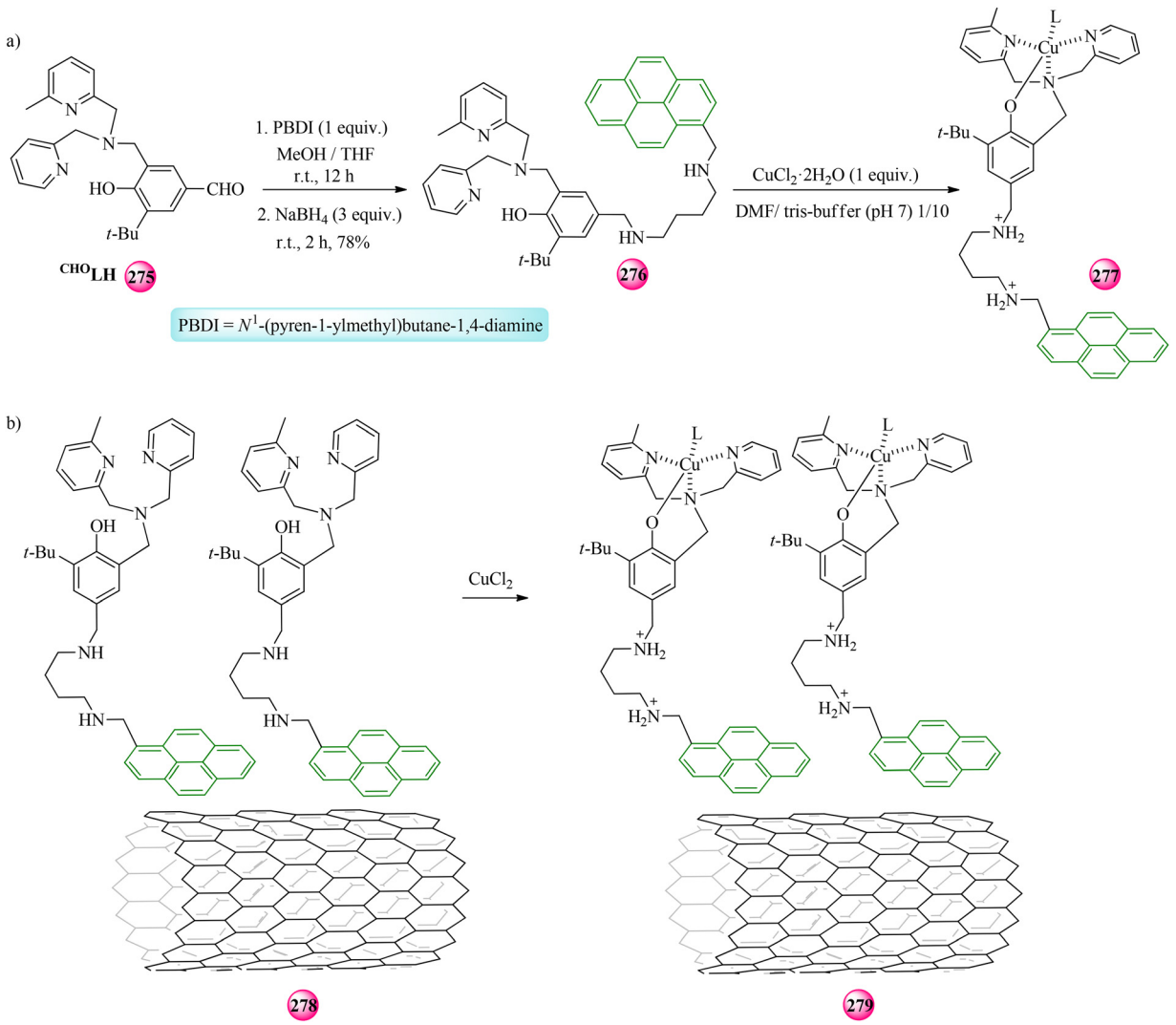

Fig. 77 Representation of (a) the synthesis of complex **277** and (b) the immobilization of Cu pyrene-tagged on MWCNTs (278). Reproduced with permission from ref. 86 copyright 2016, John Wiley and Sons.

complex **277**. In the next step, the immobilization was performed by incubating ligand **276** in dried CH_3CN on the MWCNT-modified electrodes (**278**), followed by incubation with a solution of $CuCl_2$, forming a **277**/MWCNT-based electrode (**279**). To unravel the electrocatalytic activity pathway of **277**/MWCNT (**279**), its ability to reduce H_2O_2 was examined. Cyclic voltammetry of **279** in the presence of H_2O_2 showed its electrocatalytic activity for H_2O_2 reduction at similar overpotentials to that for the ORR, validating the hypothesis of peroxide formation by two-electron reduction of O_2 and subsequent two-electron transfer, resulting in complete water production from oxygen. Since the immobilized complex **279** appears to act as a galactose oxidase mimic, reducing O_2 to Cu^{II}–OOH and H_2O_2 to H_2O, the rich redox properties of phenolate-based ligands can provide new opportunities for designing electrocatalysts inspired by the active site of galactose oxidase.

In 2017, Batista, Llobet, and their co-workers presented complex $[(L)Cu^{II}]^{2-}$ (**285**) (L = *o*-phenylenebis(oxamidate)) and $[(L_{py})Cu^{II}]^{2-}$ (**284**), which features the $(L_{py})^{4-}$, 4-pyrenyl-1,2-phenylenebis-(oxamidate) ligand, exhibiting extended π-conjugation due to a pyrene moiety covalently linked to the phenyl ring, utilizing them as a water oxidation catalyst (Fig. 78 and 79).[87] On the one hand, the ligand of complex **285** was synthesized by dissolving *o*-phenylenediamine in THF, adding ethyl chlorooxoacetate dropwise, and refluxing, followed by several processes.[88] On the other hand, in order to synthesize $[(L_{py})Cu](NMe_4)_2$ (**284**), 4-(pyren-1-yl)benzene-1,2-diamine (**151**) was prepared as schematically indicated in Fig. 78. It was then dissolved in THF, followed by the drop-wise addition of ethyl chlorooxoacetate to form **282**. Afterward, methylamine solution in MeOH was introduced to form **283**. The final complex (**284**) was obtained by the reaction of the ligand precursor and copper perchlorate. In the next step, the immobilization procedure involved preparing a solution of **284** or **285** in CH_3OH, adding graphene and forming a suspension that was sonicated and stirred. Notably, electrodes were prepared by drop-casting the suspension onto GC electrodes, which were dried under vacuum, resulting in GC@G@$[(L)Cu]^{2-}$ (**286**) and GC@G@$[(L_{py})Cu]^{2-}$ (**287**) (Fig. 79). The performance of **286** and **287**, in terms of oxygen generation,

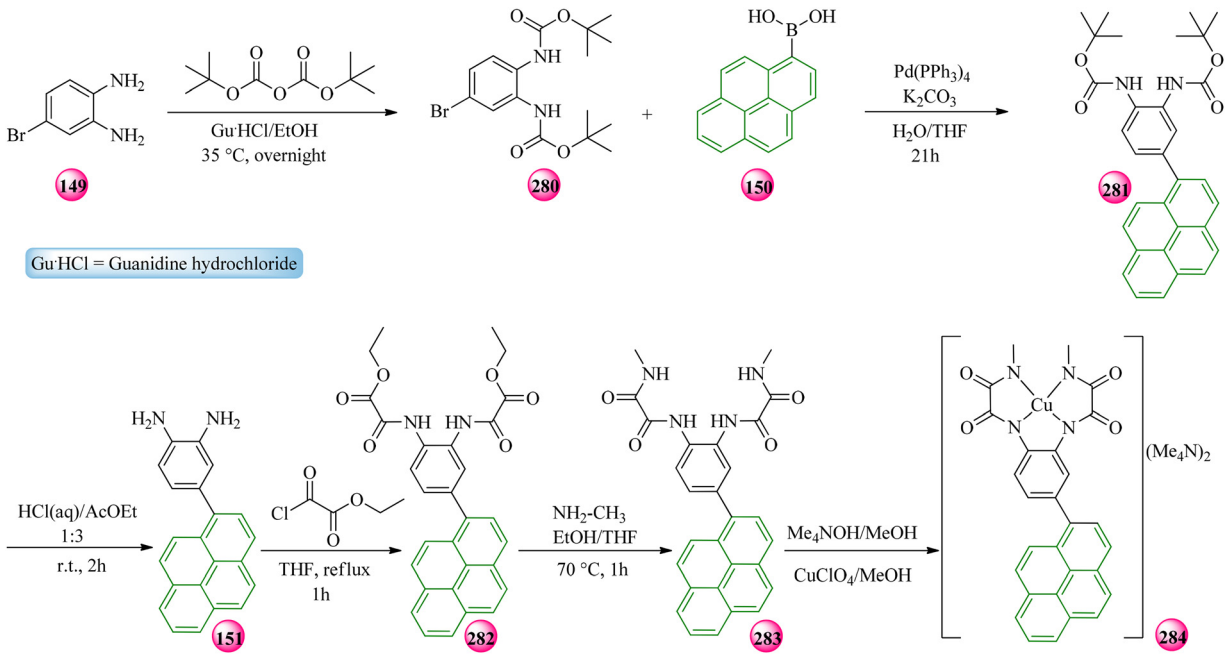

Fig. 78 The scheme procedure for the synthesis of $([L_{py})Cu]^{2-}$ (**284**). Reproduced with permission from ref. 87 copyright 2017, American Chemical Society.

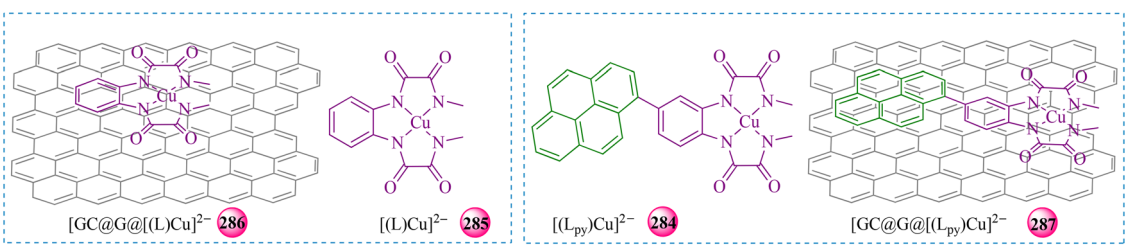

Fig. 79 Structural representation and labeling code of the complexes and the hybrid materials used in this work. Reproduced with permission from ref. 87 copyright 2017, American Chemical Society.

was evaluated using CV and rotating ring disk electrode experiments. The high stability of the anchored molecular catalysts on graphene was further analyzed, revealing no difference in charge for the anodic charge of the first oxidation wave and the respective reduction wave after the electrocatalytic analysis. Based on the obtained results, through anchoring, π-stacking interactions with graphene sheets enhance π-delocalization and the catalytic performance of both catalysts, while **287** became the most active catalyst, benefiting from the synergistic effects of both pyrene and graphene. Furthermore, the increased TOF_{max} of **287** compared to **286** implies that the enhanced π-delocalization resulting from pyrene–graphene interactions boosts electron transfer from the catalyst to the graphene electrode, which can be a beneficial molecule for WOCs and even considered as a rewarding candidate for devices that are based on direct solar water-splitting.

4.13. Pyrene-tagged gold complexes

In 2013, Riant, Hermans, and co-workers reported the synthesis of a gold catalyst bearing a pyrene tag and its immobilization onto MWCNTs *via* π–π interactions to evaluate the ability of recycling *via* the boomerang effect.[6] To synthesize the pyrene-tagged gold(I) complex (**293**), initially, 4-bromobenzonitrile (**288**) and *n*BuLi underwent a halogen/lithium exchange reaction and were then trapped with chlorodiphenylphosphine to obtain phosphine **289** (Fig. 80). Subsequently, the amine (**290**) was produced *via* nitrile reduction by $LiAlH_4$, which was then reacted with 1-pyrene butyric acid to prepare the bifunctional ligand **291**. Next, ligand **291** was exchanged with dimethylsulfide of the chloro(dimethylsulfide)gold(I) complex to obtain **292**, which was further reacted with an equivalent of silver bis(trifluoromethanesulfonyl)imide ($AgNTf_2$), leading to the pyrene-tagged gold catalyst **293**. Notably, the utilization of a polar solvent (acetone) would seem to be essential to preserve the π–π interactions through the immobilization step since both pyrene and MWCNTs are lipophilic (Fig. 81). In terms of activity and selectivity, the efficiency of **293**-MWCNT was compared with its homogeneous counterpart (**293**). The outcomes from the cyclization reaction of enynes indicate that both **293**–MWCNTs and its homogeneous analogue have good catalytic activity with the same conversions. Furthermore, the quantitative enyne cyclization was obtained up to four catalytic cycles without any activity loss. Notably, the temperature and polarity of the solvents significantly affect the π–π interactions between CNTs and pyrene; in this case, recycling can be achievable at low temperatures.

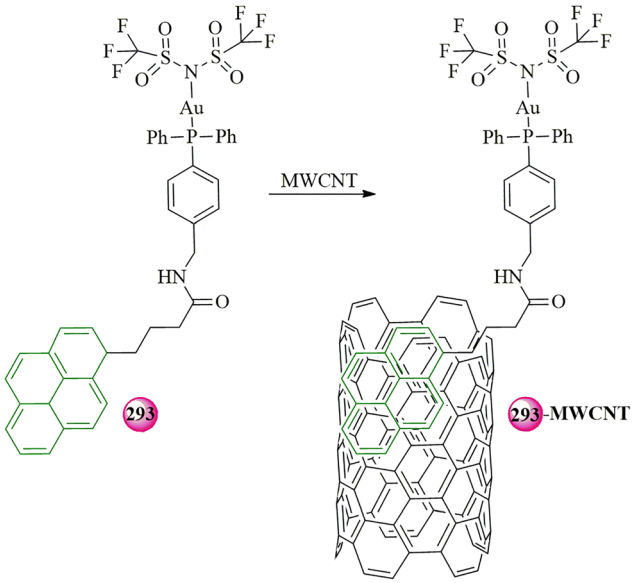

Fig. 81 The immobilization of the pyrene-tagged gold complex **293** onto MWCNTs. Reproduced with permission from ref. 6 copyright 2013, John Wiley and Sons.

In 2017, Mata and co-workers reported a procedure to synthesize and then immobilize pyrene-tagged NHC–gold complexes [(NHC)AuX] (**296**, X = Cl and **297**, X = Br) onto rGO through π-stacking interactions (Fig. 82).[89] In order to facilitate

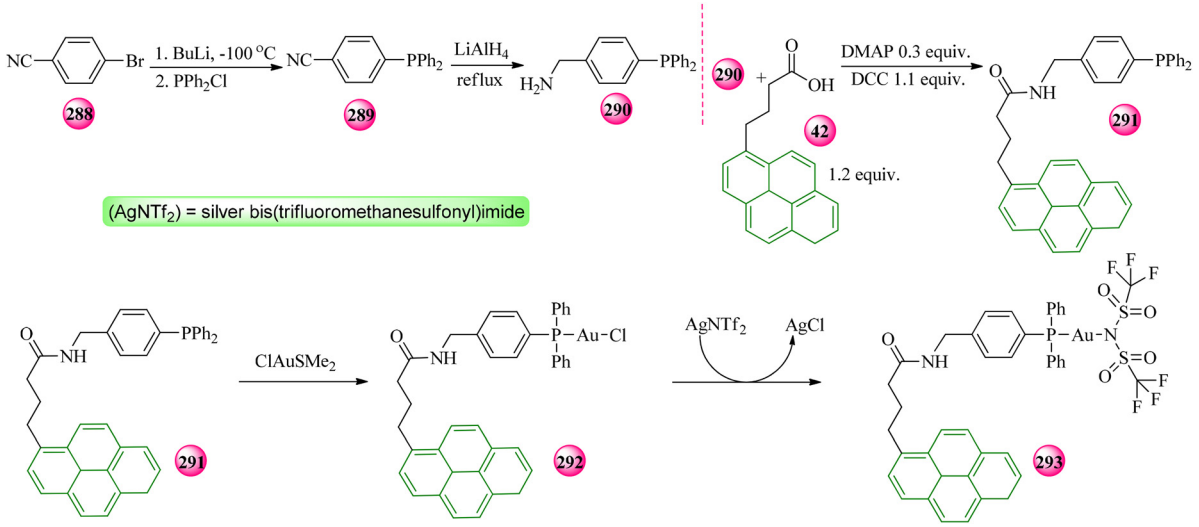

Fig. 80 Synthesis procedure for the pyrene-tagged gold complex **293**. Reproduced with permission from ref. 6 copyright 2013, John Wiley and Sons.

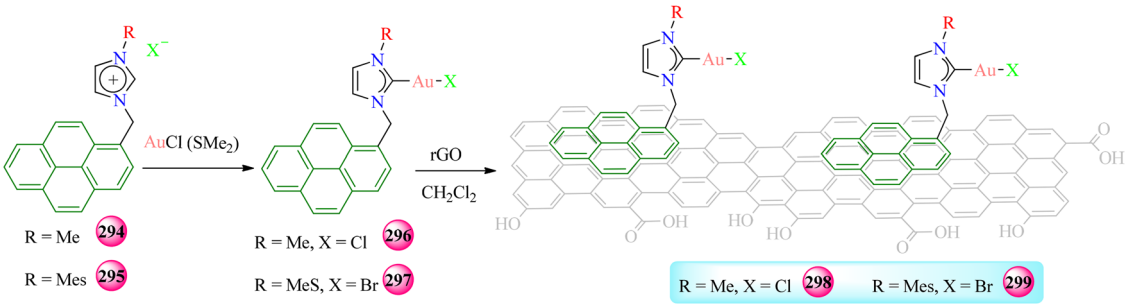

Fig. 82 Synthesis procedure for gold complexes and hybrid materials. Reproduced with permission from ref. 89 copyright 2017, Elsevier.

the direct immobilization of the organometallic gold complexes onto solid support, two pyrene-tagged imidazolium salts that function as NHC ligand precursors were initially prepared. In this regard, the methyl (or mesityl) imidazole was alkylated with 1-bromomethyl pyrene to obtain pyrene-tagged imidazolium salts **294** and **295**. The imidazolium salts can be deprotonated in the presence of $AuCl(SMe_2)$ *via* a transmetalation method or an external base to synthesize the organometallic gold complexes **296** and **297**. Afterward, these complexes were immobilized by immersing rGO in CH_2Cl_2, followed by the addition of **296** and **297** to prepare **298** and **299**. Although immobilization of molecular complexes generally reduces reaction rates due to diffusion issues, the reaction rates of the pyrene-tagged NHC–gold complexes increased after immobilization on the rGO surface. It has been shown in the hydroamination of alkynes by homogeneous and heterogeneous catalysts that the heterogeneous catalysts have higher reaction rates compared to the homogeneous counterparts, suggesting no diffusion limitations upon immobilization on graphene. In addition, the hybrid catalyst **299** was used for four runs in a row without exhibiting any noticeable loss of activity. The findings also indicated that adding aromatic rings to the NHC ligand's nitrogen improves the catalyst's stability and activity.

4.14. Pyrene-tagged zinc complexes

In 2010, Prato, Torres, Guldi, and their co-workers reported the synthesis of pyrene-tagged phthalocyanine (H_2Pc–Pyr) and zinc phthalocyanines (ZnPc–Pyr) and their immobilization onto SWCNTs to be utilized as prototype solar cells.[90] Phthalocyanine exhibited excellent light-harvesting capabilities in the visible and near-infrared (NIR) regions of the solar spectrum, high photostability, and exceptional features as excited electron donors to electron acceptors (*i.e.*, SWCNTs) through π–π interactions. On the one hand, 2,3,9,10,16,17-hexa-*tert*-butylphenoxy-23-[*p*-(4′-pyrenbutyryloxy-methyl)phenyl] phthalocyanine (H_2Pc–Pyr) (**301**) was synthesized by reacting 1-pyrenebutyric acid (**42**) with H_2Pc–OH (**300**) in DCC and DMAP in dry THF (Fig. 83). On the other hand, 2,3,9,10,16,17-hexa-*tert*-butylphenoxy-23-[*p*-(4′-pyren-butyryloxy-methyl)phenyl] phthalocyaninate Zn(II) (ZnPc–Pyr) (**302**) was synthesized by reacting **301** with $ZnCl_2$ in a mixture of *o*-dichlorobenzene (*o*-DCB) and DMF. In terms of assessing the interactions of **301** and **302** with SWCNTs, titration experiments were performed by dispersing SWCNTs in either DMF or THF. The results showed significant changes in the fluorescence and the absorption properties of the Pc fragment, including a remarkable broadening of **301** and **302** features (specifically in the Q-band region), red-shifts of the absorption bands, quantitative quenching of fluorescence, and red-shifts of the NIR absorption transitions associated with SWCNTs. These results indicate successful immobilization of **301** and **302** onto SWCNTs, while their homogeneous counterparts, lacking anchor groups, did not indicate any significant interactions. Furthermore, compared to the smaller diameter, larger SWCNTs showed stronger red-shifts, confirming that the immobilization process proceeded successfully.

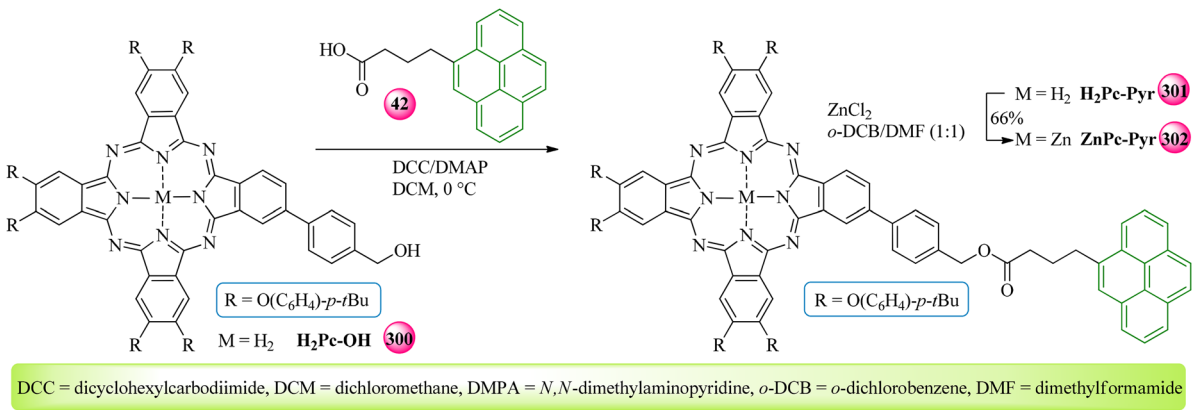

Fig. 83 Synthesis of H_2Pc–Pyr (**301**) and ZnPc–Pyr (**302**). Reproduced with permission from ref. 90 copyright 2010, American Chemical Society.

Notably, according to Raman spectroscopy data, the D-band remained unchanged in both SWCNTs and **301**/SWCNT or **302**/SWCNT hybrids, indicating that no structural damage occurred during the immobilization process. Similarly, there was no alteration for the G- and G′-bands in the suspension or solid states, and both were investigated for the electronic and structural influence of immobilizing **301**/**302** onto SWCNTs. Moreover, **301**/SWCNT and **302**/SWCNT thin films were tested in photoelectrochemical cells, showing superior solar energy conversion performance compared to earlier SWCNT hybrids.[91] Notably, throughout the NIR and visible parts of the spectrum, regarding the cells that showed the same optical absorption, **301**/SWCNT exhibited higher maximum internal photoconversion efficiency (IPCE) than **302**/SWCNT. Indeed, the **301**/SWCNT films achieved stable photocurrents with large IPCE values, among the highest reported for SWCNT systems, highlighting the advantages of non-covalent approaches in developing electron donor–acceptor hybrids.

In 2010, Hasobe, Ito, D'Souza, and co-workers reported donor–acceptor hybrid materials **303**/SWCNTs (**303** = $ZnP(pyr)_4$, P = porphyrin) by assembling specific semiconducting (7,6)- and (6,5)-SWCNTs, having different electronic band gaps, to evaluate the photoelectrochemical responses of the hybrid system (Fig. 84).[92,93] In order to synthesize **303**/(6,5)-SWCNT and **303**/(7,6)-SWCNT nanohybrids, the SWCNT was reacted with **303** in dry DMF, followed by several processes to obtain a stable black dispersion. Pyrene-tagged zinc porphyrin ($ZnP(pyr)_4$, **303**) interacts with the SWCNT surface through π–π interactions, causing exfoliation of the semiconducting CNTs, as confirmed by TEM. Based on laser Raman spectroscopy, the electronic structures of SWCNTs functionalized with **303**, (**303**)/(6,5)-SWCNT and (**303**)/(7,6)-SWCNT, exhibited no notable shift in the Raman spectra, revealing that the electronic structure of the SWCNT remained intact in the nanohybrid system. According to the obtained results, there were some differences between **303**/(6,5)-SWCNT and **303**/(7,6)-SWCNT nanohybrids; the (7,6)-SWCNT, possessing a narrower band gap, demonstrates greater efficiency in charge separation *via* the excited state of ZnP, as indicated by a higher k_{CS} (charge separation)/k_{CR} (charge recombination) ratio compared to the (6,5)-SWCNT, having a wider band gap.

In 2020, Escosura, Guldi, Torres, and co-workers reported the synthesis of pyrene-tagged tetracationic zinc phthalocyanine (ZnPc) (**310**) and its immobilization onto fullerenes (C_{60}) to mimic nanoscale photosynthetic model systems through an aqueous photoactive system of electron donor–acceptor (Fig. 85).[94] Complex **310** exhibited a distinctive mode of aggregation driven by a subtle interplay between electrostatic and π–π interactions. In order to synthesize the pyrene-tagged ZnPc complex (**310**), pyrene-1-boronic acid pinacol ester (**304**) initially underwent a Suzuki cross-coupling reaction using 5-bromo-3-hydroxypyridine (**305**) in the presence of a catalyst, $Pd(dppf)Cl_2$ (dppf = 1,1′-bis-(diphenylphosphino)ferrocene), and resulting in pyrenyl pyridyloxy derivative (**306**). It was then reacted with 4-nitrophthalonitrile (307) to obtain phthalonitrile **308**, after refluxing in DMF and purification. Subsequently, ZnPc (**309**) was formed in the presence of anhydrous zinc acetate by cyclotetramerization of **308**.

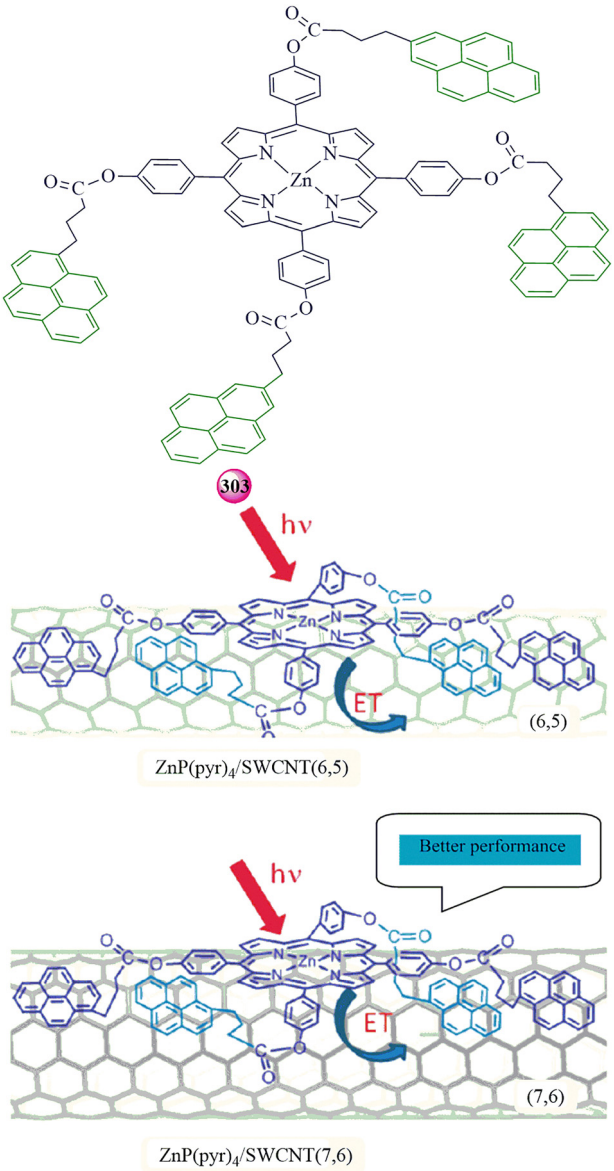

Fig. 84 The schematic structure of the $ZnP(pyr)_4$/SWCNT (6,5) and $ZnP(pyr)_4$/SWCNT (7,6). Reproduced with permission from ref. 92 and 93 copyright 2010, American Chemical Society.

Eventually, the quaternization of **309** with methyl iodide was performed to obtain the final pyrene-tagged ZnPc complex (**310**). Notably, the immobilization of **310** onto C_{60} (C_{60}–ZnPc) was achieved through wrapping of the pyrene fragments around C_{60}. The interaction between **310** and C_{60} derivatives was studied *via* absorption and fluorescence spectroscopies through the titration of **310** in pure DMSO with C_{60}. Based on titration results, a decrease and a red-shift in the absorption intensity of the Q-band, as well as quantitative quenching of the fluorescence, were observed, revealing the formation of ZnPc–C_{60}. Indeed, it has been demonstrated that two independent processes are involved in achieving high binding constants: electrostatic and π–π interactions. Additionally, following the interactions between **310** and water-soluble tetra- or octaanionic fullerene, charges were transferred to the electron-

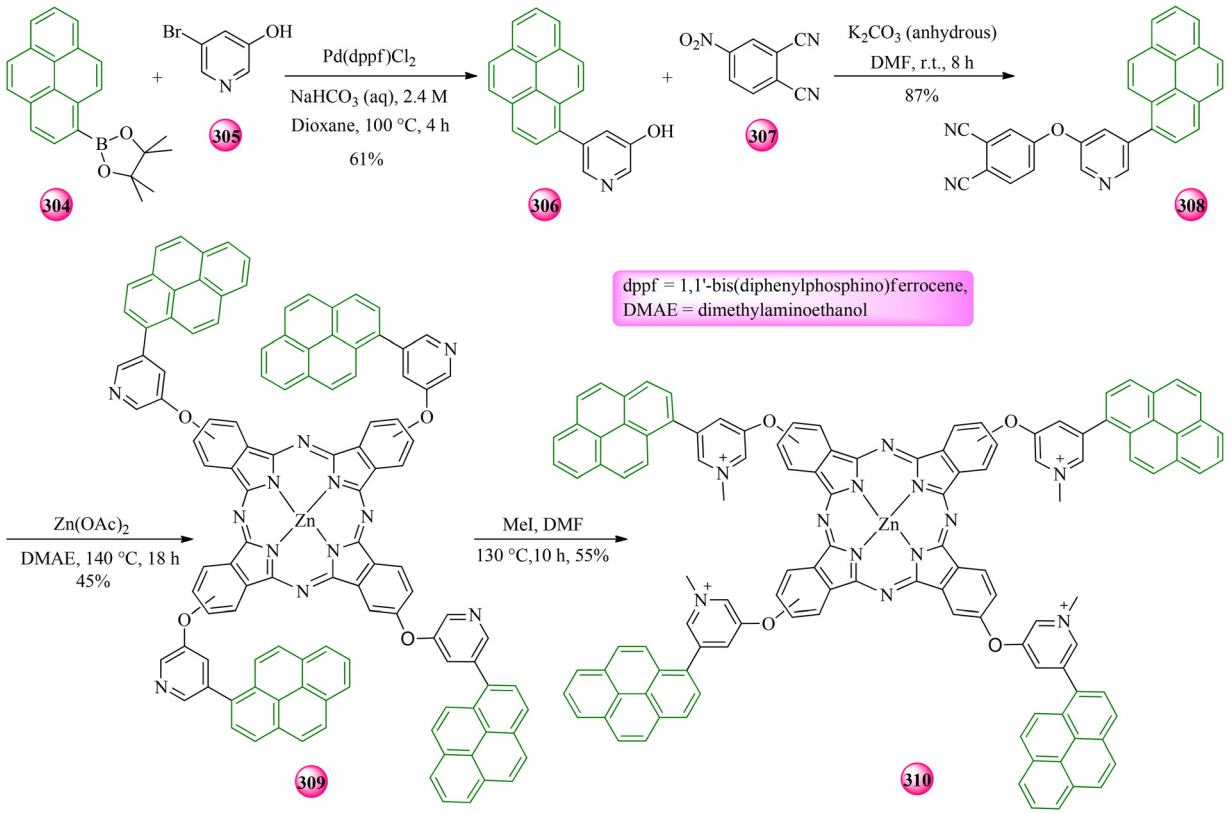

Fig. 85 The synthesis procedure of pyrene-tagged zinc complex **310**. Reproduced with permission from ref. 94 copyright 2020 John Wiley and Sons.

acceptor moiety (fullerenes), leading to longer-lived charge-separated states facilitated by the cooperation between electrostatic and π–π interactions. This versatile approach allows water to tune the synergy between several non-covalent forces, enabling the assembly of multi-chromophore supramolecular systems to achieve highly efficient artificial photosynthetic constructs.

4.15. Pyrene-tagged lanthanide complexes

Lanthanides set themselves apart from other metals due to their spatially expansive, core-like 4f orbitals and their adoption of the +3 oxidation state. In 2017, Blakemore and co-workers synthesized a series of pyrene-tagged lanthanide complexes (Ce, Nd, Sm, and Eu) (**314**) involving tripodal heptadentate ligand scaffolds and subsequently immobilized them onto carbon electrodes *via* noncovalent interactions (Fig. 86).[95] In order to prepare **314**, benzylic chloride was substituted with *N*-methyl-1-(pyren-1-yl) methanamine, followed by the reaction of the obtained aldehyde (**312**) with tris(2-aminoethyl)amine, resulting in $L^{pyr}H_3$ (**313**). Next, the desired ligand was coordinated to different M(III) f-block elements through protonolysis of the suitable tris(hexamethyldisilazide) metal precursors, ($M(N(SiMe_3)_2)_3$ (M = Ce, Nd, Sm, Eu). It is noticeable that the insolubility of $L^{pyr}M$ (**314**) complexes in less polar solvents was due to robust interactions between pyrene fragments, making it simple to isolate the precipitate from the solution of the reaction. The immobilization of **314** was performed by drop-casting carbon black material (Ketjen black) onto HOPG. The provided electrode underwent functionalization through immersion in dilute CH_2Cl_2 solutions of the **314** complexes, followed by rinsing with CH_2Cl_2 to eliminate loosely immobilized complexes. According

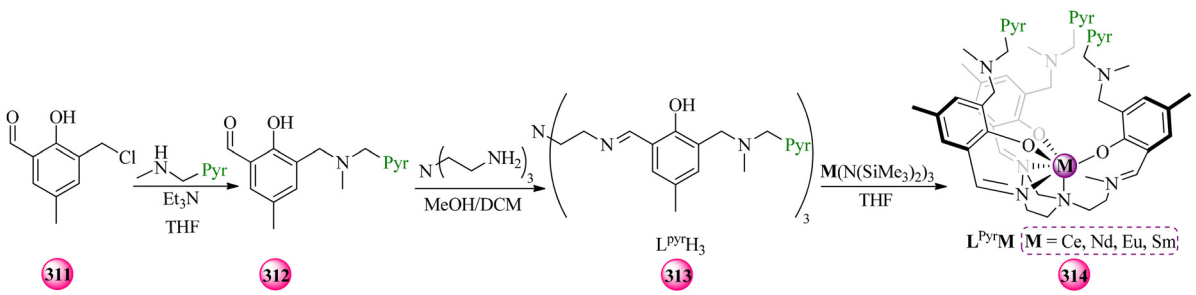

Fig. 86 Synthesis of pyrene-tagged lanthanide complexes containing heptadentate ligand $L^{Pyr}H_3$. Reproduced with permission from ref. 95 copyright 2017, Royal Society of Chemistry.

to N 1s peaks in XPS, **313** (the ligand) showed lower binding energies than **314** (the complex), which was aligned with nitrogen atoms' greater electron-rich character when they are not coordinated to the metal. In order to evaluate the stability of the surface that has been functionalized, electrodes remained in electrolyte solution, and cyclic voltammograms were recorded at 10-minute intervals. The loss of surface-bound species of the functionalized electrodes can be attributed to the tendency of the pyrene fragments in the structure of **314** complexes to engage in intramolecular π–π stacking interactions. Additionally, the cerium(III) complex was reversibly oxidized to cerium(IV) at a potential (−0.34 V) compared to the non-immobilized (−0.46 V) soluble counterpart of the same complex. The obtained results represent one of the few examples of immobilized molecular f-block complexes, verified by XPS and electrochemistry, which can be beneficial for sensors, catalytic systems, or applications of separation.

Conclusion

Impressed by the positive features of homogeneous and heterogeneous catalysts, such as high selectivity and stability, and for the latter, high recyclability and reusability, researchers have been attracted to the immobilization of pyrene-tagged complexes involving different ligands and central metals onto numerous kinds of solid supports, serving as exceptional functionalized catalysts. Functionalizing these types of supports with complexes bearing pyrene moieties, which can have a main role in the properties of the complex based on their location's tag, has received noticeable attention in the past few decades. Research groups have explored a wide range of these compounds, shedding light on understanding that not only can they promote π–π stacking interactions *via* the immobilization of complexes onto carbon-based supports, including GO, rGO, CNT, EPG, and g-C_3N_4, but they can also be immobilized onto modified supports, including gold and ITO. Indeed, thanks to taking advantage of both homogeneous and heterogeneous features, high selectivity, stability, and activity were achieved while maintaining a straightforward way of separation and recyclability, leading to a worthwhile investment in catalyst replacement. In terms of recycling, the boomerang effect (release–return phenomenon) emerges, which is utterly dependent on the temperature alteration. Furthermore, these complexes are a promising choice for a broad range of laboratory and industrial applications focused on enhancing and optimizing chemical

Table 2 Immobilized pyrene-tagged complexes classified based on their applications, including energy-related catalytic applications

O_2 reduction	Ref.	H_2 evolution/transfer	
Os^{II}–NHC (**135**) on MWCNTs[a]	57	Cobaloxime (**142b**) on g-C_3N_4	19
Co corrole (**161**) on MWCNTs	63	Cobaloxime copolymer (pPyCo, **147**) & cobaloxime (PyCo, **148**) on MWCNTs	61
Co(II) porphyrin (**164**)/Pyr–Py(**167**) on MWCNTs[b]	64	Cyclopentadienyl Rh complex (**188**) on rGO	68
Copper phenolato (**279**) on MWCNTs	86	$[Ni(P_2^{Ph}N_2^{CH_2Pyrene})_2]$ (**236**) on MWCNTs	77
CO_2 reduction		Photocatalysts	
fac-[MnBr(bpy$_{pyr}$)(CO)$_3$] (**7**) on MWCNTs[c]	33	B–Ru–P (61) on graphene[m]	44
ReQBlm-pyr (**10**) on EPG[d]	18	Tris(bipyridyl)ruthenium(II) (**62**) on SWCNTs	45
[Cp*Rh(P)Cl]Cl (**11**) & [Re(P)-(CO)$_3$Cl] (**12**) on HOPG[e]	34	Ruthenium tris(bipyridyl) and iridium bipyridine complexes (**79**) and (**80**) on HOPG	49
Iron triphenylporphyrin (**36**) on MWCNTs	40	*trans*-[Ru(pypz–pyr)(trpy)(H$_2$O)](PF$_6$) (**122**) on rGO[n]	54
Cobalt pyridyldiimine complexes (**172** and **179**) on MWCNTs	65	*trans*–*fac*-[Ru(bpea-pyrene)(bpy)OH$_2$] (PF$_6$)$_2$ (**129**) on rGO[o]	55
Iridium pincer dihydride catalyst (**209**) on CNTs	73	Rh cyclopentadienyl complex (**188**) on rGO	68
Iridium PNP-pincer complex (**234**) on MWCNTs[f]	76	Zinc phthalocyanines (ZnPc) (**302**) on SWCNT	90
[Ni^{II}(Cl)(L)]Cl (**242**) on MWCNTs[g]	79	ZnP(pyr)$_4$ (303) on SWCNTs[p]	92
Triazacyclononane Ni (**247**) on MWCNTs	80	Tetracationic zinc phthalocyanine (ZnPc) (**310**) on C_{60}	94
Water oxidation		Redox-active films	
Ru(bpa)(Pyr–Py)$_2$ (**55**) on MWCNTs[h]	43	1-Pyrenylferrocene (**39**) on modified gold	16
{Ru(tda)(L^1)$_2$} (**77a**) and {Ru(tda)(L^2)$_2$} (**77b**) on MWCNTs[i]	48	1-Pyrenylferrocene (**40**) on modified ITO	17
[(^{pyrene}bbp)Ru$_2$(OAc)(py)$_4$](PF$_6$)$_2$ (**118**) on MWCNTs[j]	53	Janus-type ruthenium monolayer complex (**75**) and bilayer Zr–phosphonate (**76**) on HOPG	47
Co salophen (**154**) on MWCNTs	62	Ruthenium bis(benzimidazolyl)pyridine complexes (**100a**, **100b**, **100c**, and **100d**) on HOPG/SWCNT/MWCNT	52
NHC IrCp*Cl$_2$ (**224**) on MWCNTs[k]	75	Tris(bipyridine)osmium(II) (**130**) on rGO	56
[(L$_{py}$)Cu^{II}]$^{2-}$ (**284**) on graphene[l]	87	[Co(tpy∼py)$_2$](PF$_6$)$_2$ (**136**) on SWCNTs[q]	59
		Lanthanide complexes (Ce, Nd, Sm, and Eu) tripodal heptadentate (**314**) on a graphitic carbon surface	95

[a] NHC: N-heterocyclic carbene. [b] pyr: pyrene, py: pyridine. [c] bpy: bipyridine. [d] ReQBlm: 2-(2′-quinolyl)benzimidazole. [e] P: pyrene-tagged bipyridine ligand. [f] PNP: phosphorus–nitrogen–phosphorus. [g] L: 241. [h] H_2bpa = 2,2′-bipyridine-6,6′-dicarboxylic acid. [i] tda^{2-}: [2,2′:6′,2″-terpyridine]-6,6″-dicarboxylato, L^1: 4-(pyrene-1-yl)-*N*-(pyridine-4-ylmethyl)butanamide and L^2: 4-(pyrene-1-yl)pyridine. [j] bbp$^-$: bis(bipyridyl)pyrazolate. [k] Cp*: C_5Me_5. [l] L$_{py}$: 4-pyrrenyl-1,2-phenylenebis(oxamidate). [m] B–Ru–P: bi(2,2′-bipyridyl)-pyrene ruthenium(II) complexes on graphene sheets. [n] Pyridinepypz-H: 2-(3-pyrazolyl), trpy: tridentate terpyridine. [o] bpea-pyrene: 1-[bis(pyridine-2-ylmethyl)amino]methylpyrene. [p] P: porphyrin. [q] tpy∼py: 4-pyren-1-yl-*N*-[5([2,2′;6′,2″]terpyridin-4′-yloxy)-pentyl]-butyramide.

reaction procedures. To clarify, the catalytic behavior of these materials in fuel production, sensing, water oxidation, photocatalytic hydrogen generation, and carbon dioxide reduction demonstrates their significant impacts, showing higher TONs, faradaic efficiency, and durability than their homogeneous counterparts. These types of catalysts can be widely used in oxygen and carbon dioxide reduction, water and glucose oxidation, asymmetric, and metathesis reactions (Tables 2–4). Thus, it could be a wise decision to extend this method to explore new metal complexes containing covalently appended pyrene fragment(s) and immobilize pyrene-tagged complexes noncovalently onto various supports, promoting the recycling of industrial catalysts in the near future. To elucidate the synergistic effects of this heterogeneous system, the metals are attached to the functionalized ligands with pyrene, enabling noncovalent π–π interactions with solid supports and resulting in effective immobilization without altering the activity of the original catalyst, compared to homogeneous catalytic systems. Additionally, the combination of two different metals has the potential of synergistic dual catalysis, a significant advantage in both experimental and industrial applications. However, in order to thoroughly understand the synergy and interaction between pyrene-tagged complexes and the supports, further investigations are still required, which may lead to optimizing the π–π stacking system to achieve increased productivity while reducing the overall cost by enhancing recyclability on a large scale. Notably, achieving a simple design for these heterogeneous catalytic systems, while maintaining their high catalytic activity and recyclability, may inspire subsequent research on novel pyrene-tagged complexes and other substituted polyaromatic systems, opening the door to additional cost-effective and environmentally friendly catalysts. On the other hand, although scientists have meticulously reported their investigations on the concept of π–π stacking immobilization, there are some unresolved challenges and debates regarding this method. Firstly, it has been verified that the number of pyrene anchors, their location, and the spacer design adjustment can affect catalyst properties; however, general design rules are still empirical and depend on specific substrates and reactions. Secondly, as demonstrated in some cases, solvent and temperature control of π–π binding for adsorption and desorption necessitate finding a solution and analyzing whether to generalize it to a broader range of systems, rather than being limited to a few specific cases. Finally, scientists' attention can be drawn to examine and expand their knowledge about the effect of combined forces, electrostatic and π–π interactions simultaneously, rather

Table 3 Immobilized pyrene-tagged complexes used in biological applications

Pyrene-tagged complexes@support	Support	Application	Ref.
3-Ferrocenyl-*N*-(pyren-1-ylmethyl)propanamide (**14**)	MWCNTs	Biosensor	35
Tris(bispyrene-bipyridine)iron(II) complex (**17**)	MWCNTs	Biosensor	36
$[Fe^{II}(L_1)_2L_2]^{2+}$ (**20**)[a]	CNTs	Biosensor	37
Cobalt(II) bis-terpyridine (**141**)	Graphene	Biosensor	38
RuQ–pyrene (**72a**)[b]	MWCNTs	Glucose oxidation	46
Ferrocene tripod **25a** & **25b**	Graphene	Protein denaturation	60
Pentamethylcyclopentadienyl rhodium(III) chloride dimer (**186**)	MWCNTs	Regenerate NADH	67
Dendritic Pd–phosphine (**263**)	Co/C	Drug synthesis	73

[a] L_1 = 4,4′-bis(biotin)-2,2′-bipyridine, L_2 = 2,2′-bipyridine-4,4′-dipyrene. [b] RuQ–pyrene: [(1,10-phenanthroline-5,6-dione)$_2$((4,4′-bis(4-pyrenyl-1-ylbutyloxy)-2,2′-bipyridine)Ru(II)] hexafluorophosphate.

Table 4 Immobilized pyrene-tagged metal complexes used as catalysts in various reactions

Pyrene-tagged complexes@support	Reactions	Ref.
Unsym-Cr-**1**@rGO	Asymmetric ring-opening of epoxides and hetero-Diels–Alder	32
Pyrphos rhodium (**181**)@CNT	Asymmetric hydrogenation of α-dehydroamino esters	66
Diphosphite ligands (**202** and **203**)@MWCNT/rGO/carbon beads	Asymmetric AHF of norbornene	70
Cu bis(oxazoline) (**274**)@charcoal/C_{60}/SWCNT	Hybrid asymmetric Henry & ene reactions	85
NHC–Pd complex (**67**) & NHC–Ru complex (**68**)@rGO	Alcohol oxidation reaction	5
NHC–Pd–Ru (**71**)@rGO	Catalyst for hydrodefluorination	9
NHC–rhodium complexes (**191** and **192**)@rGO	1,4-Addition of phenylboronic acid to cyclohex-2-one & hydrosilylation of terminal alkynes	69
NHC–iridium complexes (**214** and **216**)@rGO	β-Alkylation of secondary alcohols	74
NHC–palladium complex **251**@graphene	Aqueous hydroxycarbonylation of aryl halides	81
NHC–Pd complex (**267**)@rGO	Suzuki–Miyura cross-coupling reaction & reduction of *p*-NP reactions	83
NHC–Pd complex (**270**)@rGO	Hydrogenation and dehydrogenation of N-heterocycles	84
NHC–gold complexes (**296** and **297**)@rGO	Hydroamination of alkynes	89
Cyclometalated iridium complexes (**227**)@MWCNT	Dehydrogenation of indolines in aqueous solution	8
Hoveyda-type ruthenium (**89**)@rGO	Metathesis reactions	14
Ruthenium carbene (**45**)@SWCNTs	Ring-closing metathesis reactions	13
Rhodium(I) monophos complex (**208**)@graphene	Hydrogenation of dehydroamino acid esters	71
Terpyridine–ruthenium involving one (**47**) or five terpyridine (**49**)@graphene	Nitroarene transfer hydrogenation	41
Gold(I) phosphine bis(trifluoromethanesulfonyl)imide complex (**293**)@MWCNTs	Boomerang catalyst for the cyclization reaction of enynes	6
Fe tripod complexes (**30a** and **30b**)@MWCNTs	Ethylene polymerization	39

than π–π interactions alone, as previously reported, which shows the outperformance of the synergistic system.

Author contributions

Elham Sanaei: conceptualization, investigation, visualization, writing – original draft preparation; Gholamhossein Mohammadnezhad: conceptualization, investigation, project administration, resources, supervision, validation, writing – review and editing.

Conflicts of interest

The authors declare that they have no known competing financial interests or personal relationships that could have appeared to influence the work reported in this paper.

Data availability

No primary research results, software or code have been included and no new data were generated or analysed as part of this review.

Acknowledgements

The authors are thankful to the Research Affairs Division of the Isfahan University of Technology (IUT).

References

1 R. H. Crabtree, Multifunctional ligands in transition metal catalysis, *New J. Chem.*, 2011, **35**, 18–23, DOI: **10.1039/C0NJ00776E**.
2 E. Peris, Polyaromatic N-heterocyclic carbene ligands and π-stacking: Catalytic consequences, *Chem. Commun.*, 2016, **52**, 5777–5787, DOI: **10.1039/C6CC02017H**.
3 S. Ruiz-Botella and E. Peris, Phenylene- and biphenylene-bridged bis-imidazolylidenes of palladium: Influence of the presence of pyrene tags on the catalytic activity of the complexes, *Organometallics*, 2014, **33**, 5509–5516, DOI: **10.1021/om500765u**.
4 A. Gutierrez-Blanco, E. Peris and M. Poyatos, Pyrene-connected tetraimidazolylidene complexes of iridium and rhodium: Structural features and catalytic applications, *Organometallics*, 2018, **37**, 4070–4076, DOI: **10.1021/acs.organomet.8b00633**.
5 S. Sabater, J. A. Mata and E. Peris, Catalyst enhancement and recyclability by immobilization of metal complexes onto graphene surface by noncovalent interactions, *ACS Catal.*, 2014, **4**, 2038–2047, DOI: **10.1021/cs5003959**.
6 C. Vriamont, M. Devillers, O. Riant and S. Hermans, Catalysis with gold complexes immobilised on carbon nanotubes by π–π stacking interactions: Heterogeneous catalysis versus the boomerang effect, *Chem. – Eur. J.*, 2013, **19**, 12009–12017, DOI: **10.1002/chem.201300998**.
7 M. Esfandiari, G. Havaei, S. Zahiri and G. Mohammadnezhad, Pincer complex immobilization onto different supports: Strategies and applications, *Coord. Chem. Rev.*, 2022, **472**, 214778, DOI: **10.1016/j.ccr.2022.214778**.
8 H. Liu, J. G. Chen, C. Wang, Z. T. Liu, Y. Li, Z. W. Liu, J. Xiao and J. Lu, Immobilization of cyclometalated iridium complex onto multiwalled carbon nanotubes for dehydrogenation of indolines in aqueous solution, *Ind. Eng. Chem. Res.*, 2017, **56**, 11413–11421, DOI: **10.1021/acs.iecr.7b02804**.
9 S. Sabater, J. A. Mata and E. Peris, Immobilization of pyrene-tagged palladium and ruthenium complexes onto reduced graphene oxide: An efficient and highly recyclable catalyst for hydrodefluorination, *Organometallics*, 2015, **34**, 1186–1190, DOI: **10.1021/om501040x**.
10 L. J. Zhao, C. Zhang, S. Zhang, J. Chen, X. Lv, H. Su, X. Sun, T. Murayama and C. Qi, Dual-core drive hydrogen transfer heterogeneous catalysts based on iridium-enzyme co-modified carbon nanotubes for aromatic aldehyde hydrogenation, *J. Catal.*, 2023, **428**, 115185, DOI: **10.1016/j.jcat.2023.115185**.
11 H. Sakamoto, A. Koto, E. Takamura, H. Asakawa, T. Fukuma, T. Satomura and S. Suye, Development of biofuel cell using a complex of highly oriented immobilized His-tagged enzyme and carbon nanotube surface through a pyrene derivative, *J. Nanosci. Nanotechnol.*, 2019, **19**, 3551–3557, DOI: **10.1166/jnn.2019.16121**.
12 Y. Amano, A. Koto, S. Matsuzaki, H. Sakamoto, T. Satomura and S. Suye, Construction of a biointerface on a carbon nanotube surface for efficient electron transfer, *Mater. Lett.*, 2016, **174**, 184–187, DOI: **10.1016/j.matlet.2016.03.113**.
13 G. Liu, B. Wu, J. Zhang, X. Wang, M. Shao and J. Wang, Controlled reversible immobilization of Ru carbene on single-walled carbon nanotubes: A new strategy for green catalytic systems based on a solvent effect on π–π interaction, *Inorg. Chem.*, 2009, **48**, 2383–2390, DOI: **10.1021/ic801111h**.
14 H. Nasrallah, S. Germain, P. Queval, C. Bouvier, M. Mauduit, C. Crévisy and E. Schulz, Non-covalent immobilization of pyrene-tagged ruthenium complexes onto graphene surfaces for recycling in olefin metathesis reactions, *J. Mol. Catal. A:Chem.*, 2016, **425**, 136–146, DOI: **10.1016/j.molcata.2016.10.004**.
15 Y. J. Li, M. J. Ma, G. Yin, Y. Kong and J. J. Zhu, Phthalocyanine-sensitized graphene–CdS nanocomposites: An enhanced photoelectrochemical immunosensing platform, *Chem. – Eur. J.*, 2013, **19**, 4496–4505, DOI: **10.1002/chem.201203521**.
16 B. R. Lydon, A. Germann and J. Y. Yang, Chemical modification of gold electrodes via non-covalent interactions, *Inorg. Chem. Front.*, 2016, **3**, 836–841, DOI: **10.1039/C6QI00010J**.
17 C. M. Hanna, C. D. Sanborn, S. Ardo and J. Y. Yang, Interfacial electron transfer of ferrocene immobilized onto indium tin oxide through covalent and noncovalent interactions, *ACS Appl. Mater. Interfaces*, 2018, **10**, 13211–13217, DOI: **10.1021/acsami.8b01219**.
18 S. Sinha, A. Sonea, W. Shen, S. S. Hanson and J. J. Warren, Heterogeneous Aqueous CO_2 Reduction Using a Pyrene-Modified Rhenium(I) Diimine Complex, *Inorg. Chem.*, 2019, **58**, 10454–10461, DOI: **10.1021/acs.inorgchem.9b01060**.
19 X. W. Song, H. M. Wen, C. B. Ma, H. H. Cui, H. Chen and C. N. Chen, Efficient photocatalytic hydrogen evolution with

end-group-functionalized cobaloxime catalysts in combination with graphite-like C_3N_4, *RSC Adv.*, 2014, **4**, 18853–18861, DOI: 10.1039/C4RA01413H.

20 N. P. E. Barry and B. Therrien, Pyrene: The Guest of Honor, *Organic Nanoreactors*, Boston, 2016, pp. 421–461, DOI: 10.1016/B978-0-12-801713-5.00013-6.

21 A. Okamoto, K. Kanatani and I. Saito, Pyrene-labeled base-discriminating fluorescent DNA probes for homogeneous SNP typing, *J. Am. Chem. Soc.*, 2004, **126**, 4820–4827, DOI: 10.1021/ja039625y.

22 P. Conlon, C. J. Yang, Y. Wu, Y. Chen, K. Martinez, Y. Kim, N. Stevens, A. A. Marti, S. Jockusch, N. J. Turro and W. Tan, Pyrene excimer signaling molecular beacons for probing nucleic acids, *J. Am. Chem. Soc.*, 2008, **130**, 336–342, DOI: 10.1021/ja076411y.

23 J. M. Stadler and T. Stafforst, Pyrene chromophores for the photoreversal of psoralen interstrand crosslinks, *Org. Biomol. Chem.*, 2014, **12**, 5260–5266, DOI: 10.1039/C4OB00603H.

24 T. Otsubo, Y. Aso and K. Takimiya, Functional oligothiophenes as advanced molecular electronic materials, *J. Mater. Chem.*, 2002, **12**, 2565–2575, DOI: 10.1039/B203780G.

25 S. Diring, F. Camerel, B. Donnio, T. Dintzer, S. Toffanin, R. Capelli, M. Muccini and R. Ziessel, Luminescent ethynyl-pyrene liquid crystals and gels for optoelectronic devices, *J. Am. Chem. Soc.*, 2009, **131**, 18177–18185, DOI: 10.1021/ja908061q.

26 V. de Halleux, J. P. Calbert, P. Brocorens, J. Cornil, J. P. Declercq, J. L. Brédas and Y. Geerts, 1,3,6,8-Tetraphenylpyrene derivatives: Towards fluorescent liquid-crystalline columns, *Adv. Funct. Mater.*, 2004, **14**, 649–659, DOI: 10.1002/adfm.200400006.

27 S. Diring, F. Camerel, B. Donnio, T. Dintzer, S. Toffanin, R. Capelli, M. Muccini and R. Ziessel, Luminescent ethynyl-pyrene liquid crystals and gels for optoelectronic devices, *J. Am. Chem. Soc.*, 2009, **131**, 18177–18185, DOI: 10.1021/ja908061q.

28 Y. H. Kim, D. K. Yoon, E. H. Lee, Y. K. Ko and H. T. Jung, Photoluminescence properties of a perfluorinated supramolecular columnar liquid crystal with a pyrene core: Effects of the ordering and orientation of the columns, *J. Phys. Chem. B*, 2006, **110**, 20836–20842, DOI: 10.1021/jp063115j.

29 M. J. Sienkowska, H. Monobe, P. Kaszynski and Y. Shimizu, Photoconductivity of liquid crystalline derivatives of pyrene and carbazole, *J. Mater. Chem.*, 2007, **17**, 1392–1398, DOI: 10.1039/B612253A.

30 M. J. Sienkowska, J. M. Farrar, F. Zhang, S. Kusuma, P. A. Heiney and P. Kaszynski, Liquid crystalline behavior of tetraaryl derivatives of benzo[*c*]cinnoline, tetraazapyrene, phenanthrene, and pyrene: The effect of heteroatom and substitution pattern on phase stability, *J. Mater. Chem.*, 2007, **17**, 1399–1411, DOI: 10.1039/B615545F.

31 X. Liu, F. Tian, Y. Han, T. Song, X. Zhao and J. Xiao, Synthesis, physical properties and electroluminescence of functionalized pyrene derivative, *Dyes Pigm.*, 2019, **167**, 22–28, DOI: 10.1016/j.dyepig.2019.04.006.

32 M. Abd El Sater, M. Mellah, D. Dragoe, E. Kolodziej, N. Jaber and E. Schulz, Chiral chromium salen@rGO as multipurpose and recyclable heterogeneous catalyst, *Chem. – Eur. J.*, 2021, **27**, 9454–9460, DOI: 10.1002/chem.202101003.

33 B. Reuillard, K. H. Ly, T. E. Rosser, M. F. Kuehnel, I. Zebger and E. Reisner, Tuning product selectivity for aqueous CO_2 reduction with a Mn(bipyridine)-pyrene catalyst immobilized on a carbon nanotube electrode, *J. Am. Chem. Soc.*, 2017, **139**, 14425–14435, DOI: 10.1021/jacs.7b06269.

34 J. D. Blakemore, A. Gupta, J. J. Warren, B. S. Brunschwig and H. B. Gray, Noncovalent immobilization of electrocatalysts on carbon electrodes for fuel production, *J. Am. Chem. Soc.*, 2013, **135**, 18288–18291, DOI: 10.1021/ja4099609.

35 A. Le Goff, F. Moggia, N. Debou, P. Jegou, V. Artero, M. Fontecave, B. Jousselme and S. Palacin, Facile and tunable functionalization of carbon nanotube electrodes with ferrocene by covalent coupling and π-stacking interactions and their relevance to glucose bio-sensing, *J. Electroanal. Chem.*, 2010, **641**, 57–63, DOI: 10.1016/j.jelechem.2010.01.014.

36 A. Le Goff, K. Gorgy, M. Holzinger, R. Haddad, M. Zimmerman and S. Cosnier, Tris(bispyrene-bipyridine)iron(II): A supramolecular bridge for the biofunctionalization of carbon nanotubes via π-stacking and pyrene/β-cyclodextrin host-guest interactions, *Chem. – Eur. J.*, 2011, **17**, 10216–10221, DOI: 10.1002/chem.201101283.

37 R. Haddad, K. Gorgy, M. Holzinger and S. Cosnier, In situ synthesis of stable mixed ligand Fe^{2+} complexes on bipyridinyl functionalized electrodes and nanotube supports, *Chem. Commun.*, 2012, **48**, 6121–6123, DOI: 10.1039/C2CC31645E.

38 J. A. Mann and W. R. Dichtel, Improving the Binding Characteristics of Tripodal Compounds on Single Layer Graphene, *ACS Nano*, 2013, **7**, 7193–7199, DOI: 10.1021/nn402599x.

39 L. Zhang, W. Zhang, P. Serp, W. H. Sun and J. Durand, Ethylene polymerization catalyzed by pyrene-tagged iron complexes: The positive effect of π-conjugation and immobilization on multiwalled carbon nanotubes, *ChemCatChem*, 2014, **6**, 1310–1316, DOI: 10.1002/cctc.201301063.

40 A. Maurin and M. Robert, Noncovalent immobilization of a molecular iron-based electrocatalyst on carbon electrodes for selective, efficient CO_2-to-CO conversion in water, *J. Am. Chem. Soc.*, 2016, **138**, 2492–2495, DOI: 10.1021/jacs.5b12652.

41 H. Asri, O. Dautel and A. Ouali, Terpyridine–Ru complexes noncovalently supported on cobalt magnetic nanoparticles for nitroarene transfer hydrogenation, *ACS Appl. Nano Mater.*, 2020, **3**, 11811–11818, DOI: 10.1021/acsanm.0c02337.

42 M. Keller, V. Collire, O. Reiser, A.-M. Caminade, J.-P. Majoral and A. Ouali, Pyrene-tagged dendritic catalysts noncovalently grafted onto magnetic Co/C nanoparticles: An efficient and recyclable system for drug synthesis, *Angew. Chem., Int. Ed.*, 2013, **52**, 3626–3629, DOI: 10.1002/anie.201209969.

43 F. Li, B. Zhang, X. Li, Y. Jiang, L. Chen, Y. Li and L. Sun, Highly Efficient Oxidation of Water by a Molecular Catalyst Immobilized on Carbon Nanotubes, *Angew. Chem., Int. Ed.*, 2011, **51**, 12276–12279, DOI: 10.1002/anie.201105044.

44 S. Li, X. Zhong, H. Yang, Y. Hu, F. Zhang, Z. Niu, W. Hu, Z. Dong, J. Jin, R. Li and J. Ma, Noncovalent modified

graphene sheets with ruthenium(II) complexes used as electrochemiluminescent materials and photosensors, *Carbon*, 2011, **49**, 4239–4245, DOI: 10.1016/j.carbon.2011.05.058.

45 S. N. Ding, D. Shan, S. Cosnier and A. Le Goff, Single-Walled Carbon Nanotubes Noncovalently Functionalized by Ruthenium(II) Complex Tagged with Pyrene: Electrochemical and Electrogenerated Chemiluminescence Properties, *Eur. J. Org. Chem.*, 2012, 11564, DOI: 10.1002/chem.201201543.

46 B. Reuillard, A. Le Goff and S. Cosnier, Non-covalent double functionalization of carbon nanotubes with a NADH oxidation Ru(II)-based molecular catalyst and a NAD-dependent glucose dehydrogenase, *Chem. Commun.*, 2014, **50**, 11731, DOI: 10.1039/C4CC04758C.

47 L. Yang, H. Ozawa, M. Koumoto, K. Yoshikawa, M. Matsunaga and M. Haga, "Janus-type" Ruthenium Complex Bearing Both Phosphonic Acids and Pyrene Groups for Functionalization of ITO and HOPG Surfaces, *Chem. Lett.*, 2015, **44**, 160–162, DOI: 10.1246/cl.140979.

48 J. Creus, R. Matheu, I. Peñafiel, D. Moonshiram, P. Blondeau, J. Benet-Buchholz, J. García-Antón, X. Sala, C. Godard and A. Llobet, A Million Turnover Molecular Anode for Catalytic Water Oxidation, *Angew. Chem., Int. Ed.*, 2016, **55**, 15382–15386, DOI: 10.1002/ange.201609167.

49 A. Gupta, J. D. Blakemore, B. S. Brunschwig and H. B. Gray, Immobilization and electrochemical properties of ruthenium and iridium complexes on carbon electrodes, *J. Phys.:Condens. Matter*, 2016, **28**, 094002, DOI: 10.1088/0953-8984/28/9/094002.

50 D. Ventura-Espinosa, C. Vicent, M. Bayac and J. A. Mata, Ruthenium molecular complexes immobilized on graphene as active catalysts for the synthesis of carboxylic acids from alcohol dehydrogenation, *Catal. Sci. Technol.*, 2016, **6**, 8024, DOI: 10.1039/C6CY01455K.

51 H. Clavier, F. Caijo, E. Borré, D. Rix, F. Boeda, S. P. Nolan and M. Mauduit, Towards long-living metathesis catalysts by tuning the N-heterocyclic carbene (NHC) ligand on trifluoroacetamide-activated boomerang Ru complexes, *Eur. J. Org. Chem.*, 2009, 4254–4265, DOI: 10.1002/ejoc.200900407.

52 M. Kohmoto, H. Ozawa, L. Yang, T. Hagio, M. Matsunaga and M. A. Haga, Controlling the adsorption of ruthenium complexes on carbon surfaces through noncovalent bonding with pyrene anchors: An electrochemical study, *Langmuir*, 2016, **32**, 4141–4152, DOI: 10.1021/acs.langmuir.6b00405.

53 S. Rajabi, F. Ebrahimi, G. Lole, J. Odrobina, S. Dechert, C. Jooss and F. Meyer, Water oxidizing diruthenium electrocatalysts immobilized on carbon nanotubes: Effects of the number and positioning of pyrene anchors, *ACS Catal.*, 2020, **10**, 10614–10626, DOI: 10.1021/acscatal.0c01577.

54 E. Clerich, S. Affès, E. Anticó, X. Fontrodona, F. Teixidor and I. Romero, Molecular and supported ruthenium complexes as photoredox oxidation catalysts in water, *Inorg. Chem. Front.*, 2022, **9**, 5347–5359, DOI: 10.1039/D2QI01504H.

55 S. Affès, A. M. Stamatelou, X. Fontrodona, A. Kabadou, C. Viñas, F. Teixidor and I. Romero, Enhancing photoredox catalysis in aqueous environments: Ruthenium aqua complex derivatization of graphene oxide and graphite rods for efficient visible-light-driven hybrid catalysts, *ACS Appl. Mater. Interfaces*, 2024, **16**, 507–519, DOI: 10.1021/acsami.3c13156.

56 A. Le Goff, B. Reuillard and S. Cosnier, A pyrene-substituted tris(bipyridine)osmium(II) complex as a versatile redox probe for characterizing and functionalizing carbon nanotube- and graphene-based electrodes, *Langmuir*, 2013, **29**, 8736–8742, DOI: 10.1021/la401712u.

57 N. Lalaoui, B. Reuillard, C. Philouze, M. Holzinger, S. Cosnier and A. Le Goff, Osmium(II) complexes bearing chelating N-heterocyclic carbine and pyrene-modified ligands: Surface electrochemistry and electron transfer mediation of oxygen reduction by multicopper enzymes, *Organometallics*, 2016, **35**, 2987–2992, DOI: 10.1021/acs.organomet.6b00508.

58 E. W. McQueen and J. I. Goldsmith, Electrochemical Analysis of Single-Walled Carbon Nanotubes Functionalized with Pyrene-Pendant Transition Metal Complexes, *J. Am. Chem. Soc.*, 2009, **131**, 17554–17556, DOI: 10.1021/ja907294q.

59 H. L. Smith, R. L. Usala, E. W. McQueen and J. I. Goldsmith, Novel Polyaromatic-Terminated Transition Metal Complexes for the Functionalization of Carbon Surfaces, *Langmuir*, 2010, **26**, 3342–3349, DOI: 10.1021/la9031249.

60 J. A. Mann, J. Rodríguez-López, H. D. Abruna and W. R. Dichtel, Multivalent binding motifs for the noncovalent functionalization of graphene, *J. Am. Chem. Soc.*, 2011, **133**, 17614–17617, DOI: 10.1021/ja208239v.

61 B. Reuillard, J. Warnan, J. J. Leung, D. W. Wakerley and E. Reisner, A Poly(cobaloxime)/Carbon Nanotube Electrode: Freestanding Buckypaper with Polymer-Enhanced H2-Evolution Performance, *Angew. Chem., Int. Ed.*, 2016, **55**, 3952–3957, DOI: 10.1002/anie.201511378.

62 T. T. Li, J. Qian, Q. Zhou, J. L. Lin and Y. Q. Zheng, A pyrene-modified cobalt salophen complex immobilized on multi-walled carbon nanotubes acting as a precursor for efficient electrocatalytic water oxidation, *Dalton Trans.*, 2017, **46**, 13020–13026, DOI: 10.1039/C7DT03033A.

63 H. Lei, C. Liu, Z. Wang, Z. Zhang, M. Zhang, X. Chang, W. Zhang and R. Cao, Noncovalent immobilization of a pyrene-modified cobalt corrole on carbon supports for enhanced electrocatalytic oxygen reduction and oxygen evolution in aqueous solutions, *ACS Catal.*, 2016, **6**, 6429–6437, DOI: 10.1021/acscatal.6b01579.

64 I. K. Attatsi, W. Zhu and X. Liang, Noncovalent immobilization of Co(II) porphyrin through axial coordination as an enhanced electrocatalyst on carbon electrodes for oxygen reduction and evolution, *New J. Chem.*, 2020, **44**, 4340–4345, DOI: 10.1039/C9NJ02408E.

65 B. Andrin, P. J. M. Cordeiro Junior, D. Provost, S. Diring, Y. Pellegrin, M. Robert and F. Odobel, Carbon nanotube heterogenization improves cobalt pyridyldiimine complex CO_2 reduction activity in aqueous carbonate buffer, *Chem. Commun.*, 2024, **60**, 5022–5025, DOI: 10.1039/D4CC00629A.

66 L. Xing, J. H. Xie, Y. S. Chen, L. X. Wang and Q. L. Zhou, Simply Modified Chiral Diphosphine: Catalyst Recycling *via* Non-covalent Absorption on Carbon Nanotubes, *Adv. Synth. Catal.*, 2008, **350**, 1013–1016, DOI: 10.1002/adsc.200700617.

67 B. Tan, D. P. Hickey, R. D. Milton, F. Giroud and S. D. Minteer, Regeneration of the NADH cofactor by a

rhodium complex immobilized on multi-walled carbon nanotubes, *J. Electrochem. Soc.*, 2015, **162**, H102, DOI: 10.1149/2.0111503jes.

68 S. J. Park, S. Kim, T. F. Anjong, S. E. Lee and J. Kim, The vital role of reduced graphene oxide in enhanced hydrogen photoproduction with a pyrene-pendant rhodium catalyst and platinum nanoparticles, *Carbon*, 2015, **94**, 448–454, DOI: 10.1016/j.carbon.2015.06.083.

69 S. Ruiz-Botella and E. Peris, Immobilization of pyrene-adorned N-heterocyclic carbene complexes of rhodium(I) on reduced graphene oxide and study of their catalytic activity, *ChemCatChem*, 2018, **10**, 1874–1881, DOI: 10.1002/cctc.201701277.

70 A. Cunillera, C. Blanco, A. Gual, J. M. Marinkovic, E. J. Garcia-Suarez, A. Riisager, C. Claver, A. Ruiz and C. Godard, Highly efficient Rh-catalysts immobilised by π–π stacking for the asymmetric hydroformylation of norbornene under continuous flow conditions, *ChemCatChem*, 2019, **11**, 2195–2205, DOI: 10.1002/cctc.201900211.

71 E. J. Hao, G. X. Li, Z. Z. Lv, F. S. Li, Y. Q. Chen, S. J. Lin, C. Z. Shi and L. Shi, "In situ immobilization" of a multicomponent chiral catalyst (MCC) via non-covalent interactions for heterogeneous asymmetric hydrogenation reactions, *Org. Chem. Front.*, 2020, **7**, 345–349, DOI: 10.1039/C9QO01331H.

72 C. Caix, S. Chardon-Noblat and A. Deronzier, Electrocatalytic reduction of CO_2 into formate with $[(\eta^5\text{-}Me_5C_5)M(L)Cl]^+$ complexes (L = 2,2′-bipyridine ligands; M = Rh(III) and Ir(III)), *J. Electroanal. Chem.*, 1997, **434**, 163–170, DOI: 10.1016/S0022-0728(97)00058-2.

73 P. Kang, S. Zhang, T. J. Meyer and M. Brookhart, Rapid selective electrocatalytic reduction of carbon dioxide to formate by an iridium pincer catalyst immobilized on carbon nanotube electrodes, *Angew. Chem., Int. Ed.*, 2014, **53**, 8709–8713, DOI: 10.1002/anie.201310722.

74 S. Ruiz-Botella and E. Peris, Unveiling the Importance of π-Stacking in Borrowing-Hydrogen Processes Catalysed by Iridium Complexes with Pyrene Tags, *Chem. – Eur. J.*, 2015, **21**, 15263–15271, DOI: 10.1002/chem.201502948.

75 J. M. Koelewijn, M. Lutz, R. J. Detz and J. N. H. Reek, Anode preparation strategies for the electrocatalytic oxidation of water based on strong interactions between multiwalled carbon nanotubes and cationic acetylammonium pyrene moieties in aqueous solutions, *ChemPlusChem*, 2016, **81**, 1098–1106, DOI: 10.1002/cplu.201600235.

76 J. De Tovar, A. C. Ghosh, T. Di Santo, M. Curtil, D. Aldakov, M. Koepf and M. Gennari, Electrochemical CO_2 Reduction with a Heterogenized Iridium–Pincer Catalyst in Water, *ChemCatChem*, 2023, **15**, e202300049, DOI: 10.1002/cctc.202300049.

77 P. D. Tran, A. Le Goff, J. Heidkamp, B. Jousselme, N. Guillet, S. Palacin, H. Dau, M. Fontecave and V. Artero, Noncovalent Modification of Carbon Nanotubes with Pyrene-Functionalized Nickel Complexes: Carbon Monoxide Tolerant Catalysts for Hydrogen Evolution and Uptake, *Angew. Chem., Int. Ed.*, 2011, **50**, 1371–1374, DOI: 10.1002/anie.201005427.

78 P. D. Tran, A. Morozan, S. Archambault, J. Heidkamp, P. Chenevier, H. Dau, M. Fontecave, A. Martinent, B. Jousselme and V. Artero, A noble metal-free proton-exchange membrane fuel cell based on bio-inspired molecular catalysts, *Chem. Sci.*, 2015, **6**, 2050, DOI: 10.1039/C4SC03774J.

79 S. Pugliese, N. T. Huan, J. Forte, D. Grammatico, S. Zanna, B. L. Su, Y. Li and M. Fontecave, Functionalization of Carbon Nanotubes with Nickel Cyclam for the Electrochemical Reduction of CO_2, *ChemSusChem*, 2020, **13**, 6449–6456, DOI: 10.1002/cssc.202002092.

80 U. Contaldo, M. Curtil, J. Pérard, C. Cavazza and A. Le Goff, A Pyrene-Triazacyclononane Anchor Affords High Operational Stability for CO_2RR Reduction Reaction by a CNT-Supported Histidine-Tagged CODH, *Angew. Chem.*, 2022, **134**, e202117212, DOI: 10.1002/ange.202117212.

81 S. Wittmann, A. Schütz, R. N. Grass, W. J. Stark and O. Reiser, A Recyclable Nanoparticle-Supported Palladium Catalyst for the Hydroxycarbonylation of Aryl Halides in Water, *Angew. Chem., Int. Ed.*, 2010, **10**, 1867–1870, DOI: 10.1002/anie.200906166.

82 M. Keller, V. Collière, O. Reiser, A. M. Caminade, J. P. Majoral and A. Ouali, Pyrene-Tagged Dendritic Catalysts Noncovalently Grafted onto Magnetic Co/C Nanoparticles: An Efficient and Recyclable System for Drug Synthesis, *Angew. Chem., Int. Ed.*, 2013, **52**, 3626–3629, DOI: 10.1002/anie.201209969.

83 K. Karami, A. Ramezanpour, M. Zakariazadeh and C. Silvestru, Catalytic activity and facile recovery of a cyclometalated N-heterocyclic carbene palladium(II) complex immobilized by non-covalent interactions on reduced graphene oxide, *Appl. Organomet. Chem.*, 2019, **33**, e4907, DOI: 10.1002/aoc.4907.

84 A. Mollar-Cuni, S. Martín, G. Guisado-Barrios and J. A. Mata, Dual role of graphene as support of ligand-stabilized palladium nanoparticles and carbocatalyst for (de)hydrogenation of N-heterocycles, *Carbon*, 2023, **206**, 314–324, DOI: 10.1016/j.carbon.2023.02.014.

85 D. Didier and E. Schulz, π-Stacking interactions at the service of [Cu]-bis(oxazoline) recycling, *Tetrahedron:Asymmetry*, 2013, **24**, 769–775, DOI: 10.1016/j.tetasy.2013.05.008.

86 S. Gentil, D. Serre, C. Philouze, M. Holzinger, F. Thomas and A. Le Goff, Electrocatalytic O_2 Reduction at a Bioinspired Mononuclear Copper Phenolato Complex Immobilized on a Carbon Nanotube Electrode, *Angew. Chem.*, 2016, **128**, 2563–2566, DOI: 10.1002/ange.201509593.

87 P. Garrido-Barros, C. Gimbert-Suriñach, D. Moonshiram, A. Pićon, P. Monge, V. S. Batista and A. Llobet, Electronic π-Delocalization Boosts Catalytic Water Oxidation by Cu(II) Molecular Catalysts Heterogenized on Graphene Sheets, *J. Am. Chem. Soc.*, 2017, **139**, 12907–12910, DOI: 10.1021/jacs.7b06828.

88 P. Garrido-Barros, I. Funes-Ardoiz, S. Drouet, J. Benet-Buchholz, F. Maseras and A. Llobet, Redox Non-innocent Ligand Controls Water Oxidation Overpotential in a New Family of Mononuclear Cu-Based Efficient Catalysts, *J. Am. Chem. Soc.*, 2015, **137**, 6758–6761, DOI: 10.1021/jacs.5b03977.

89 D. Ventura-Espinosa, S. Sabater and J. A. Mata, Enhancement of gold catalytic activity and stability by immobilization on the

surface of graphene, *J. Catal.*, 2017, **352**, 498–504, DOI: 10.1016/j.jcat.2017.06.021.

90 J. Bartelmess, B. Ballesteros, G. de la Torre, D. Kiessling, S. Campidelli, M. Prato, T. Torres and D. M. Guldi, Phthalocyanine-Pyrene Conjugates: A Powerful Approach toward Carbon Nanotube Solar Cells, *J. Am. Chem. Soc.*, 2010, **132**, 16202–16211, DOI: 10.1021/ja107131r.

91 S. Campidelli, B. Ballesteros, A. Filoramo, D. Díaz Díaz, G. de la Torre, T. Torres, G. M. A. Rahman, C. Ehli, D. Kiessling, F. Werner, V. Sgobba, D. M. Guldi, C. Cioffi, M. Prato and J. P. Bourgoin, Facile Decoration of Functionalized Single-Wall Carbon Nanotubes with Phthalocyanines *via* "Click Chemistry", *J. Am. Chem. Soc.*, 2008, **130**, 11503–11509, DOI: 10.1021/ja8033262.

92 E. Maligaspe, A. S. D. Sandanayaka, T. Hasobe, O. Ito and F. D'Souza, Sensitive Efficiency of Photoinduced Electron Transfer to Band Gaps of Semiconductive Single-Walled Carbon Nanotubes with Supramolecularly Attached Zinc Porphyrin Bearing Pyrene Glues, *J. Am. Chem. Soc.*, 2010, **132**, 8158–8164, DOI: 10.1021/ja101776p.

93 F. D'Souza, A. S. D. Sandanayaka and O. Ito, SWNT-Based Supramolecular Nanoarchitectures with Photosensitizing Donor and Acceptor Molecules, *J. Phys. Chem. Lett.*, 2010, **1**, 2586–2593, DOI: 10.1021/jz1009407.

94 E. Anaya-Plaza, J. Joseph, S. Bauroth, M. Wagner, C. Dolle, M. Sekita, F. Grçhn, E. Spiecker, T. Clark, A. de la Escosura, D. M. Guldi and T. Torres, Synergy of Electrostatic and π–π Interactions in the Realization of Nanoscale Artificial Photosynthetic Model Systems, *Angew. Chem., Int. Ed.*, 2020, **59**, 18786–18794, DOI: 10.1002/anie.202006014.

95 D. Lionetti, V. W. Day and J. D. Blakemore, Noncovalent immobilization and surface characterization of lanthanide complexes on carbon electrodes, *Dalton Trans.*, 2017, **46**, 11779–11789, DOI: 10.1039/C7DT02577G.